Monte Carlo study of charge and phonon transport in graphene

Marco Coco

Dipartimento di Matematica e Informatica
Università degli Studi di Catania

"This dissertation is submitted in partial fulfillment for the degree of"
Doctor of Philosophy

Advisor
Prof. PhD Vittorio Romano

January 2017

Abstract

In this thesis, we investigate charge transport in graphene. Graphene is one of the most important new materials with a wide range of properties, rarely together in the same material, and it is the ideal candidate for future electronic devices. The dynamics of electrons in the conduction band is analyzed, by considering values of Fermi levels high enough to neglect the dynamics in the valence band. This is equivalent to a n-type doping for traditional semiconductors.

Degeneracy effects are very important in graphene and then it becomes mandatory to consistently include the Pauli exclusion principle.

We develop a new Direct Simulation Monte Carlo (DSMC) procedure to solve the Boltzmann transport equation, that properly takes into account the Pauli principle. For a cross-validation of the results, we also solve the Boltzmann equation in a deterministic way by using the Discontinuous Galerkin method. The agreement of the results is excellent. A comparison of the new DSMC results with those obtained by means of well established hydrodynamical models are presented as well, and again the agreement is very good.

This new approach is applied to study the transport properties in suspended monolayer graphene and then in a layer of graphene on different substrates, obtaining the expected results as the degradation of mobilities.

Regarding phonon transport, we investigate the thermal effects in a suspended monolayer graphene due to the charge flow under an applied electric field. A complete model is considered, with all the phonon branches, both in-plane and out of plane ones. Moreover, we describe the phonon populations without any approximation of the distribution with an equivalent Bose-Einstein one. The distribution is built by means of the intermediate results arising from the new DSMC, by counting the number of the emission and absorption processes due to the interaction between electrons and phonons. The phonon-phonon interaction is treated in a standard way with a BGK approximation.

We are able to determine the increase of the temperature due to the charge flow and to predict its raise for any values of electric fields and Fermi energies. Moreover, it is shown that the inclusion of a complete phonon model leads to a lower heating effect with respect to other simplified models.

Key words: Graphene, Pauli's exclusion principle, Monte Carlo method, Discontinuous Galerkin method, Heating effects, Maximum Entropy Principle

Sommario

L'argomento principale di questa tesi è lo studio dei fenomeni di trasporto nel grafene. Il graphene è uno dei nuovi materiali più importanti e gode di un ampio spettro di ottime proprietà, che sono raramente presenti assieme in uno stesso materiale, ed è considerato il candidato ideale per lo sviluppo di futuri dispositivi elettronici. Si studierà la dinamica degli elettroni nella banda di conduzione, considerando livelli di Fermi sufficientemente alti per potere trascurare la dinamica di quelli nella banda di valenza. Questa condizione è equivalente a un doping di tipo n per i semiconduttori tradizionali.

Gli effetti di degenerazione sono particolarmente importanti nel grafene e la corretta inclusione del principio di Pauli non è più evitabile.

Per risolvere l'equazione di Boltzmann, è stata sviluppata una nuova procedura di simulazione Monte Carlo (Direct Simulation Monte Carlo) capace di trattare correttamente il principio di Pauli. Per una validazione dei risultati, l'equazione di Boltzmann è stata risolta anche in maniera deterministica ricorrendo a uno schema numerico basato sul metodo Discontinuous Galerkin. L'accordo tra i risultati è eccellente. Si è fatto un confronto anche con i risultati ottenuti utilizzando un consolidato modello idrodinamico e anche in questo caso l'accordo è molto buono.

La nuova procedura è stata applicata per lo studio del trasporto di cariche in un singolo strato di grafene sospeso e successivamente in uno strato di grafene appoggiato su differenti substrati. Si sono confermati gli effetti del substrato, come la diminuzione della mobilità.

Si è investigato anche il trasporto dei fononi e sono stati analizzati gli effetti termici in presenza di un campo elettrico. Si è fatto uso di un modello completo, comprensivo di tutte le branche di fononi, sia quelli nel piano che quelli ortogonali al piano. La popolazione dei fononi è stata descritta senza ricorrere all'approssimazione con una distribuzione di Bose-Einstein ed è calcolata sfruttando i risultati della simulazione Monte Carlo, contando il numero dei processi di emissione e assorbimento dovuti all'interazione degli elettroni con i fononi. Il contributo dovuto all'interazione fonone-fonone è trattato con un' approssimazione BGK.

È stato possibile determinare l'aumento della temperatura dovuto al flusso di cariche e prevederne l'andamento per qualsiasi valore del campo elettrico e del livello di Fermi. Infine, si è dimostrato come l'inclusione di tutte le branche dei fononi predica effetti termici minori rispetto ad altri modelli semplificati.

Contents

List of figures

List of tables

Introduction

The Boltzmann equation is the basic starting point for transport problems; it was initially developed for gas dynamics and its semiclassical formulation has become the standard model for charge transport in semiconductors. The semiclassical formulation includes into the Boltzmann equation the appropriate form of the energy bands, and therefore the relation for the group velocity, arising from the solution of the Schroedinger equation with a periodic potential on account of the periodicity of the crystall lattice. An useful formulation for the collision operator is another fundamental element into a semiclassical picture. Usually, it is derived into the constraints given by the Fermi Golden Rule and the Born approximation.

Starting from the Boltzmann equation, several models and methods have been developed for the modeling of transport problems in semiconductors in order to describe and simulate the underlying physical phenomena and the behaviour of real electronic devices. Many deterministic numerical methods give a direct solution of the Boltzmann equation, but can be computationally expensive for simulation purposes.

A standard way to overcome such a difficulty was the development of macroscopic continuous models, as the famous Drift-Diffusion and Hydrodynamical ones. These are obtained by means of moments of the Boltzmann equation with respect to opportune weight functions and have the same form as the equations for fluid-dynamics. They became one of the most useful models for Computer Aided Design (CAD). Actually, the study and simulation of charge problem has to be integrated into the more general production process typical of Computational Electronics. The development of a new electronic device cannot anymore be reached with the standard trial-and-error technique and a general integrated simulation procedure able to deal both with the physical phenomena and the device properties has become fundamental. With the shrinking of the dimension of the electronic device the basic assumptions underlying the macroscopic models are less and less valid. Furthermore, quantum effects start to be not negligible.

Particle-based methods have become increasingly important.

Monte Carlo method was developed some hundreds years ago and is a consolidated way to deal with charge transport in semiconductors. Its most important and apparently

contradictory feature is together its greatest strength and advantage: it is a probabilistic method able to solve also deterministic problems, as the Boltzmann equation. Indeed, its probabilistic character makes it a natural way to look at charge transport in a *direct* way. This means that we can deduce the properties of a real ensemble just by following the dynamics of only a sample of particles. Furthermore, it naturally results as an experimental technique that allows us to study physical phenomena for which direct experiments are no possible and to predict properties of new materials and devices.

Great mathematical difficulties arise in the Boltzmann equation when we deal with non diluted ensembles because we must consider the availability of the final states into the collision operator, introducing strong non linearity.

Degeneracy effects were a hard task also for Monte Carlo simulations and a lot of attempts were made to treat correctly the Pauli principle. A standard method has become that developed by Lugli and Ferry [28] for an Ensemble Monte Carlo (EMC) simulation, starting from the pioneering work of Bosi and Jacoboni [27] for the one-particle Monte Carlo simulation. The results show how important the degeneracy effects are but predict incorrect distribution functions, exceeding the maximum value equal to 1. Some improvements can be found in literature, for example with the introduction of ad hoc scattering-out terms [31, 32] or with some approximations of the distribution function [33, 34] but the problem of the derivation of a correct distribution function remained unsolved. In several applications, this effect was not so relevant because the mean values were accurate enough but the problem is fundamental from a theoretical point of view. Moreover, in the presence of high densities, the Pauli exclusion principle becomes more and more important and it is mandatory to accurately describe the distribution function.

The first aim of this thesis is to deal with such degeneracy effects and to develop a new Direct Simulation Monte Carlo strategy in order to properly take into account the Pauli principle.

The Boltzmann equation intrinsically appears as a balance between two distinct parts with different meaning and structure. In the left hand side, the effect of the Liouvillian differential operator represents the rigid motion of the distribution as a whole over the trajectories of the phase space, according to the semiclassical equations of motion; this in turn balances the action of the collisional operator.

Keeping this structure in mind, we use a hybrid DSMC simulation strategy, splitting the Monte Carlo solution of the Boltzmann equation into two steps: first, we solve analytically the left part, and then we treat the scattering mechanisms, in a similar way as in the standard EMC simulation. We obtain correct occupation numbers and can properly take into account

the Pauli exclusion principle. Moreover, the computational cost is comparable with that of the standard approaches.

Charge transport in a homogeneous suspended monolayer graphene is studied.

Graphene is one of the most important new material and shows a wide range of important properties, rarely together in the same material. It is one of the most promising candidate for future electronic devices due to its electric and thermal properties; for example, its electrical conductivity is an order of magnitude greater than the conventional semiconductors. It was theorized many years ago but it was discovered only a few years ago, so charge transport in graphene is still an open field and much is to be well understood both from a mathematical and from a physical point of view. For example, one can find great uncertainty about the values of the coupling constants. From a modeling point of view, it is important to underline that graphene is a zero-gap semiconductor, it has a linear dispersion relation and the electrons moving inside can be treated as mass-less Dirac fermions. Degeneracy effects and Pauli's principle seem to be very effective in graphene and the work in this thesis could be an important contribution in this field.

We apply the previous scheme to investigate the transport properties of graphene, as the average velocity and energy under the effect of an applied electric field. We analyze the dynamics of the conduction band by using values of the Fermi level high enough to consider the valence band completely filled, so that the dynamics of the electrons into the valence band can be neglected.

In the second part of the thesis, the case of a graphene layer on different substrates is considered, obtaining the expected results as, for example, the degradation of the mobilities. The influence of the distance from the substrate is deeply analyzed.

For a cross-validation of the results, we also solve the Boltzmann equation by using a numerical scheme based on Discontinuous Galerkin method, already largely used for conventional semiconductors. The agreement of the results is excellent.

The results for the suspended case are compared as well with those obtained by means of well established hydrodynamical models, and again the agreement is good. The overall discrepancy of the hydrodynamical model is acceptable from a practical point of view for Computer Aided Design (CAD) purposes.

In order to investigate thermal effects in graphene, in the last part of the thesis we study the phonon transport. We consider a complete phonon model with all phonon branches, both in plane and out of plane (flexural) ones. These latter do not contribute in the interaction with electrons but are very important in the determination of the thermal behaviour of graphene. Moreover, we describe the phonon populations without any approximation of the distribution by an equivalent Bose-Einstein one. The phonon distribution is obtained by

means of the intermediate results of the DSMC part, by counting the number of emission and absorption processes. The right statistical weight of each process is properly calculated. The phonon-phonon interaction is modeled by a standard BGK approximation.

We are able to determine the increase of the temperature due to the charge flow and to predict its raise for any values of electric fields and Fermi energies. It is also shown that the inclusion of a complete phonon model leads to a lower heating effect with respect to simplified models.

Outline of the thesis

The plan of the thesis is as follows.

In chapter 1, basic concepts about the Boltzmann equation and the properties of graphene are presented, and the general kinetic description for charge transport in graphene is discussed.

In chapter 2, we summarize the standard Ensemble Monte Carlo simulation and then we describe the original part, the new proposed DSMC strategy. We give computational details and show the results. A comparison is made between the new DSMC results and the standard EMC ones and then a comparison with the deterministic solution of the Boltzmann equation obtained with Discontinuous Galerkin method. We also show some results obtained with other approaches similar to those already present in literature and that suffer from physical inconsistencies.

In chapter 3, Discontinuous Galerkin method is delineate, discussing in particular the discretization of the drift and collision terms.

In chapter 4, we study the case of a graphene layer on different substrates, and the influence of the distance from the substrate and the distribution of impurities are analyzed. The results agree with the expected degradation of transport properties due to the presence of the substrate and its impurities.

In chapter 5, we deal with phonon transport in order to analyze thermal effects in a suspended monolayer graphene. A complete phonon model, with all phonon branches, is considered, We show and comment the results of the simulation and deduce the rate of rise in temperature versus time. In the second part, we perform a regression analysis on the simulation data and we find a way to predict the raise of the temperature for any values of the electric field and of the Fermi energy. The chapter is concluded by comparison with a simplified model.

In chapter 6, macroscopic models are briefly presented and a hydrodynamical model is obtained by using the Maximum Entropy Principle for the needed closure relations. A

comparison between the results of the new DSMC strategy and of the Hydrodynamical model is shown.

Some mathematical details about derivation and properties of the Boltzmann equation are postponed in the Appendix A. The semiclassical framework is underlined.

Chapter 1

Mathematical model for charge transport in graphene

1.1 The Boltzmann equation

The Boltzmann equation is the fundamental basis for transport problems, from the original gas dynamics ones to those related to charge transport in semiconductors. For more rigorous details we refer to Appendix A.

Given a gas with N particles [1, 2], the space and velocity coordinates, $\mathbf{x} \in \mathbb{R}^3_{\mathbf{x}}$, $\mathbf{v} \in \mathbb{R}^3_{\mathbf{v}}$ respectively, the *distribution function* $f(\mathbf{x},\mathbf{v},t)$ is defined in such a way that

$$f(\mathbf{x},\mathbf{v},t)\, d\mathbf{x}\, d\mathbf{v} \tag{1.1}$$

represents the number of particles in the infinitesimal volume $d\mathbf{x}\, d\mathbf{v}$ at time t. The normalization condition for f is

$$\int_{\mathbb{R}_{\mathbf{v}}} \int_{\mathbb{R}_{\mathbf{x}}} f(\mathbf{x},\mathbf{v},t)\, d\mathbf{x}\, d\mathbf{v} = N. \tag{1.2}$$

The spatial density $n(\mathbf{x},t)$ at time t is given by

$$n(\mathbf{x},t) = \int_{\mathbb{R}_{\mathbf{v}}} f(\mathbf{x},\mathbf{v},t)\, d\mathbf{v}. \tag{1.3}$$

Given an ensemble of electrons, we consider the distribution function $f(\mathbf{x},\mathbf{k},t)$, where $\mathbf{k} \in B$ is the wave-vector; B is the Brilluoin zone, the primitive cell of the reciprocal lattice. $\mathbf{k}$ assumes a set of discrete values, due to the discrete nature of lattice. $\hbar\mathbf{k}$ is the crystal momentum.

In a standard way, we can replace sums over $\mathbf{k}$ with integrals by mean of the following rule

$$\sum_{\mathbf{k}} \longmapsto \frac{(l)^d}{(2\pi)^d} \int_B, \tag{1.4}$$

where d is the dimensionality of the electron gas and l the size of the crystal. For graphene, $d = 2$. $f(\mathbf{x},\mathbf{k},t)$ is proportional to the number of particles in $d\mathbf{x}d\mathbf{k}$ and the normalization conditions are

$$\frac{2}{(2\pi)^2} \int_B \int_{\mathbb{R}_\mathbf{x}} f(\mathbf{x},\mathbf{k},t) d\mathbf{x} d\mathbf{k} = N, \qquad \frac{2}{(2\pi)^2} \int_B f(\mathbf{x},\mathbf{k},t) d\mathbf{k} = n(\mathbf{x},t). \tag{1.5}$$

The factor 2 takes into account the spin of electrons. The time evolution of the distribution function is given by the Boltzmann Transport Equation

$$\partial_t f + \mathbf{v}(\mathbf{k}) \cdot \nabla_\mathbf{x} f - \frac{e}{\hbar} \mathbf{E} \cdot \nabla_\mathbf{k} f = C[f](\mathbf{k}), \tag{1.6}$$

where $\mathbf{E}$ is the external force, in our case the applied electric field, e the elementary (positive) charge of electron, $\nabla_\mathbf{x}$ and $\nabla_\mathbf{v}$ denote the gradient with respect to the position and the wave-vector, respectively, and $C[f](\mathbf{k})$ is the collision operator. The l.h.s of the Boltzmann Equation describes the flow of particles in the phase space and it represents the effect on $f(\mathbf{x},\mathbf{k},t)$ of the Liouvillian operator

$$L = \frac{\partial}{\partial t} + \mathbf{v} \cdot \nabla_\mathbf{x} - \dot{\mathbf{k}} \cdot \nabla_\mathbf{k}. \tag{1.7}$$

$\mathbf{v}(\mathbf{k})$ is the group velocity of an electron wave packet and it is linked to the energy band $\varepsilon(\mathbf{k})$, arising from the solution of the Schroedinger equation with a static periodic potential, by the following relation

$$\mathbf{v}(\mathbf{k}) = \frac{1}{\hbar} \nabla_\mathbf{k} \varepsilon(\mathbf{k}). \tag{1.8}$$

The collision operator describes the contribution of several type of electron scatterings and, omitting the dependence on space and time for the sake of simplicity, also justified by the fact that the collision operator is considered local in space and time, its general form is

$$C[f](\mathbf{k}) = \int_B \left[P(\mathbf{k}',\mathbf{k}) f(\mathbf{k}') \left(1 - f(\mathbf{k})\right) - P(\mathbf{k},\mathbf{k}') f(\mathbf{k}) \left(1 - f(\mathbf{k}')\right) \right] d\mathbf{k}'. \tag{1.9}$$

The first term is the gain of electrons into the state $\mathbf{k}$ (*scattering in*) and it is proportional to the initial state occupancy $f(\mathbf{k}')$ and to the availability of the finale state $(1 - f(\mathbf{k}))$, on account of the Pauli exclusion principle; the second term is the loss of electrons from the state $\mathbf{k}$ (*scattering out*). $P(\mathbf{k}',\mathbf{k})$ is the scattering rate, the transition probability per unit time,

that an electron in the state $\mathbf{k}'$ is transferred into the state $\mathbf{k}$. The collisions do not induce spin flip. With the previous collision operator, the Boltzmann Equation becomes a non linear integro-differential equation. In general, the rate of a transition from a state $|\mathbf{i}\rangle$ into a state $|\mathbf{j}\rangle$ due to a process with the interaction Hamiltonian H_I is given by means of the Fermi Golden Rule and is equal to

$$P_{|\mathbf{i}\rangle\to|\mathbf{j}\rangle} = \frac{2\pi}{\hbar}\,|\langle\mathbf{i}|H_I|\mathbf{j}\rangle|^2\,\delta(\varepsilon_\mathbf{i}-\varepsilon_\mathbf{j}), \tag{1.10}$$

where $\varepsilon_\mathbf{i}$ and $\varepsilon_\mathbf{j}$ take into account the energy of electrons in the state $|\mathbf{i}\rangle$ and $|\mathbf{j}\rangle$, respectively.

For a non homogeneous system the transition rates depend upon also the position, i.e. $P = P(\mathbf{x},\mathbf{k}',\mathbf{k})$, and if the non homogeneity is too strong, the semiclassical description could fail and one has to recur to solutions directly based on the Schroedinger equation [1].

The most important scattering mechanisms we will consider are those with the crystal lattice, whose vibrations are described by (quasi)-particles, the phonons, able to exchange quanta of energy with electrons. When the electron loses a quantum of energy, we have an *emission* process, otherwise an *absorption* one. The general scattering rate of electron phonon-interaction can be written as a sum of emission and absorption contributions

$$P(\mathbf{k}',\mathbf{k}) = s(\mathbf{q})\left\{[(g(\mathbf{q})+1)]\,\delta(\varepsilon(\mathbf{k})-\varepsilon(\mathbf{k}')+\hbar\omega)\;+g(\mathbf{q})\delta(\varepsilon(\mathbf{k})-\varepsilon(\mathbf{k}')-\hbar\omega)\right\}. \tag{1.11}$$

$\mathbf{q}$ is the phonon wave-vector, $g(\mathbf{x},\mathbf{q},t)$ is the phonon distribution, $s(\mathbf{q})$ is the scattering potential and $\hbar\omega$ is the phonon energy. The term $+1$ added to $g(\mathbf{q})$ in the emission case is due to the so-called *spontaneous emission*, a quantum effect that describes the possibility of electrons to interact with the phonon field even when phonons are not present and it is as the zero-point vibrations of quantum harmonic oscillator; the term proportional to $g(\mathbf{q})$ is due to the phonons already present in the crystal and is called *stimulated emission*. At equilibrium, the electrons are described by the Fermi-Dirac distribution and the phonons, that are bosons and do not obey to Pauli's exclusion principle, by the Bose-Einstein distribution, given respectively by

$$f(\mathbf{k}) = \frac{1}{1+\exp\frac{\varepsilon(\mathbf{k})-\varepsilon_F}{k_BT}} \quad , \tag{1.12}$$

$$g(\mathbf{q}) = \frac{1}{1-\exp\frac{\hbar\omega(\mathbf{q})}{k_BT}} \quad , \tag{1.13}$$

where k_B is the Boltzmann constant, T the temperature and ε_F the Fermi level.

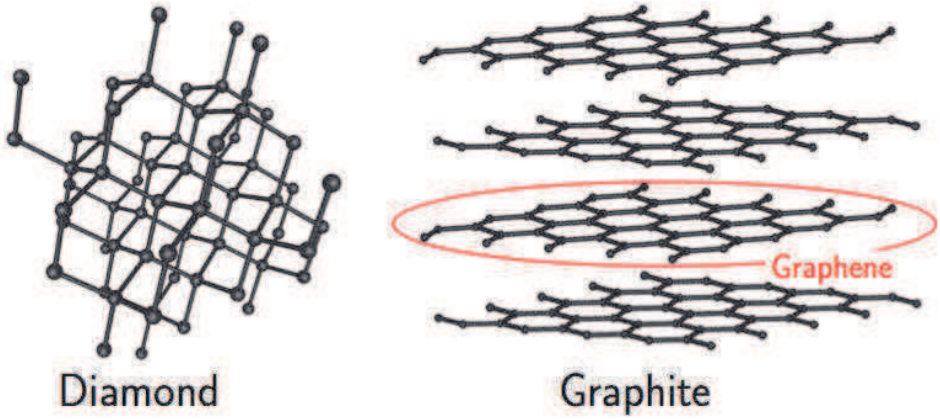

Fig. 1.1 Graphite and Graphene

1.2 Electronic properties of graphene

Graphene is one of the most important new material, really promising as an ideal candidate for future applications in electronic devices. It has a lot of very good properties, some of them in general difficult to find together in the same material: it is the thinnest object ever obtained but at the same time one of the strongest material in the world; it is also very elastic and impermeable to any molecule. It is extremely electrically and thermally conductive, with an electrical conductivity an order of magnitude greater than the conventional semiconductors. The starting material is just the graphite used for pencils, Fig. 1.1. With the original scotch tape method Andre Geim and Kostya Novoselov [3] (awarded with the Nobel Prize in Physics in 2010), at the University of Manchester, were able to produce relatively large isolated graphene samples from graphite. Also from a mathematical modeling point of view, one of the most important feature of graphene is that the charges moving inside it do no more respect the effective mass approximation model and have to be considered as mass less Dirac fermions with an effective speed of light $c_* = 10^6$ ms^{-1} ([4], [5], [6]).
Graphene is a single layer of sp^2 carbon atoms arranged into a honeycomb hexagonal lattice and can also be deformed in order to have 1-dimensional or 0-dimensional structures, the carbon nanotubes and the fullerene, respectively (Fig. 1.2). The lattice has a biatomic basis with the lattice vectors

$$\mathbf{a}_1 = \frac{a}{2}\left(3, \sqrt{3}\right), \qquad \mathbf{a}_2 = \frac{a}{2}\left(3, -\sqrt{3}\right) \quad , \tag{1.14}$$

where $a = 0.142$ nm is the carbon-carbon bond length. Since we have a biatomic basis, the lattice constant is $a\sqrt{3} = 0.246$ nm. The nearest neighbors of each carbon atom are displaced

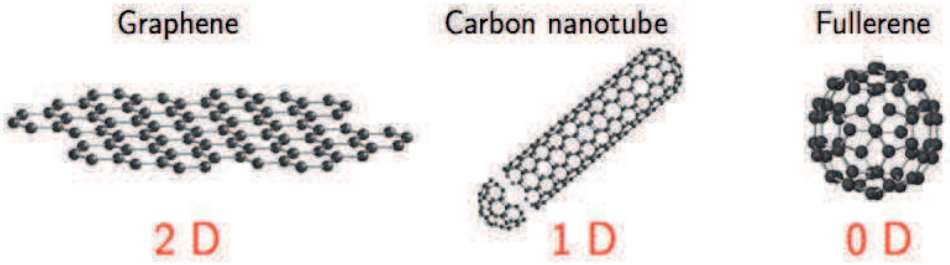

Fig. 1.2 Graphene configurations

by the following vectors

$$\boldsymbol{\delta}_1 = \frac{a}{2}\left(1,\sqrt{3}\right), \qquad \boldsymbol{\delta}_2 = \frac{a}{2}\left(1,-\sqrt{3}\right), \qquad \boldsymbol{\delta}_3 = -a\,(1,0) \quad ; \tag{1.15}$$

the six second-nearest neighbors are located at

$$\boldsymbol{\delta'}_1 = \pm\mathbf{a}_1, \qquad \boldsymbol{\delta'}_2 = \pm\mathbf{a}_2, \qquad \boldsymbol{\delta}'_3 = \pm(\mathbf{a}_2 - \mathbf{a}_1) \quad . \tag{1.16}$$

The primitive cell of the reciprocal lattice, the (first) Brillouin zone (Fig. 1.3), is hexagonal as that of the real space lattice but rotated by $\frac{\pi}{2}$, and its basis vectors are

$$\mathbf{b}_1 = \frac{2\pi}{3a}\left(1,\sqrt{3}\right), \qquad \mathbf{b}_2 = \frac{2\pi}{3a}\left(1,-\sqrt{3}\right) \quad . \tag{1.17}$$

Thanks to the periodicity of the reciprocal lattice, all the corners can be treated considering only the two points K and K', called *Dirac points*, with coordinates

$$K = \left(\frac{2\pi}{3a}, \frac{2\pi}{3\sqrt{3}a}\right), \qquad K' = \left(\frac{2\pi}{3a}, -\frac{2\pi}{3\sqrt{3}a}\right). \tag{1.18}$$

Solving the Schroedinger equation, taking into account the periodicity of the crystal potential, one obtains the numerical energy bands of Fig.1.4. With the standard tight-binding Hamiltonian approach [7] the energy bands have the general form

$$E_{\pm}(\mathbf{q}) = \pm t\sqrt{3 + f(\mathbf{q})} - t' f(\mathbf{q}) \tag{1.19}$$

where $\mathbf{q}$ is the wave-vector evaluated from the Γ point, the plus and minus signs are for upper (π^*) and lower (π) band, the conduction and valence band, respectively, $t = 2.8$ eV, $t' = 0.1$

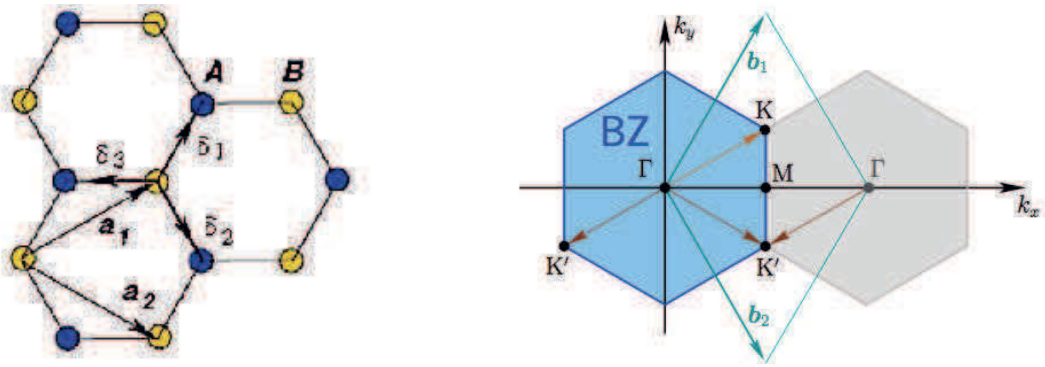

Fig. 1.3 Graphene lattice (left) and Brillouin zone (right)

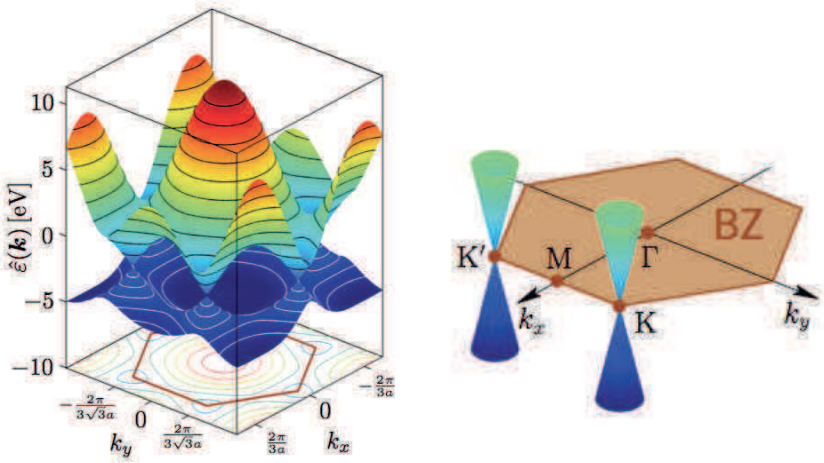

Fig. 1.4 Energy bands in graphene

eV and $f(\mathbf{q})$ is given by

$$f(\mathbf{q}) = 2\cos\left(\sqrt{3}q_x a\right) + 4\cos\left(\frac{\sqrt{3}}{2}q_y a\right)\cos\left(\frac{3}{2}q_x a\right) \quad . \tag{1.20}$$

The two bands touch at K and K, meaning that graphene is a zero gap semiconductor, and they are exactly symmetric if $t' = 0$. The region of the Brillouin zone around the Dirac points is the most occupied from electrons and then the most important in the study of charge transport. Around the Dirac points the dispersion relation has a conical shape according to the approximation

$$E_{\pm}(\mathbf{k}) = \pm\hbar v_F |\mathbf{k}| + O\left(\frac{|\mathbf{k}|}{|\mathbf{K}|}\right)^2 \tag{1.21}$$

where $\mathbf{k} = \mathbf{q} - \mathbf{K}$, $\mathbf{K}$ is the lattice vector relative to the Dirac point K, $v_F = 3ta/2$ is the Fermi velocity, equal to 10^6 m/s, $\hbar$ is the reduced Planck constant and $\mathbf{k}$ is the wave-vector considered from the Dirac point K (or K'). Considering only the first term, the previous relation is the same for both Dirac points, so that the valleys around K and K' can be treated as equivalent. It holds when $|\mathbf{k}| << |\mathbf{K}|$, so practically always because all the electrons are around the Dirac points. At zero temperature, the valance band is totally occupied by electrons and the conduction band has only unoccupied states. In intrinsic graphene, in ideal conditions, the Fermi level is equal to zero. In the following, we will consider higher values of the Fermi level taking into account the effects of imperfections of the material or of an external applied voltage, in order to have a condition equivalent to a n type doping in standard semiconductors; in this way, it is possible to neglect the dynamics of the holes because the valence band is completely filled and we will refer only to the electrons dynamics.

1.3 Semiclassical kinetic model

In a semiclassical kinetic setting, the charge transport in graphene is described by four Boltzmann equations, one for electrons in the valence band (π) and one for electrons in the conduction band (π^*), that in turn can belong to the K or K' valley,

$$\frac{\partial f_{\ell,s}(t,\mathbf{x},\mathbf{k})}{\partial t} + \mathbf{v}_{\ell,s}\cdot\nabla_{\mathbf{x}} f_{\ell,s}(t,\mathbf{x},\mathbf{k}) - \frac{e}{\hbar}\mathbf{E}\cdot\nabla_{\mathbf{k}} f_{\ell,s}(t,\mathbf{x},\mathbf{k}) = \left.\frac{df_{\ell,s}}{dt}(t,\mathbf{x},\mathbf{k})\right|_{e-ph}, \tag{1.22}$$

where $f_{\ell,s}(t,\mathbf{x},\mathbf{k})$ represents the distribution function of charge carriers, in the band π or π^* ($s = -1$ or $s = 1$) and valley ℓ (K or K'), at position $\mathbf{x}$, time t, and with wave-vector

$\mathbf{k}$. We denote by $\nabla_{\mathbf{x}}$ and $\nabla_{\mathbf{k}}$ the gradients with respect to the position and the wave-vector, respectively. The group velocity $\mathbf{v}_{\ell,s}$ is related to the band energy $\varepsilon_{\ell,s}$ by

$$\mathbf{v}_{\ell,s} = \frac{1}{\hbar}\nabla_{\mathbf{k}}\,\varepsilon_{\ell,s}\,.$$

With a very good approximation [4] a linear dispersion relation holds for the band energies $\varepsilon_{\ell,s}$ around the equivalent Dirac points; so that

$$\varepsilon_{\ell,s} = s\hbar\, v_F\,|\mathbf{k}-\mathbf{k}_\ell|\,, \tag{1.23}$$

where v_F is the (constant) Fermi velocity, $\hbar$ the Planck constant divided by 2π, and $\mathbf{k}_\ell$ is the position of the Dirac point corresponding to valley ℓ. The elementary (positive) charge is denoted by e, and $\mathbf{E}$ is the electric field obtained by the Poisson equation, which must be coupled with Eqs (1.22). The right hand side of Eqs. (1.22) is the collision term representing the interactions of electrons with acoustic, optical and K phonons. Acoustic phonon scattering is intra-valley and intra-band. Optical phonon scattering is intra-valley and can be longitudinal optical (LO) and transversal optical (TO); it can be intra-band, leaving the electrons in the same band, or inter-band, pushing the electrons from the initial band toward another one. Scattering with phonons of K type pushes electrons from a valley to a one nearby (inter-valley scattering).

The general form of the collision term can be written as (see [4, 35–38] for more details)

$$\begin{aligned}\left.\frac{df_{\ell,s}}{dt}(t,\mathbf{x},\mathbf{k})\right|_{e-ph} = \sum_{\ell',s'}\Bigg[&\int_B S_{\ell',s',\ell,s}(\mathbf{k}',\mathbf{k})\,f_{\ell',s'}(t,\mathbf{x},\mathbf{k}')\left(1-f_{\ell,s}(t,\mathbf{x},\mathbf{k})\right)d\mathbf{k}'\\ &-\int_B S_{\ell,s,\ell',s'}(\mathbf{k},\mathbf{k}')\,f_{\ell,s}(t,\mathbf{x},\mathbf{k})\left(1-f_{\ell',s'}(t,\mathbf{x},\mathbf{k}')\right)d\mathbf{k}'\Bigg]\,,\end{aligned}$$

where the total transition rate $S_{\ell',s',\ell,s}(\mathbf{k}',\mathbf{k})$ is given by the sum of the contributions of the several types of scatterings described above

$$\begin{aligned}S_{\ell',s',\ell,s}(\mathbf{k}',\mathbf{k}) &= \sum_\nu \left|G^{(\nu)}_{\ell',s',\ell,s}(\mathbf{k}',\mathbf{k})\right|^2\\ &\times\left[\left(n^{(\nu)}_{\mathbf{q}}+1\right)\delta\left(\varepsilon_{\ell,s}(\mathbf{k})-\varepsilon_{\ell',s'}(\mathbf{k}')+\hbar\,\omega^{(\nu)}_{\mathbf{q}}\right)+n^{(\nu)}_{\mathbf{q}}\,\delta\left(\varepsilon_{\ell,s}(\mathbf{k})-\varepsilon_{\ell',s'}(\mathbf{k}')-\hbar\,\omega^{(\nu)}_{\mathbf{q}}\right)\right].\end{aligned} \tag{1.24}$$

The index ν labels the νth phonon mode. The $\left|G^{(\nu)}_{\ell',s',\ell,s}(\mathbf{k}',\mathbf{k})\right|^2$'s are the electron-phonon coupling matrix elements, which describe the interaction mechanism of an electron with a νth phonon, from the state of wave-vector $\mathbf{k}'$ belonging to the valley ℓ' and band s' to the state

$\mathbf{k}$ belonging to the valley ℓ and band s. The symbol δ denotes the Dirac distribution, $\omega_{\mathbf{q}}^{(\nu)}$ is the νth phonon frequency, $n_{\mathbf{q}}^{(\nu)}$ is the Bose-Einstein distribution for the ν-type phonons

$$n_{\mathbf{q}}^{(\nu)} = \frac{1}{e^{\hbar\,\omega_{\mathbf{q}}^{(\nu)}/k_B T} - 1}, \tag{1.25}$$

where k_B is the Boltzmann constant and T the graphene lattice temperature and with $\mathbf{q}$ the phonon wave-vector belonging to B. When, for a phonon ν_*, $\hbar\,\omega_{\mathbf{q}}^{(\nu_*)} \ll k_B T$, the scattering with the phonon ν_* can be assumed elastic. In this case, we eliminate in Eq. (1.24) the term $\hbar\,\omega_{\mathbf{q}}^{(\nu_*)}$ inside the delta distribution and we use the approximation $n_{\mathbf{q}}^{(\nu_*)} \approx k_B T/\hbar\,\omega_{\mathbf{q}}^{(\nu)} - \frac{1}{2}$. By applying a gate voltage transversal with respect to the graphene sheet, it is possible to modify the Fermi energy ε_F and therefore the charge density. If a high positive value of the Fermi potential is considered, the electrons responsible for the current are those belonging to the conduction band. Therefore only the transport equation for electrons in the conduction band is considered and interband electron transitions are neglected. Moreover the valleys K and K' are considered as equivalent. A reference frame centered in the K-point will be used. Of course, we simplify the notation, omitting the indexes s and ℓ and denoting with f the only relevant distribution function.

The expressions of the electron-phonon scattering matrices used in our simulations are as follows. For acoustic phonons, we consider the elastic approximation according to which we have

$$\left(2\,n_{\mathbf{q}}^{(ac)} + 1\right)\left|G^{(ac)}(\mathbf{k}',\mathbf{k})\right|^2 = \frac{1}{(2\,\pi)^2}\,\frac{\pi\,D_{ac}^2\,k_B\,T}{2\,\hbar\,\sigma_m\,v_p^2}\left(1+\cos\vartheta_{\mathbf{k},\mathbf{k}'}\right), \tag{1.26}$$

where D_{ac} is the acoustic phonon coupling constant, v_p is the sound speed in graphene, σ_m the graphene density, and $\vartheta_{\mathbf{k},\mathbf{k}'}$ is the convex angle between $\mathbf{k}$ and $\mathbf{k}'$.
The electron-phonon coupling matrix elements of the longitudinal optical (LO), the transversal optical (TO) and the K phonons are (see for example [38])

$$\left|G^{(LO)}(\mathbf{k}',\mathbf{k})\right|^2 = \frac{1}{(2\,\pi)^2}\,\frac{\pi\,D_O^2}{\sigma_m\,\omega_O}\left(1-\cos(\vartheta_{\mathbf{k},\mathbf{k}'-\mathbf{k}}+\vartheta_{\mathbf{k}',\mathbf{k}'-\mathbf{k}})\right) \tag{1.27}$$

$$\left|G^{(TO)}(\mathbf{k}',\mathbf{k})\right|^2 = \frac{1}{(2\,\pi)^2}\,\frac{\pi\,D_O^2}{\sigma_m\,\omega_O}\left(1+\cos(\vartheta_{\mathbf{k},\mathbf{k}'-\mathbf{k}}+\vartheta_{\mathbf{k}',\mathbf{k}'-\mathbf{k}})\right) \tag{1.28}$$

$$\left|G^{(K)}(\mathbf{k}',\mathbf{k})\right|^2 = \frac{1}{(2\,\pi)^2}\,\frac{2\pi\,D_K^2}{\sigma_m\,\omega_K}\left(1-\cos\vartheta_{\mathbf{k},\mathbf{k}'}\right), \tag{1.29}$$

where D_O is the optical phonon coupling constant, ω_O the optical phonon frequency, D_K is the K phonon coupling constant and ω_K the K phonon frequency. The angles $\vartheta_{\mathbf{k},\mathbf{k}'-\mathbf{k}}$

Table 1.1 Physical parameters for the scattering rates.

σ_m	7.6×10^{-8} g/cm^2
v_F	10^6 m/s
v_p	2×10^4 m/s
D_{ac}	6.8 eV
$\hbar\omega_O$	164.6 meV
D_O	10^9 eV/cm
$\hbar\omega_K$	124 meV
D_K	3.5×10^8 eV/cm

and $\vartheta_{\mathbf{k}',\mathbf{k}'-\mathbf{k}}$ denote the convex angles between $\mathbf{k}$ and $\mathbf{k}'-\mathbf{k}$ and between $\mathbf{k}'$ and $\mathbf{k}'-\mathbf{k}$, respectively.

In the literature there are several values for the coupling constants entering the collision terms. For example for the acoustic deformation potential one can find values ranging from 2.6 eV to 29 eV. A similar degree of uncertainty is found for the optical and K phonon coupling constants as well. In our numerical simulations of monolayer graphene, the parameters proposed in [8, 17] have been adopted. They are reported in Table 1.1.

Regarding the optical and K phonons we will assume the Einstein approximation: $\hbar\omega_\eta$ is constant, $\eta = LO, TO, K$. Instead, for the acoustic phonon the Debye approximation will be assumed, $\hbar\omega_{ac} = \hbar v_s q$ with v_s the sound speed in graphene, and the Brillouin zone will be consistently extended to $\mathbb{R}^2$. For an accurate description of phonon dispersion relations and thermal conductivity in graphene, we refer the interested reader to [68, 69].

The transition rate (collision frequency) associated to the Ath type of scattering mechanism is defined as

$$\Gamma_A(\mathbf{k}) = \int S_A(\mathbf{k},\mathbf{k}')\, d\mathbf{k}' \,. \tag{1.30}$$

We introduce the polar coordinates (ε,θ); taking into account the dispersion relation (1.23), we have

$$\mathbf{k} = (k_x, k_y) \longmapsto \frac{\varepsilon}{\hbar v_F}(\cos\theta, \sin\theta) \,, \tag{1.31}$$

$$d\mathbf{k} = k\, dk\, d\theta = \frac{\varepsilon}{(\hbar v_F)^2}\, d\varepsilon\, d\theta \,, \tag{1.32}$$

with $\varepsilon \in [0,+\infty)$ and $\theta \in [0,2\pi]$. We set $\theta = \vartheta_{\mathbf{k},\mathbf{k}'}$ and solve the difficulty arising from the angular terms of scattering rates for optical phonons by using the following result [44]

$$\cos(\vartheta_{\mathbf{k},\mathbf{k}'-\mathbf{k}} + \vartheta_{\mathbf{k}',\mathbf{k}'-\mathbf{k}}) = \frac{(\varepsilon^2+\varepsilon'^2)\cos\theta - 2\varepsilon\varepsilon'}{\varepsilon'^2 - 2\varepsilon\varepsilon'\cos\theta + \varepsilon^2} \,. \tag{1.33}$$

With the previous transformation of coordinates, skipping for the sake of simplicity the details of the integration, we can get the transition rates as function of energy alone, i.e $\Gamma_A(\mathbf{k}) = \Gamma_A(\varepsilon)$. For the acoustic phonon scattering we get

$$\Gamma_{ac}(\varepsilon) = \frac{D_{ac}^2 k_B T}{4\hbar^3 v_F^2 \sigma_m v_p^2} \varepsilon \,, \tag{1.34}$$

while for the total optical phonon scattering, given by the sum of the longitudinal and transversal contribution, we have

$$\Gamma_{op}(\varepsilon) = \frac{D_O^2}{\sigma_m \omega_O \hbar^2 v_F^2} \left[(\varepsilon - \hbar\omega_O) \left(n_{\mathbf{q}}^{(O)} + 1 \right) H(\varepsilon - \hbar\omega_O) + (\varepsilon + \hbar\omega_O) \, n_{\mathbf{q}}^{(O)} \right], \tag{1.35}$$

where the fact that the coupling constants are the same for both the longitudinal and the transversal optical phonons has been used. In Eq. (1.35) H is the Heaviside function and $n_{\mathbf{q}}^{(O)}$ the equilibrium optical phonon distribution as given by Eq. (1.25). The expression of the transition rate for the K phonon scattering is the same as for the optical phonon

$$\Gamma_K(\varepsilon) = \frac{D_K^2}{\sigma_m \omega_K \hbar^2 v_F^2} \left[(\varepsilon - \hbar\omega_K) \left(n_{\mathbf{q}}^{(K)} + 1 \right) H(\varepsilon - \hbar\omega_K) + (\varepsilon + \hbar\omega_K) \, n_{\mathbf{q}}^{(K)} \right]. \tag{1.36}$$

Above $n_{\mathbf{q}}^{(K)}$ is the equilibrium K phonon distribution. In Fig.1.5 the scattering rates for each type of phonons are shown.

A review of the properties of the transport equations in semiconductors can be found in [18]. Most part of the results are valid only for regularized collision operators. The existence and uniqueness of the solution, without any regularization of the collisional kernel, have been proved for the homogeneous semiconductor Boltzmann equations, in the case of zero electric field in [19, 20], where it has also been shown that $0 \leq f \leq 1$ provided that such a condition is satisfied by the initial data. The general situation is still an open problem.

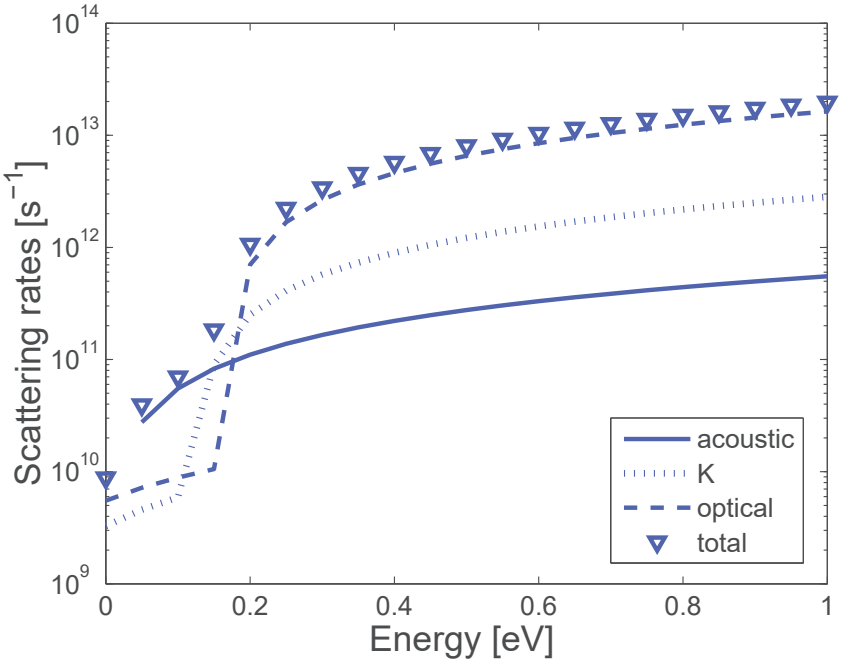

Fig. 1.5 Scattering rates.

Chapter 2

A new Direct Simulation Monte Carlo Method to properly take into account the Pauli exclusion principle

2.1 The standard Monte Carlo Method

The Monte Carlo method is based on the use of random numbers and can be used for solving both stochastic and deterministic problems, such as the evaluation of integrals and the solution of algebraic or integral equations. A classical example to understand how a statistical method can be used for the solution of a deterministic problem is the calculation of the number π, that is equivalent to the evaluation of the integral that gives the area of a circle of radius a. We can solve this problem by considering a square of side $2a$ with the circle inscribed and by generating pairs of random numbers (x, y), evenly distributed between $-a$ and a, to be used as coordinates of points inside the square. The expectation value of the fraction f of the points falling inside the circle is given by the ration between the area of the circle, πa^2, and that of the square, a^2, i.e. the expectation value is equal to π. Thus, practically, π can be evaluated by means of the ration between the number of points falling inside the circle and the total number of points used. Clearly, one obtains a result even more exact when the number of points is increased. This is one of the most typical feature of the Monte Carlo method, i.e. the dependence from the statistical sample. The Monte Carlo method has been used from remote times, already in 1777 by the French Encyclopedist Georges-Louis Leclerc, Compte de Buffon, and by Laplace. The official birth with this name, due to the Monte Carlo casino where roulettes generate random numbers, is due to the work of the Los Alamos group for the development of nuclear weapons, in particular the paper "The Monte

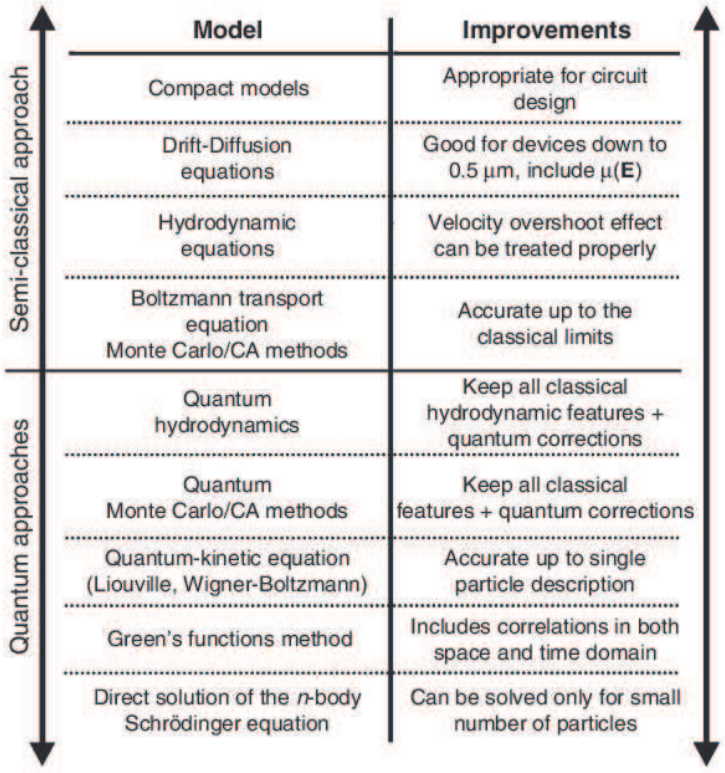

Fig. 2.1 Hierarchy of transport models.

Carlo method" by Metropolis and Ulam in 1949 [9]. Thereafter [10–13, 29, 14], the MC method had a wide range of applicability and became a standard method for the solution of transport problems, as a very effective method to solve the Boltzmann Transport Equation. The MC methos is very flexible due to the possibility of adapting its statistical nature both for the solution of deterministic problems and of intrinsically statistical ones; in this latter case, it can be considered as a *Direct Simulation* of the phenomenon. In this way, it is used for the solution of the BE for charge transport as a direct simulation of the dynamics of the particles inside the crystal. This property of MC method make us able to link directly with the physical situation under study and make it a very useful tool also as an *experimental technique*, i.e. we can simulate physical phenomena that cannot be analyzed experimentally, predict the properties of new materials and simulate the behaviour of electronic devices, without resorting to the very expensive industrial technique of the trial-and-error. The Monte Carlo method fits in the middle of a hierarchy of transport models, when the macroscopic ones, as Drift Diffusion or Hydrodynamical, fail and the quantum effects are not so strong to invalidate the approximations behind the semiclassical Boltzmann Equation itself; an illustration of such a hierarchy [15] is reported in Fig.2.1.

A first important classification is in

- one-particle Monte Carlo simulation;
- Ensemble Monte Carlo simulation (EMC).

In the first case, one simulates the motion of only one carrier and it is enough for a steady-state homogeneous phenomenon; actually, from ergodicity, one can assume that a path long enough of only a single carrier can give information on the behaviour of the entire gas of particles. The second method is necessary for time or space dependent phenomena, when for example it is important the effect of the transient dynamic response to an applied field; in this case, we have to independently simulate a large number of particles, according to an appropriate setting of initial conditions. Each particle in EMC is a super particle with a statistical weight representative of the sub-ensemble of real particles whose behaviour it describes. Usually, if N^* is the real number of electrons and N the number of the simulated particles, the statistical weight is equal to N^*/N. If the number of particles is large enough, the average value of a certain quantity, $\langle A(t)\rangle$ on this sample ensemble is very close to average one on the entire gas:

$$\langle A(t)\rangle = \frac{1}{N}\sum_i A_i(t). \tag{2.1}$$

Obviously, there is an error more little larger the number of particles is; the standard error is

$$s = \frac{\sigma}{\sqrt{N}}, \tag{2.2}$$

with σ^2 the variance that can be estimated as [21]

$$\sigma^2 \cong \frac{N}{N-1}\left[\frac{1}{N}\sum_{i=1}^{N} A_i^2 - \langle A\rangle^2\right]. \tag{2.3}$$

One follows each particle into a time window Δt, wherein the motion of each carrier is synchronized. The particle motion is constituted by a free flight, governed by the semiclassical equations of motion, interrupted by instantaneous random collision events, that change the energy and the momentum of the particle. Thus, the main steps of every Monte Carlo method, all based on the generation of random numbers, are the following:

- choose of the free flight duration;
- choose of the type of scattering event;
- determination of the new energy and momentum of the particle.

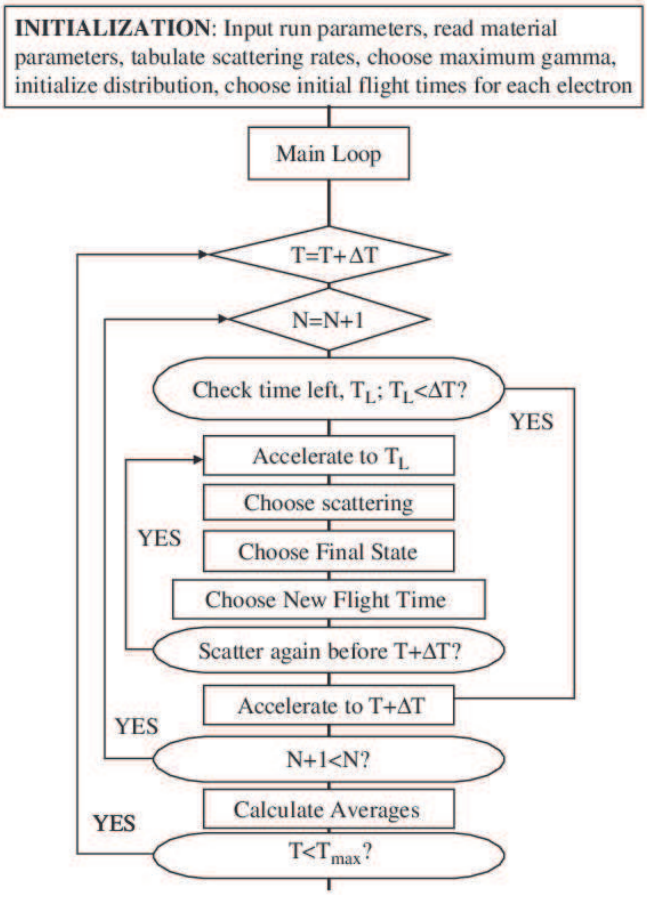

Fig. 2.2 Flow chart of a standard EMC simulation.

This procedure is continued for each particle until the time window Δt is reached, and then one can extract the average values of the quantities of interest, as the distribution function, the mean drift velocity, energy, etc. In Fig. 2.2 is reported a schematic fow chart of a typical standard EMC simulation.

The probability that an electron suffers a collision in the time t around dt is equal to $\Gamma(\mathbf{k}(t))$dt, where $\Gamma(\mathbf{k}(t))$ is the total scattering rate of an electron with wavevector $\mathbf{k}(t)$, given by the sum of the scattering rates due to each scattering mechanism, $\Gamma_A(\mathbf{k})$ or $\Gamma_A(\varepsilon)$, discussed in the previous chapter. Thus, the probability that an electron suffers a collision at time t around dt after a free flight of duration t is given by the joint probability

$$P(t)dt = \Gamma(\mathbf{k}(t))\exp\left\{-\int_0^t \Gamma(\mathbf{k}(t'))dt'\right\}dt. \tag{2.4}$$

Random free flight times t_r can be generated according to the probability density $P(t)$ by means of

$$r = \int_0^{t_r} P(t)dt \tag{2.5}$$

where r is a random number evenly distributed in the range $[0,1]$. By inserting (2.4) into (2.5), one obtains

$$r = 1 - \exp\left\{ -\int_0^{t_r} \Gamma(\mathbf{k}(t'))dt' \right\}. \tag{2.6}$$

Since r is statistically the same as $1-r$, from (2.6) we have the fundamental equation for the generation of random free flight times after each collision

$$-\ln r = \int_0^{t_r} \Gamma(\mathbf{k}(t'))dt'. \tag{2.7}$$

It could be very difficult and computational expensive to solve the previous equation due to the analytical form of $\Gamma(\mathbf{k}(t))$. A standard way to overcome such a difficulty is to introduce a fictitious scattering [23, 24], the so-called *self-scattering*, whose scattering rate varies in order to ensure that the total scattering rate Γ remains constant

$$\Gamma = \text{const} = \sum_A \Gamma_A(\mathbf{k}(t)) + \Gamma_{self}(\mathbf{k}(t)). \tag{2.8}$$

The self-scattering does not introduce any change in the energy and momentum of the particles, that will begin the next free flight starting from the same state before the self-sattering event. Hence, Eq. (2.7) becomes

$$t_r = -\frac{1}{\Gamma}\ln r. \tag{2.9}$$

Γ must be chosen in such a way that it is always greater than the real maximum one during all the simulation. It can be fixed at the beginning of the simulation (constant gamma method) or, in a more computationally efficient way, at each time step [16]. In order to select the scattering mechanism that interrupts the free flight, one generates a random number r, uniformly distributed between 0 and 1, and compares the number $r\Gamma$ with the successive sums of the Ath scattering rates, $\sum_A \Gamma_A$. One selects the mechanism that makes the sum greater than $r\Gamma$ (see Fig. 2.3).

After the scattering mechanism has been chosen, one has to update the values of energy and momentum of the particles. The new energy is easily recovered by considering that electrons and phonons exchange quanta of energy and that the energy remains unchanged if the scattering is (quasi)-elastic, as we will assume for acoustic phonons. Defining a spherical

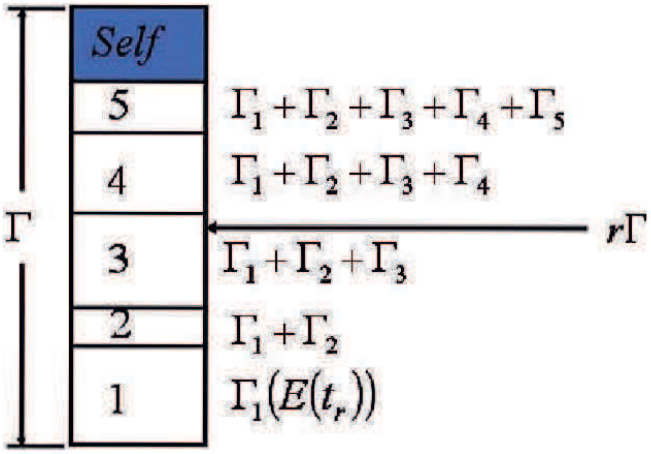

Fig. 2.3 Selection of the scattering mechanism terminating the free flight.

coordinate system around the initial wavevector $\mathbf{k}$, the final wavevector is given by $|\mathbf{k}'|$, that one calculates by means of energy, and, in the general 3D case, by the azimuthal and polar angles, ϕ and θ respectively. In general, ϕ can be chosen in a isotropic way, as $\phi = 2\pi r$, and θ according to the angular dependence of the scattering rate arising from the expression of $\Gamma_A(\mathbf{k})$. In principle, one can use the probability to scatter into a certain angle $P(\theta)d\theta$ and an uniformly distributed random number r according to (2.5). If $P(\theta)$ cannot easily be integrated, Eq. (2.5) can be treated by using a standard rejection technique [29, 30].

2.1.1 Degeneracy effects

Degeneracy effects arise when the particles concentration is high; in this case, we cannot neglect the Pauli exclusion principle and the term $(1-f(\mathbf{k}'))$, representing the availability of the final state $\mathbf{k}'$, has to be taken into account in the determination of the scattering rate $\Gamma(\mathbf{k})$. This is a hard task in EMC simulation because, when we have to determine the scattering rate, we do not know the exact final state $\mathbf{k}'$ that will be reached after the collision.

A standard way to overcome such a difficulty, as it was developed by Bosi and Jacoboni [27] for one-particle Monte Carlo and by Lugli and Ferry [28] for EMC, is to calculate the scattering rates without the term $(1-f(\mathbf{k}'))$, to select the final state and then to add a control on the final state availability. A random number r, uniformly distributed between 0 and 1, is generated and a rejection technique is used to check the final state. If r is greater than $f(\mathbf{k}')$ the scattering is accepted, energy and momentum of particles changed, otherwise it is treated as a self-scattering without any change in energy and momentum. We remind that $0 \leq f \leq 1$.

The improvements in results showed how much important the degeneracy effects are, but the obtained distribution function can exceed the maximum value 1, and this is an unphysical result that one should consider when the degeneracy effects are very effective.

It is indeed very important to include the Pauli exclusion principle in a correct way, in order to obtain correct distribution functions.
In the next section, we show the procedure we used to solve such a problem.

2.2 A new Direct Simulation Monte Carlo Method to properly take into account the Pauli exclusion principle

In [26], we developed a new algorithm for Direct Simulation Monte Carlo that properly takes into account the Pauli exclusion principle also in the degenerate case; we can also derive mean values of the charge energy and velocity more correct and stable in the case of high charge densities than those obtained with the traditional methods.
Direct Simulation Monte Carlo (DSMC) method has been intensively used in several fields of physical, life and social sciences. In particular a huge amount of literature is devoted to the simulations of charge transport in electron devices. The problem is well understood when the degeneracy effects are neglected. This is justified for low or moderate doping concentration, as it happens in many cases of electron device design. In the case of high charge concentrations, in the collision terms the occupation probability of the final state cannot be approximated as equal to one and this fact must be included in the selection of the final state after a scattering event.

A first way to deal with the degeneracy effects in bulk semiconductors was proposed in a pioneering work in [27]. An extension to a more general case was devised in [28] and has become the standard approach. However, due to round-off errors, the reconstruction of the occupation number can exceed the unit, see for example [31]. In several applications this effect is not so relevant because the mean values are still accurate but, from a theoretical point of view, it needs an improvement if we require a good estimation of the occupation number. Moreover, a treatment of the degeneracy effects, which is not accurate enough, might alter the evaluation of the scattering rate and the availability of the final states. In order to improve the approach of [28], an ad hoc scattering-out term has been added in [31, 32], while in [33, 34] ad hoc approximations of the distribution function have been proposed for the evaluation of the degeneracy effects.

We use a hybrid DSMC simulation strategy that guarantees correct occupation numbers maintaining a computational cost comparable with that of the standard DSMC approach. In

order to validate the proposed DSMC strategy, the electron transport equation is also solved by means of a numerical scheme based on the discontinuous Galerkin (DG) method. This method has been already successfully applied to more conventional semiconductor materials, like silicon [42, 43], and therefore represents a valid approach to test and compare different techniques. It will be performed a comparison of the results obtained both with DSMC and DG methods furnishing a cross-validation of the two approaches and confirming the validity of the proposed DSMC algorithm.

We consider at first the homogeneous case. In a homogeneous suspended monolayer graphene, the Boltzmann equation in the generic K valley reduces to

$$\frac{\partial f(\mathrm{t},\mathbf{k})}{\partial \mathrm{t}} - \frac{e}{\hbar}\mathbf{E}\cdot\nabla_{\mathbf{k}} f(t,\mathbf{k}) = \int S(\mathbf{k}',\mathbf{k})\, f(t,\mathbf{k}')\,(1-f(t,\mathbf{k}))\, d\mathbf{k}' - \int S(\mathbf{k},\mathbf{k}')\, f(t,\mathbf{k})\,\big(1-f(t,\mathbf{k}')\big)\, d\mathbf{k}'\,. \tag{2.10}$$

A similar equation holds for the K' valley.
The $\mathbf{k}$-space is approximated by the set $[-k_{xmax},k_{xmax}]\times[-k_{ymax},k_{ymax}]$ with k_{xmax} and k_{ymax} such that the number of electrons with a wave-vector $\mathbf{k}$ outside such a set is practically negligible. The $\mathbf{k}$-space is partitioned into a uniform rectangular grid. We shall denote by C_{ij} the generic cell of the grid centered at the $\mathbf{k}_{ij}$ wave-vector.
The distribution function is approximated with a piecewise constant function in each cell. Initially, the n_P particles used for the simulation are distributed in each cell according to the equilibrium Fermi-Dirac distribution:

$$f(0,\mathbf{k}) = \frac{1}{1+\exp\left(\dfrac{\varepsilon(\mathbf{k})-\varepsilon_F}{k_B T}\right)}\,,$$

where $T = 300$ K, and ε_F is the Fermi energy, which is related to the initial charge density by

$$\rho(0) = \frac{2}{(2\pi)^2}\int f(0,\mathbf{k})\, d\mathbf{k}\,. \tag{2.11}$$

Note that in the unipolar case, when only one band is considered, ρ remains constant, $\rho(t)=\rho(0)$, as consequence of charge conservation. The motion of each particle alternates free-flight and scattering. The latter is the most involved and delicate part and in graphene it is particularly important to include the Pauli principle. This implies a heavy computational cost and, more importantly, requires a continuous update of the distribution function.

In the standard approach the free-flight is performed according to the semiclassical equation of motion

$$\hbar\dot{\mathbf{k}} = -e\,\mathbf{E}\,. \tag{2.12}$$

$\mathbf{E}$ will be considered as a constant external field. Therefore, in a free-flight time Δt one has a variation of momentum given by

$$\hbar\Delta\mathbf{k} = -e\,\mathbf{E}\,\Delta t\,.$$

The time interval Δt is chosen for each particle in a random way by

$$\Delta t = -\frac{\ln\xi}{\Gamma_{tot}}\,, \tag{2.13}$$

ξ being a random number with uniform distribution in the interval $[0,1]$ and Γ_{tot} being the total scattering rate (see for example [29])

$$\Gamma_{tot} = \Gamma_{ac} + \Gamma_{op} + \Gamma_K + \Gamma_{ss}\,.$$

Γ_{ss}, called *self-scattering rate*, is the scattering rate associated to a fictitious scattering that does not change the state of the electron. It is introduced so that Γ_{tot} is constant leading to the simple relation (2.13). To fix the value of Γ_{tot} one considers the range of the energy involved in the simulation and takes the maximum value Γ_M of the sum $\Gamma_{ac}+\Gamma_{op}+\Gamma_K$. Γ_{tot} is then $\alpha\Gamma_M$ with $\alpha > 1$ a tuning parameter.

The main drawback is that the range of Γ_{ac}, Γ_{op}, Γ_K can be very large resulting in a huge amount of self-scatterings with a consequent high computational cost. In the range of energy we encounter in the simulations, the scattering rates can vary by two orders of magnitude as shown in Fig. 1.5. Therefore it is evident that the use of a constant total scattering rate could be too expensive from a computational point of view. A good variant is to use a variable Γ_{tot} which depends on the energy $\varepsilon(t)$ of the considered particle at the current time t

$$\Gamma_{tot} = \alpha\left[\Gamma_{ac}(\varepsilon(t)) + \Gamma_{op}(\varepsilon(t)) + \Gamma_K(\varepsilon(t))\right].$$

We will use this procedure and set $\alpha = 1.1$ in our simulations.

The scattering rates are given by equations (1.34), (1.35), (1.36) of the previous chapter, that we rewrite for convenience of reading:

$$\Gamma_{ac}(\varepsilon) = \frac{D_{ac}^2\,k_B\,T}{4\hbar^3\,v_F^2\,\sigma_m\,v_p^2}\,\varepsilon,$$

$$\Gamma_{op}(\varepsilon) = \frac{D_O^2}{\sigma_m\,\omega_O \hbar^2\, v_F^2}\left[(\varepsilon-\hbar\,\omega_O)\left(n_{\mathbf{q}}^{(O)}+1\right)H(\varepsilon-\hbar\,\omega_O)+(\varepsilon+\hbar\,\omega_O)\,n_{\mathbf{q}}^{(O)}\right],$$

$$\Gamma_K(\varepsilon) = \frac{D_K^2}{\sigma_m\,\omega_K \hbar^2\, v_F^2}\left[(\varepsilon-\hbar\,\omega_K)\left(n_{\mathbf{q}}^{(K)}+1\right)H(\varepsilon-\hbar\,\omega_K)+(\varepsilon+\hbar\,\omega_K)\,n_{\mathbf{q}}^{(K)}\right].$$

After the free-flight, the scattering is randomly selected according to the values of the transition rates and the Pauli exclusion principle is taken into account as in [28]. Once the state after the scattering has been determined, let us denote by $\mathbf{k}'$ its wave-vector, the initial state is changed or left the same with a rejection technique: a random number ξ is generated and if $\xi < 1 - f(\mathbf{k}')$ the transition is accepted otherwise rejected.

At fixed times the momentum, velocity, energy of each electron are recorded and the mean values are evaluated along with the distribution of electrons among the cells in the $\mathbf{k}$-space in order to follow the time evolution of the system.

The maximum number n_{ij}^* of simulated particles can be accommodate in each cell is easily evaluated (see [28]). Let N_{ij} be the number of real particles in the cell C_{ij} and let n_{ij} be the number of simulated particles in the same cell. By observing that N/n_P is the statistical weight of each simulated particle and taking into account the condition $0 \le f \le 1$, one has

$$\begin{aligned} n_{ij} &= \frac{N_{ij}}{N} n_P = \frac{n_P}{N}\frac{2}{(2\pi)^2} A \int_{C_{ij}} f\, d\,\mathbf{k} \le \frac{n_P}{N}\frac{2}{(2\pi)^2} A \int_{C_{ij}} d\,\mathbf{k} \\ &= \frac{2}{(2\pi)^2}\mathrm{meas}(C_{ij})\frac{n_P}{N}A = \frac{2}{(2\pi)^2}\mathrm{meas}(C_{ij})\frac{n_P}{\rho} = n_{ij}^*\,, \end{aligned} \tag{2.14}$$

where A is the area of the sample, N is the number of real particles in the sample, $N = \rho A$, and $\mathrm{meas}(C_{ij})$ is the measure of the cell C_{ij}. Of course n_{ij}^* is not in general an integer, therefore rounding errors are introduced. Usually, the problem is solved by using a number of particles n_P great enough to make negligible such errors. The convergence of the procedure is otften checked just by comparing the results with different n_P.

The main concern with the procedure delineated above is that, according to the semi-classical approximation, the compatibility with Pauli's principle of the positions occupied during the free flight is not checked. *It may occur that the particle at the end of the free-flight reaches a cell in the* $\mathbf{k}$*-space already fully occupied making the occupation number greater than the maximum one* (see Fig. 2.4).

For high values of the Fermi energy the maximum occupation number can greatly exceed the maximum one. This is of course unphysical, although the average quantities could be

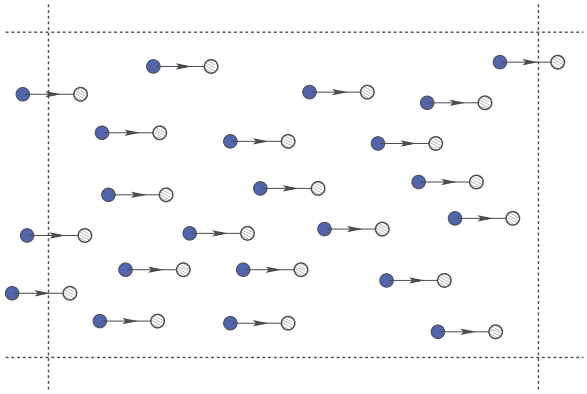

Fig. 2.4 Dynamics of the simulated particles in given cells of the **k**-space. Under the action of the electric field the wave-vector changes and it may happen that some particles enter in an adjacent cell. If the number of entering particles is sufficiently higher than that of the exiting ones, the maximum occupation number can be exceeded since during the free-flight no control on Pauli's principle is performed.

acceptable according to the large number law. Even if the scattering can redistribute the particles among the cells, in general it is not able to eliminate the presence of anomalous occupation numbers.

We have implemented the standard DSMC procedure and evaluated the distribution function at steady state, approximately after about 5 ps. In Fig. 2.5 the distribution function is plotted for an electric field $E = 10$ kV/cm and a Fermi energy equal to 0.4 eV. A violation of Pauli's exclusion principle is evident. In Fig. 2.6 the case with $E = 1$ kV/cm and a Fermi energy equal to 0.3 eV has been considered. Although we have a smaller density, and therefore the degeneracy effects could be less relevant, again a violation of Pauli's principle is observed. When the Fermi level is increased, the maximum occupation number, as expected, increases as Fig. 2.7 clearly shows.

In [39] it has been proposed for overcoming the problem to apply the rejection technique not only to the scattering event but also at the end of each free-flight. However, even implementing this variant, the same drawbacks are still present and also the mean values can change, as shown later.

In order to avoid such a difficulty we propose the following approach.

The crucial point in the previous procedure is the step concerning the free-flight. If we go back to the original transport equation, we can use a splitting scheme to avoid unphysical results. The basic idea is to reformulate the splitting method in terms of a particle method.

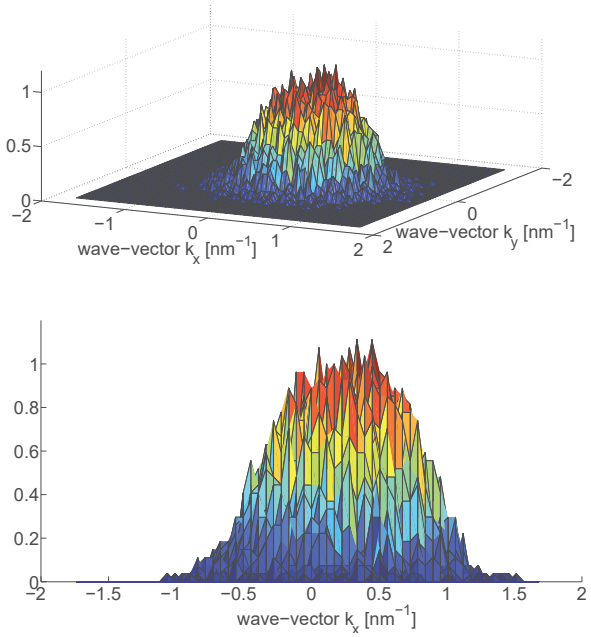

Fig. 2.5 Steady-state distribution function and its longitudinal view in the case of an applied electric field of 10 kV/cm and a Fermi level equal to 0.4 eV by adopting the standard DSMC. Note that the maximum value exceeds one.

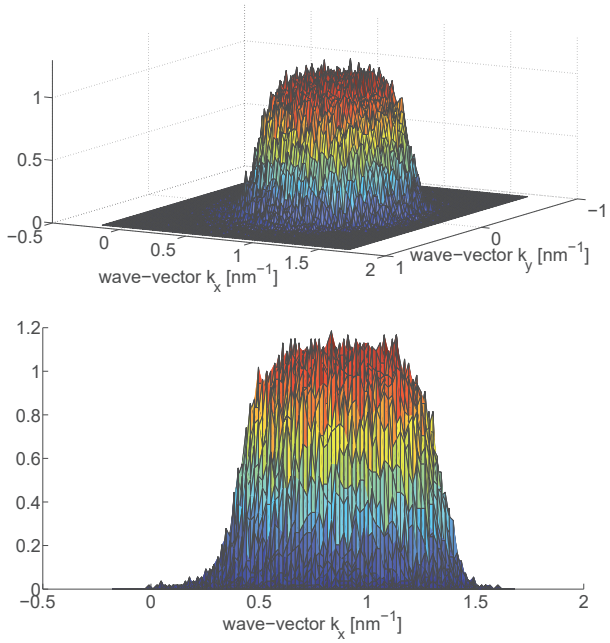

Fig. 2.6 Steady-state distribution function and its longitudinal view in the case of an applied electric field of 1 kV/cm and a Fermi level equal to 0.3 eV by adopting the standard DSMC. Although we have a smaller density, again a violation of Pauli's principle is observed.

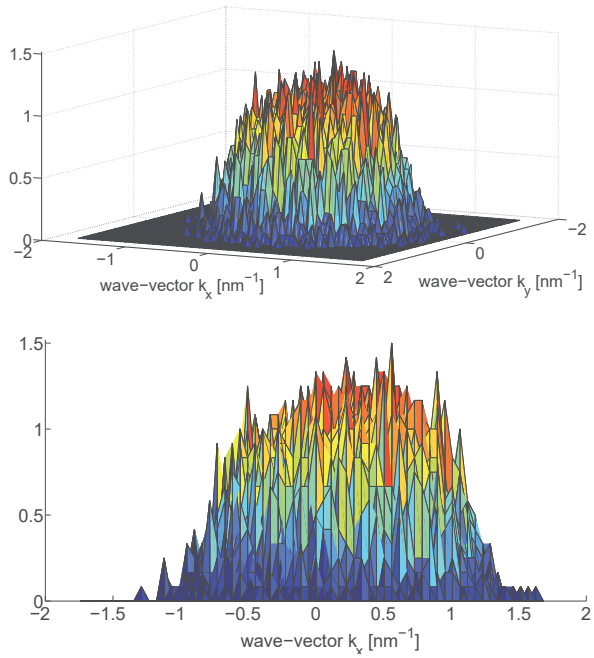

Fig. 2.7 Steady-state distribution function and its longitudinal view in the case of an applied electric field of 10 kV/cm and a Fermi level equal to 0.6 eV by adopting the standard DSMC.

In a time interval Δt, first we solve the drift part of the equation corresponding to the free-flight in the analogous DSMC approach,

$$\frac{\partial f(t,\mathbf{k})}{\partial t} - \frac{e}{\hbar}\mathbf{E}\cdot\nabla_{\mathbf{k}} f(t,\mathbf{k}) = 0\,, \tag{2.15}$$

taking as initial condition the distribution at time t, and then the collision part

$$\frac{\partial f(t,\mathbf{k})}{\partial t} = \frac{df}{dt}(t,\mathbf{k})\bigg|_{e-ph}\,, \tag{2.16}$$

taking as initial condition the solution of Eq. (2.15). The global procedure gives a numerical approximation of $f(t+\Delta t,\mathbf{x},\mathbf{k})$ up to first order in Δt. The solution of Eq. (2.15) is just a *rigid* translation of the distribution function as a whole along the characteristics and can be reformulated from a particle point of view as a free-flight of the same duration for each electron. In this way the cells in the $\mathbf{k}$-space are moved with the displacement vector $\hbar\Delta\mathbf{k} = -e\mathbf{E}\Delta t$ but without changing the occupation number of the cells themselves. To avoid considering a too large computational domain, instead of moving the cells we adopt a Lagrangian approach and move the grid, adapting it to the new position of the cells.

Eq. (2.16) is solved by considering a sequence of collision steps for each particle during the time interval $[t, t+\Delta t]$ in a standard way: choice of the scattering, including also the self one, and selection of the final state. Since the collision mechanisms take into account the Pauli principle, the occupation number cannot exceed the maximum occupation number in this second step as well. Hence, neither the drift nor the collision step give rise to the possibility of having more particles in a single cell greater than the maximum occupation number.

In a schematic way, the algorithm we propose is summarized in the following steps.

1. Let us consider a uniform temporal grid $t_1 = \Delta t$, $t_1 = 2\Delta t$, $\cdots$, $t_r = r\Delta t$, $\cdots$.

2. Let f_{ij}^r be the piecewise constant approximation of the distribution function in C_{ij} at the rth time step.

3. For each particle we update the momentum

$$\hbar\mathbf{k}(t_{r+1}) = \hbar\mathbf{k}(t_r) - e\,\mathbf{E}\,\Delta t \tag{2.17}$$

   and then we move in the same way the center (k_i^c, k_j^c) of each C_{ij} so that the relative positions of the electrons with respect to the grid remain unchanged.

4. For a time interval Δt we consider for each particle only scattering events selected in the standard way. After the scattering of each particle, the occupation numbers of the cells involved in the collision, both the initial state and the final state, are updated.

The overall scheme is a hybrid approach which furnishes a first order in time approximation of the distribution function.
Average quantities can be evaluated as well by taking the mean values of the quantities of interest, e.g. velocity and energy.

The main difference between the standard and the new DSMC approach is schematically summarized in Figs. 2.8 and 2.9.

Remark 1 *The previous procedure consists of a splitting of the Boltzmann equation into two parts; one represents the effect of the Liouvillian differential operator through a rigid motion of the distribution function as a whole over the phase-space trajectories; the other, scattering part, takes into account the re-distribution of electrons due to the collisions. Thus, this procedure respects the intrinsic nature of the Boltzmann equation and in particular the role of the time. The l.h.s of the Boltzmann equation takes into account the time evolution while in the r.h.s the collisions are considered instantaneously, time is a frozen parameter. Is*

Fig. 2.8 The standard DSMC scheme.

Fix the time step Δt

```
for n=1 to the total number of electrons
      do{
            find the free flight time
            move the particle in k-space
            calculate f
            perform a scattering or a self-scattering
      } until the time step Δt is reached;
end loop
```

Repeat until the final time is reached.

Fig. 2.9 The new DSMC scheme.

Fix the time step Δt

step 1: Solve the simple equation

$$\frac{\partial f}{\partial t} - \frac{e}{\hbar}\mathbf{E} \cdot \nabla_{\mathbf{k}} f = 0$$

step 2: for n=1 to the total number of electrons
      do{
            calculate f
            perform a scattering or a self-scattering
      } until the time step Δt is reached;
end loop

Repeat until the final time is reached.

it a coincidence that a numerical solution which respects this double role of time also gives a right solution? In this way, the splitting, that allow us to respect the intrinsic nature of the Boltzmann equation also in the numerical procedure, seems to be not only a sufficient condition but also a necessary condition. I think that the problem is to be investigated deeper and that it could lead to useful suggestions, at least from a philosophical point of view, for example about the relationship between a physical phenomenon, its analytical model and the corresponding numerical approximations.

2.2.1 Numerical results and comparison between stochastic and deterministic solutions

In this section the results of simulating a monolayer graphene with different Fermi levels and electric fields are presented in order to check the validity of both the new DSMC simulation and the DG method by a cross-validation. Details about the Discontinuous Galerkin method are given in the following chapter.

The value of the Fermi level is chosen high enough for neglecting the inter-band interactions and hole dynamics. The lattice temperature is kept equal to 300 K.

For the numerical solution of the ODE system arising after applying the DG discretization, the TVD third order Runge-Kutta scheme has been used as in [51] with a time step which depends on the electric field. We remark that the overall numerical scheme guarantees charge conservation. In the Monte Carlo simulations a time step of 1 fs is used for the applied fields.

Regarding the computational costs, the execution time of the two approaches is comparable. On the average each simulation requires at most three minutes with a 2.3 GHz Intel Core i7 processor.

The DSMC calculations have been performed by discretizating the **k**-space with $\hbar k_{xmax} = \hbar k_{ymax} = 4$ eV·ps /μm and 641 $\times$ 641 cells when the electric fields are equal to 1, 2, 4 kV/cm. In the cases of applied fields equal to 10 and 20 kV/cm, we have set $\hbar k_{xmax} = \hbar k_{ymax} = 12$ eV·ps /μm but retaining the same number of cells.

In the simulations with the DG method, the **k**-space has been discretized with 9600 cells while the time step depends on the values of the electric fields. For the higher considered electric field, 20 kV/cm, we used a time step of 0.75 fs.

Firstly, the Fermi level is set equal to 0.4 eV and 10^4 particles are employed. In Fig.2.10 the distribution functions, obtained with the two approaches, are compared. Apart the good agreement, it is evident that the occupation probability never exceeds one and no violation of the Pauli exclusion principle appears with the new DSMC, in contrast with the results showed in Fig. 2.5.

eV	kV/cm	**V** (10^8 cm/s)	$\sigma_{mean\,velocity}$ (10^8 cm/s)	W (eV)	$\sigma_{mean\,energy}$ (eV)
0.40	1	0.1989	0.0022	0.2816	0.0004
0.40	2	0.2320	0.0022	0.2883	0.0004
0.40	4	0.2761	0.0021	0.3026	0.0004
0.40	10	0.3314	0.0021	0.3544	0.0005
0.40	20	0.3481	0.0021	0.4429	0.0007
0.60	1	0.1215	0.0022	0.4078	0.0005
0.60	2	0.1449	0.0022	0.4110	0.0005
0.60	4	0.1694	0.0022	0.4172	0.0005
0.60	10	0.2229	0.0022	0.4424	0.0006
0.60	20	0.2715	0.0022	0.5044	0.0007

Table 2.1 Estimation of the sample standard deviation for the steady state mean values of velocity and energy. In the first and the second columns the Fermi level and the electric field are reported.

In order to check the validity of the proposed approaches also for a higher density, we have performed simulations in the case of a Fermi level equal to 0.6 eV as well by using 10^5 particles. In Fig. 2.11 the solutions are plotted. The goodness of the agreement remains the same and again no violation of Pauli's exclusion principle is observed in contrast with Fig.2.7.

We have compared also the results of the average values of the electron velocity **V** and energy W. These quantities are defined as

$$\mathbf{V} = \frac{1}{\rho}\frac{2}{(2\pi)^2}\int \mathbf{v} f(t,\mathbf{k})\, d\mathbf{k}\,, \tag{2.18}$$

$$W = \frac{1}{\rho}\frac{2}{(2\pi)^2}\int \varepsilon f(t,\mathbf{k})\, d\mathbf{k}\,. \tag{2.19}$$

In Table 2.1 the standard deviation of the sample mean for energy and velocity, evaluated according to $\sigma_{mean} = \sigma/\sqrt{n_p - 1}$ with σ^2 denoting the variance of the energy or velocity of the electron population, are reported at the steady state showing a good statistical performance. Indeed the standard deviation is a small fraction of the mean value.

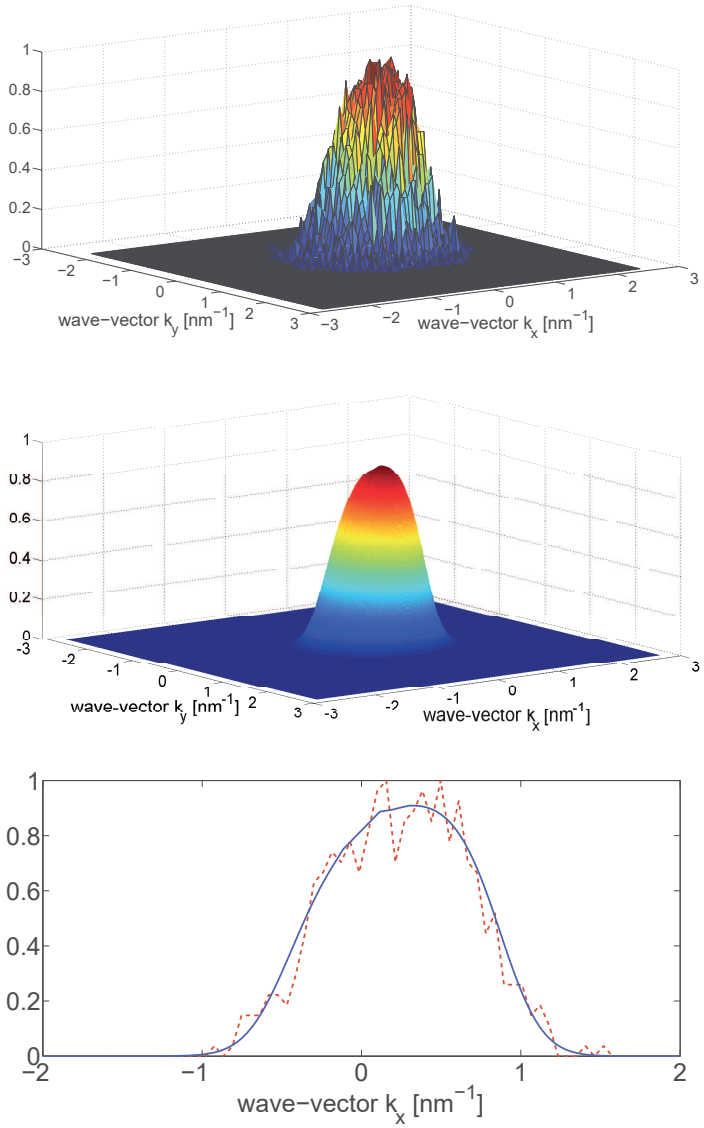

Fig. 2.10 Steady-state distribution function in the case of an applied electric field of 10 kV/cm and a Fermi level equal to 0.4 eV by adopting the new DSMC method and the DG method. Note that the maximum value does not exceed one. In the bottom figure the longitudinal section, $k_y = 0$, obtained with the DG (continuos line) and the DSMC (dashed line) methods is plotted.

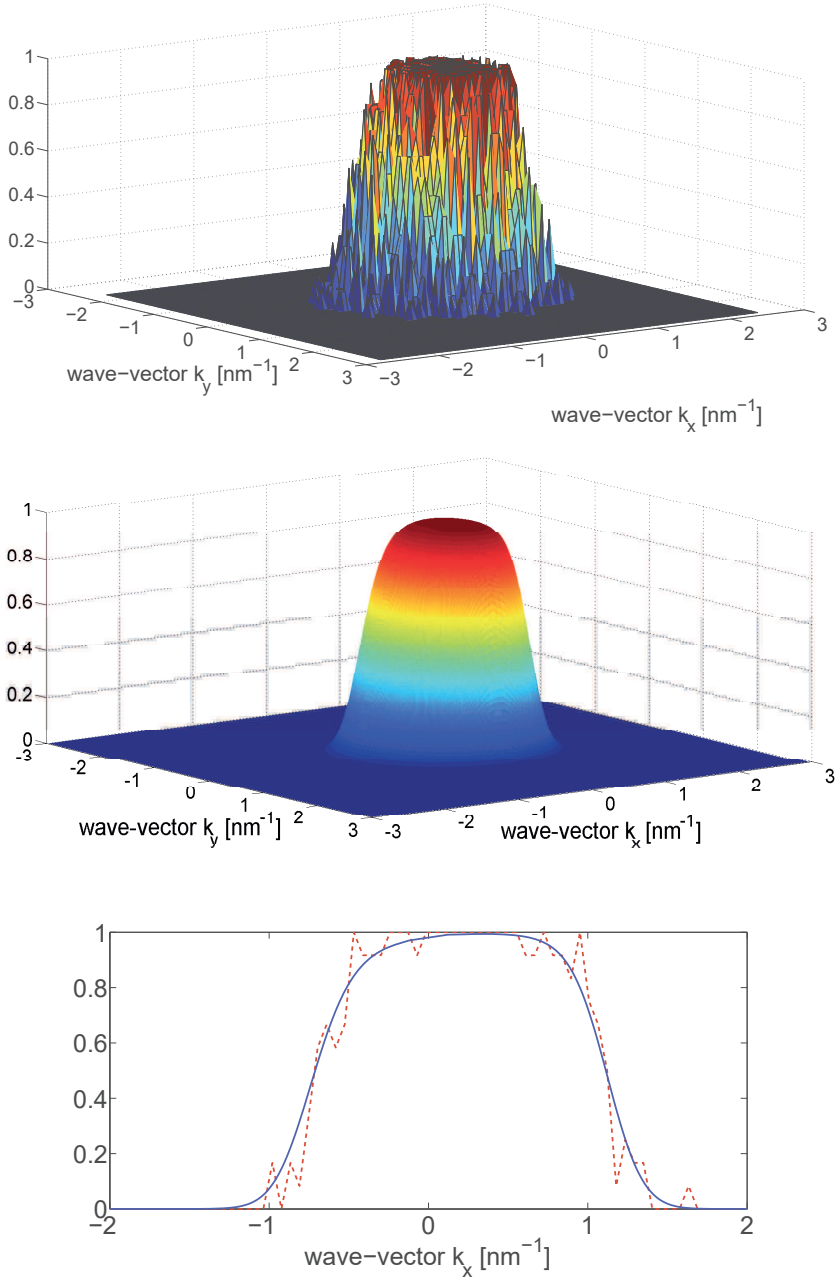

Fig. 2.11 Steady-state distribution function in the case of an applied electric field of 10 kV/cm and a Fermi level equal to 0.6 eV by adopting the new DSMC method and the DG method. In the bottom figure the longitudinal section, $k_y = 0$, obtained with the DG (continuos line) and the DSMC (dashed line) methods is plotted. Again no violation of Pauli's exclusion principle is observed.

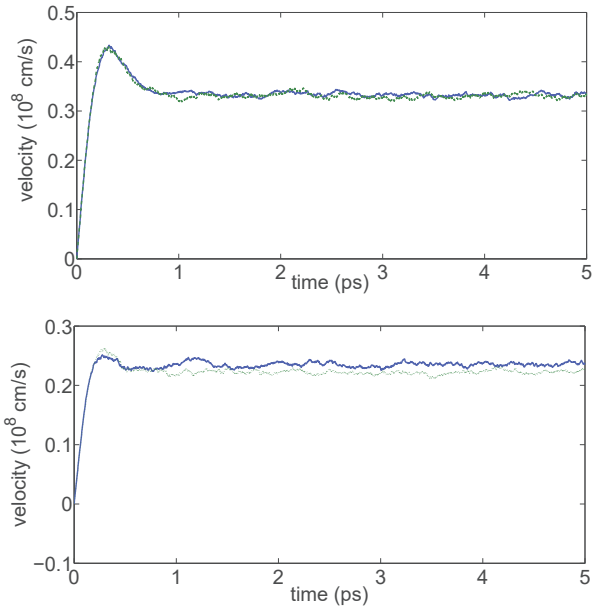

Fig. 2.12 Comparison of the average velocity versus time obtained with the standard DSMC (continuous line) and the new DSMC (dashed line) approaches in the case of an applied electric field of 10 kV/cm and a Fermi level equal to 0.4 eV (top) and 0.6 eV (bottom).

In Figs 2.12, 2.13, a comparison between the mean values obtained with the standard and the new DSMC approach is plotted. It is clear that evident differences arise at a higher Fermi energy, which is the case when the importance of the degeneracy effects increases.

In order to further investigate the accuracy of the new DSMC method, in Figs 2.14, 2.15, 2.16, 2.17 the results of the average values of the electron velocity and energy obtained with the DG method and the new DSMC method are compared.

There is an excellent agreement between the new DSMC and the DG methods in correspondence with the considered electric fields. Of course, DSMC presents some statistical noise which is more evident in correspondence of the overshoot but the discrepancy is very small.

In order to estimate the differences between the average quantities u_{MC} and u_{DG}, where u stands for velocity or energy, obtained by using the new DSMC and the DG methods respectively, we introduce the estimator

$$d_u = \frac{\max_t \{|u_{MC}(t) - u_{DG}(t)|\}}{\mathbb{E}\left[|u_{DG}(t)|\right]},$$

where $\mathbb{E}$ is the expectation value. The time t belongs to the interval $[0,5]$ (in ps). The results are reported in Table 2.2 and they clarify the overall agreement. Of course, to assess whether

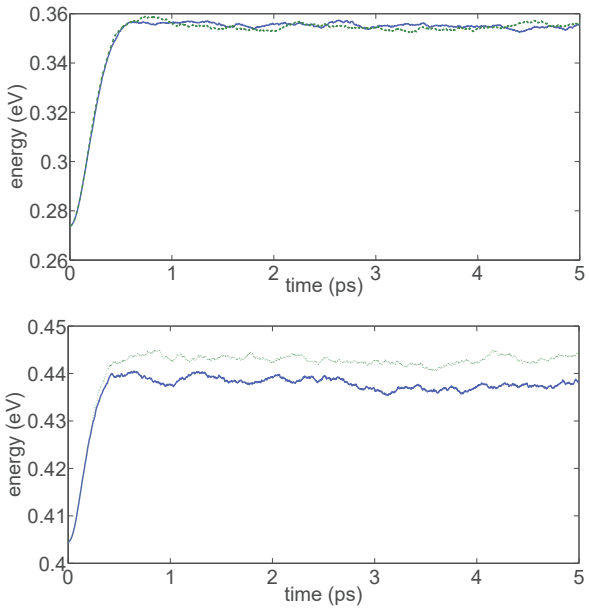

Fig. 2.13 Comparison of the average energy versus time obtained with the standard DSMC (continuous line) and the new DSMC (dashed line) approaches in the case of an applied electric field of 10 kV/cm and a Fermi level equal to 0.4 eV (top) and 0.6 eV (bottom).

the DSMC or the DG approach is more accurate is just a fictitious question because the differences of the results are within the measurement errors.

Finally, we want to stress that the numerical distribution obtained with the DG method is always positive. It is apparent that the used DG scheme preserves the positivity of the solution, supporting the validity of the theoretical results, proved in [40], also for the problem under consideration.

2.2.2 Failure of other approaches

In this section, we show other attempts to solve the problem of a proper inclusion of the Pauli exclusion principle. The method is the same as in the standard EMC simulation and the differences are in the treatment of the availability of the final state.

- Variant 1

In a similar way as in [39], a rejection technique is used not only for the scattering events but also for the final state after the free flight. In this way, the free flight trajectories are treated not in a really semiclassical picture. Only if the state after the free flight is accepted,

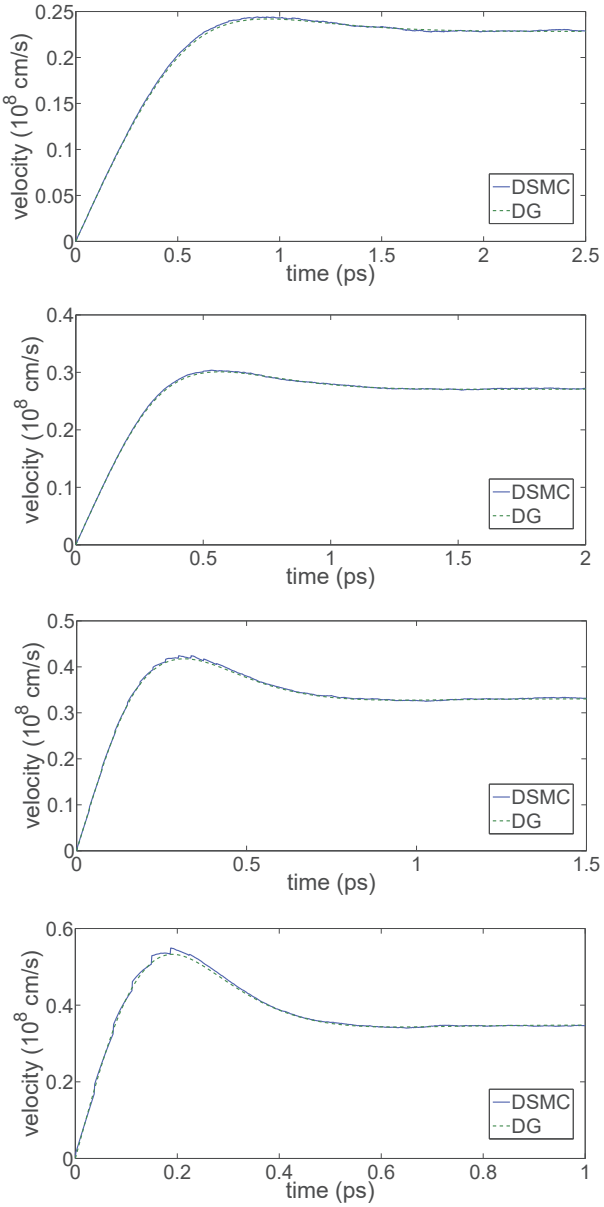

Fig. 2.14 Comparison of the average velocity versus time obtained with the new DSMC and the DG method in the case of an applied electric field of 2 kV/cm, 4 kV/cm, 10 kV/cm, 20 kV/cm and a Fermi level equal to 0.4 eV.

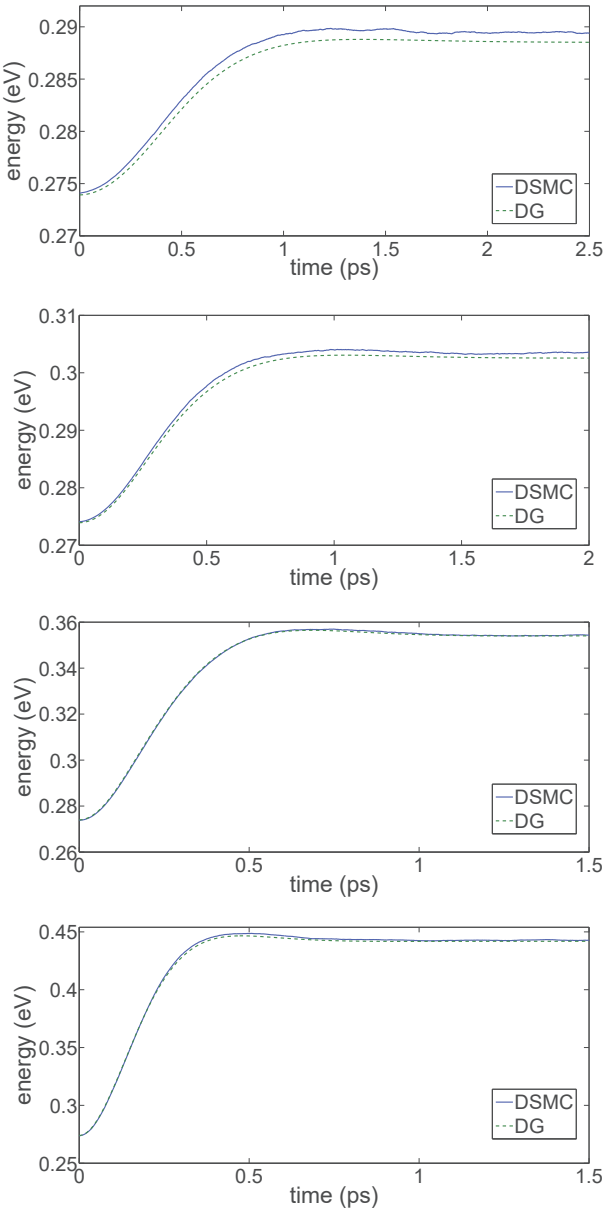

Fig. 2.15 Comparison of the average energy versus time obtained with the new DSMC and the DG method in the case of an applied electric field of 2 kV/cm, 4 kV/cm, 10 kV/cm, 20 kV/cm and a Fermi level equal to 0.4 eV.

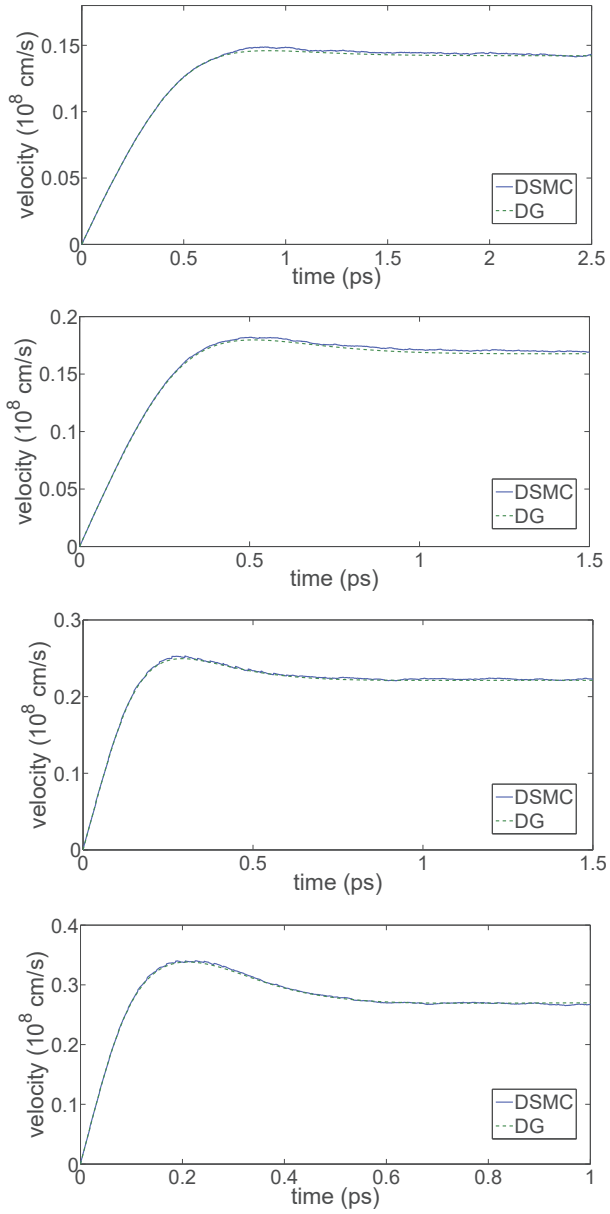

Fig. 2.16 Comparison of the average velocity versus time obtained with the new DSMC and the DG method in the case of an applied electric field of 2 kV/cm, 4 kV/cm, 10 kV/cm, 20 kV/cm and a Fermi level equal to 0.6 eV.

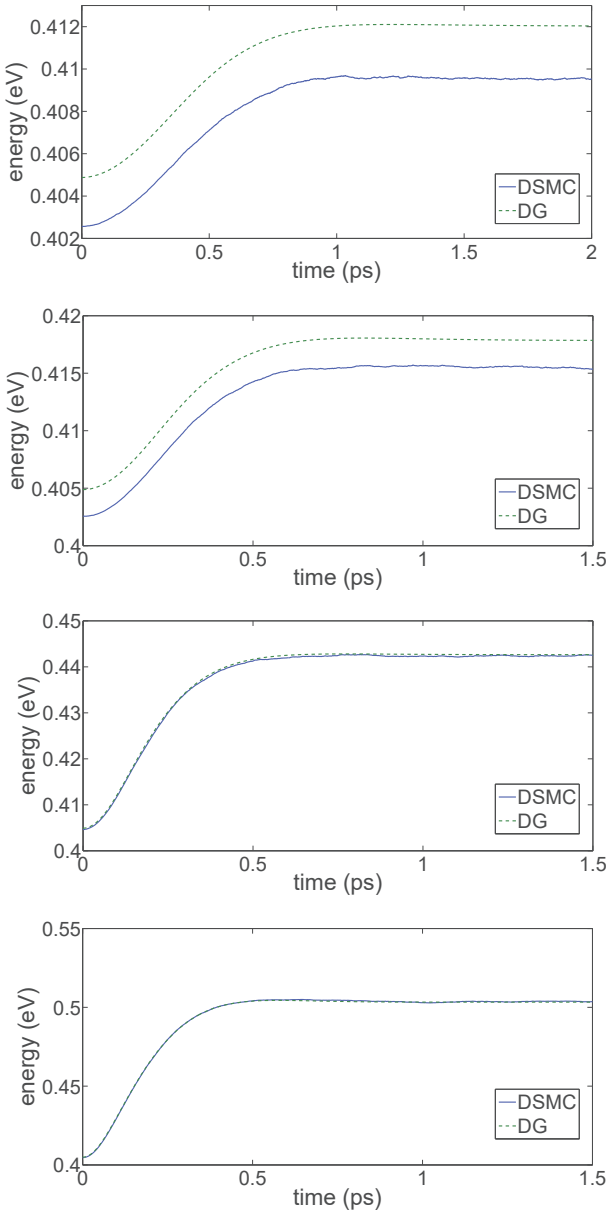

Fig. 2.17 Comparison of the average energy versus time obtained with the new DSMC and the DG method in the case of an applied electric field of 2 kV/cm, 4 kV/cm, 10 kV/cm, 20 kV/cm and a Fermi level equal to 0.6 eV.

eV	kV/cm	$d_{velocity}$	d_{energy}
0.40	1	0.015631	0.003603
0.40	2	0.013698	0.003849
0.40	4	0.013873	0.004049
0.40	10	0.022464	0.004015
0.40	20	0.046947	0.005564

eV	kV/cm	$d_{velocity}$	d_{energy}
0.60	1	0.027146	0.006616
0.60	2	0.024401	0.006717
0.60	4	0.027201	0.006411
0.60	10	0.021336	0.001423
0.60	20	0.016653	0.003023

Table 2.2 Estimation of the differences of the results obtained with the DMSC and the DG methods. In the first and the second columns the Fermi level and the electric field are reported.

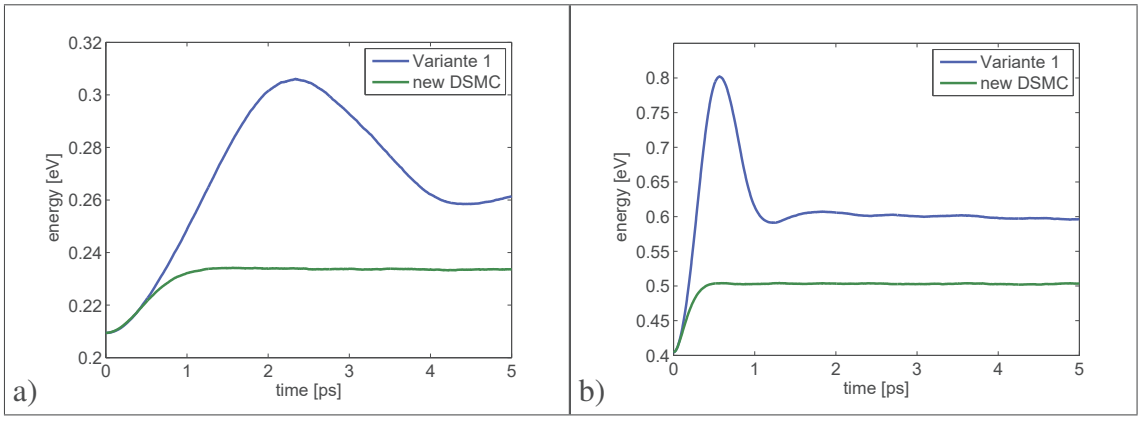

Fig. 2.18 Comparison of the average energy versus time obtained with the variant 1 and the new DSMC when $E = 2$ kV/cm and $\varepsilon_F = 0.3$ eV a), and when $E = 20$ kV/cm and $\varepsilon_F = 0.6$ eV b).

one considers the scattering events; if the final state after the scattering is accepted, as in a standard way, one changes the electron energy and momentum, otherwise it is treated as a self scattering. In both cases, the time is updated from t to $t + dt$, dt being the free flight duration. If the final state after the free flight is not accepted, nothing happens and one only updates the time. In Figs 2.18, 2.19, the mean values of energy and velocity are reported.There is a great disagreement with the results of the new DSMC, mainly in the transient overshoot. The obtained distribution functions could have values exceeding the maximum ones, even if less than the standard procedure, and they present also negative unphysical values, as shown in Fig.2.20.

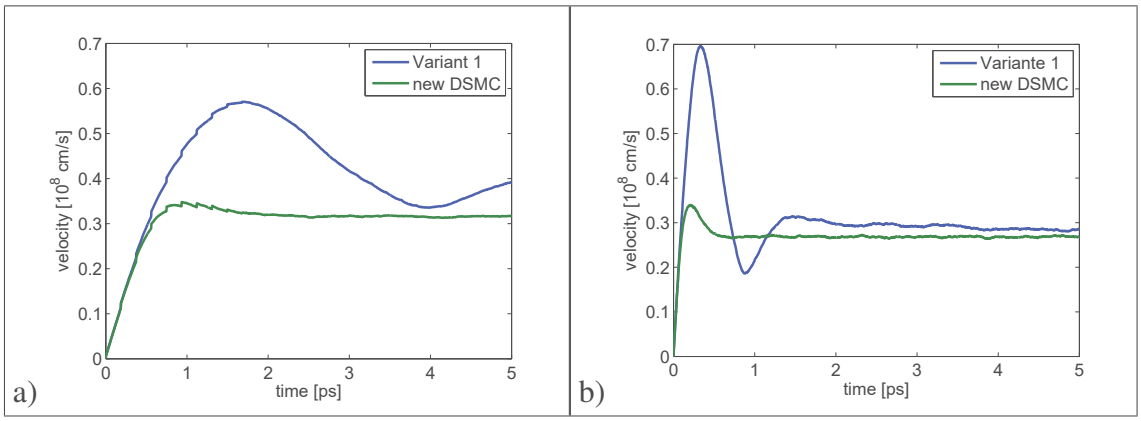

Fig. 2.19 Comparison of the average velocity versus time obtained with the variant 1 and the new DSMC when $E = 2$ kV/cm and $\varepsilon_F = 0.3$ eV a), and when $E = 20$ kV/cm and $\varepsilon_F = 0.6$ eV b).

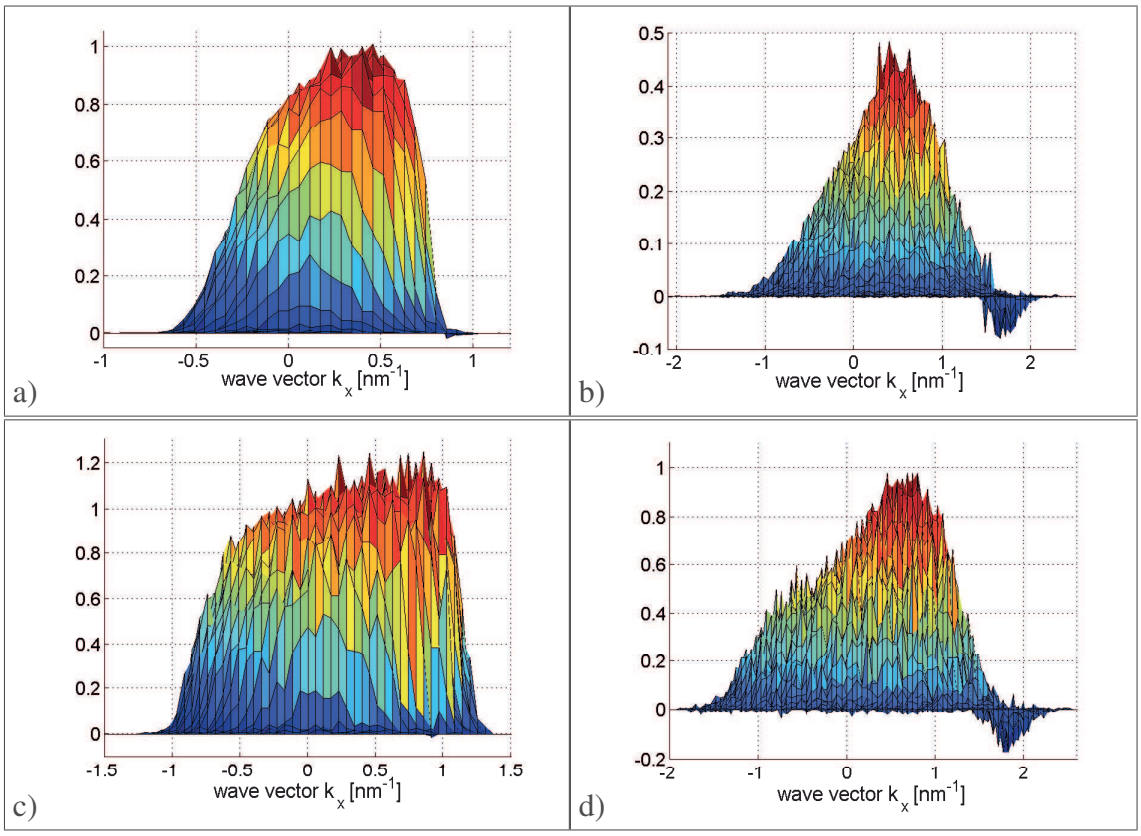

Fig. 2.20 Distribution function section along the field direction with variant 1. $\varepsilon_F = 0.3$ eV and $E = 2$ kV/cm a), $\varepsilon_F = 0.3$ eV and $E = 20$ kV/cm b), $\varepsilon_F = 0.6$ eV and $E = 2$ kV/cm c), $\varepsilon_F = 0.6$ eV and $E = 20$ kV/cm d).

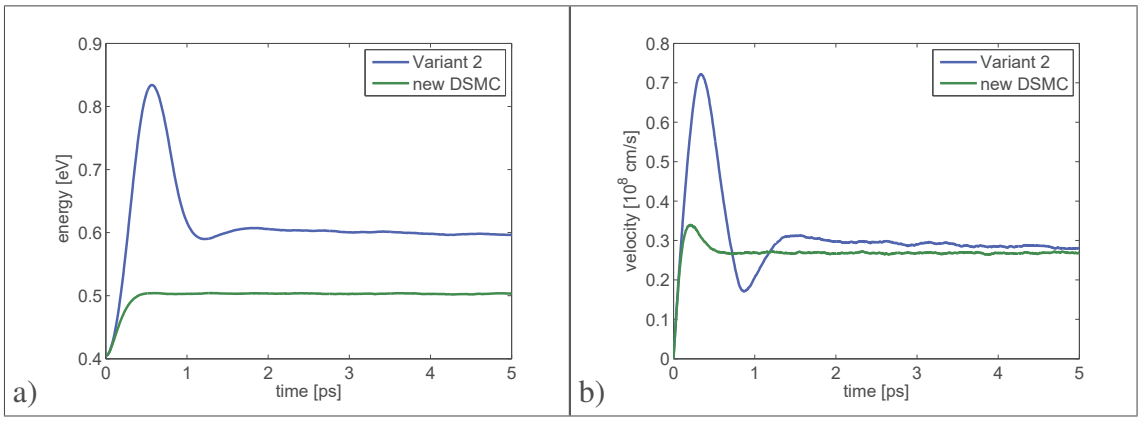

Fig. 2.21 Comparison of the average energy a) and velocity b) versus time obtained with the variant 2 and the new DSMC when $E = 20$ kV/cm and $\varepsilon_F = 0.6$ eV.

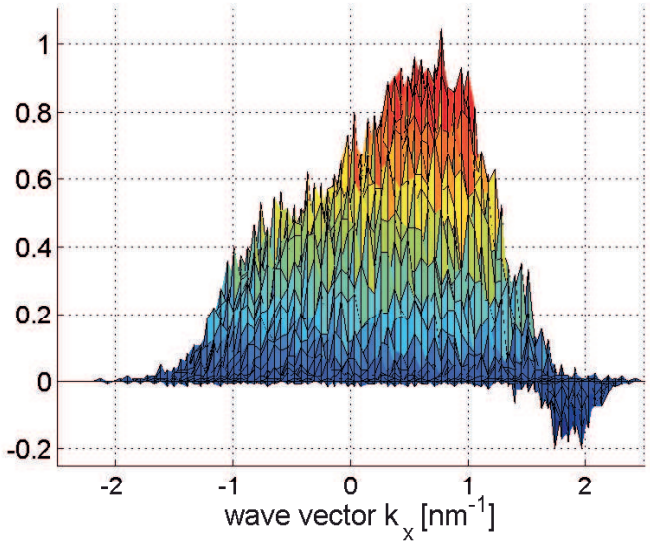

Fig. 2.22 Distribution function section along the field direction with variant 2 when $E = 20$ kV/cm and $\varepsilon_F = 0.6$ eV.

- Variant 2

It is the same procedure of the variant 1, but the time is updated only if the state after the free flight is accepted. Mean energy and velocity, compared with the new DSMC ones, are shown in Fig.2.21.They have the same behaviuor of those in variant 1 and are very similar. This shows how ineffective the updtating procedure for the simulation time is. The distribution functions in Fig.2.25 can exceed again the maximum value 1 and have negative values.

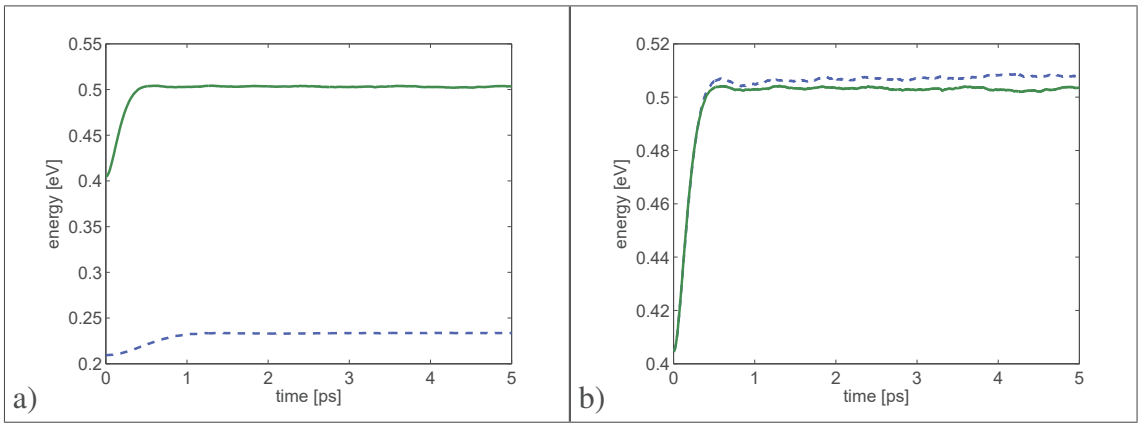

Fig. 2.23 Comparison of the average energy versus time obtained with the variant 3 (dashed line) and the new DSMC (continuous line) when $E = 2$ kV/cm and $\varepsilon_F = 0.3$ eV a), and when $E = 20$ kV/cm and $\varepsilon_F = 0.6$ eV.

- Variant 3

Unlike the variant 1, at first one uses a rejection technique on the states after the scattering events as in the standard EMC simulation; the free flight is performed and the scattering mechanism is chosen. If this is accepted the simulation time and the electron state are updated; if it is not accepted, then ones checks also the free flight state before the scattering; if this is accepted one updates the electron energy and momentum according to the free flight and updates the simulation time, otherwise all remain unchanged and only the simulation time is updated. This is a variant closer both to standard one and to new DSMC approach; actually, some average values for energy and velocity seem good at high fields and Fermi levels, see Figs 2.23, 2.24, but the distribution function have values exceeding the maximum one see Fig. 2.25.

- Variant 4

It is the same as the variant 3, but the simulation time is updated to $t + dt$ only if the state after the scattering or after the free flight is accepted. Again, the updating of the simulation time it is not so important and we have practically the same results of the variant 3, see Fig. 2.26, with the same problems in the distribution functions, see Fig.2.27.

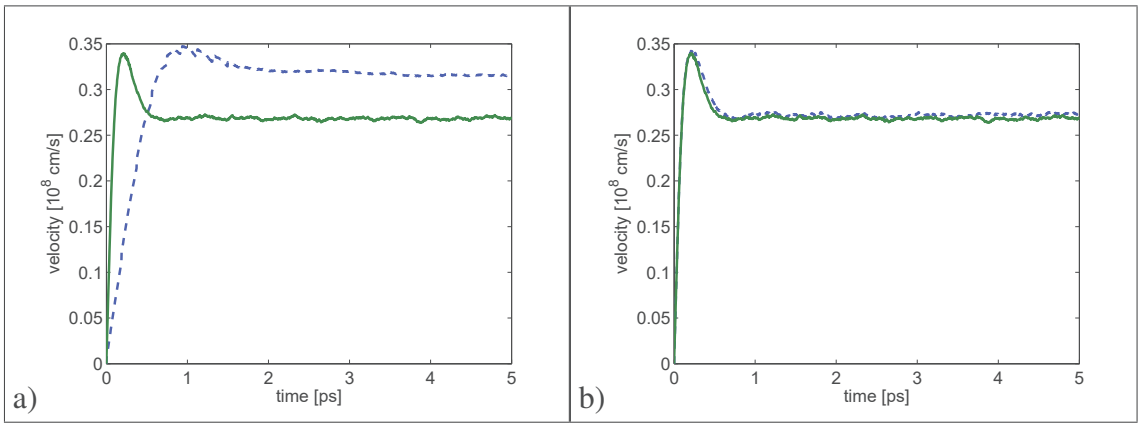

Fig. 2.24 Comparison of the average velocity versus time obtained with the variant 3 (dashed line) and the new DSMC (continuous line) when $E = 2$ kV/cm and $\varepsilon_F = 0.3$ eV a), and when $E = 20$ kV/cm and $\varepsilon_F = 0.6$ eV b).

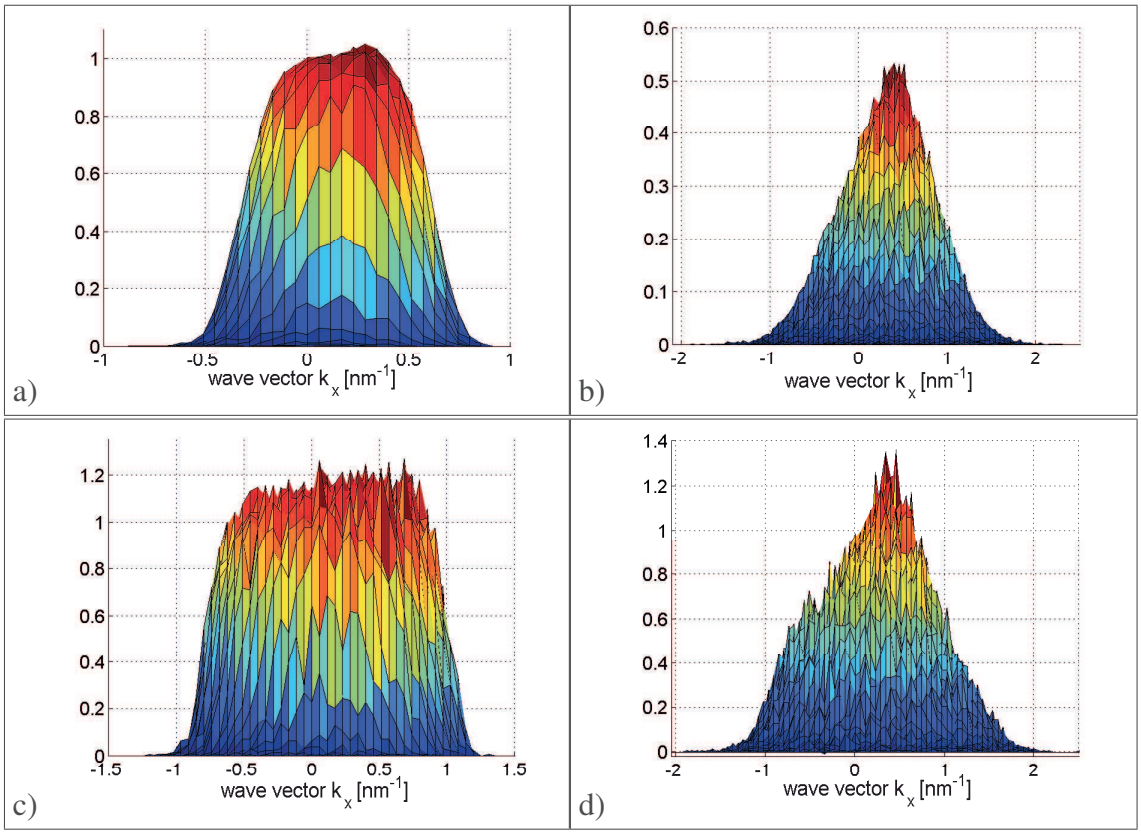

Fig. 2.25 Distribution function section along the field direction with variant 3. $\varepsilon_F = 0.3$ eV and $E = 2$ kV/cm a), $\varepsilon_F = 0.3$ eV and $E = 20$ kV/cm b), $\varepsilon_F = 0.6$ eV and $E = 2$ kV/cm c), $\varepsilon_F = 0.6$ eV and $E = 20$ kV/cm d).

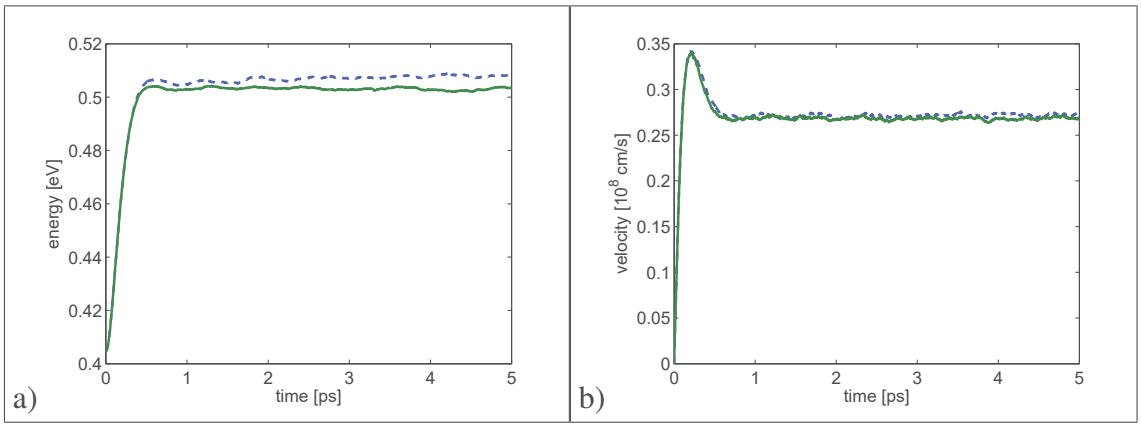

Fig. 2.26 Comparison of the average energy a) and velocity b) versus time obtained with the variant 4 (dashed line) and the new DSMC (continuous line) when $E = 20$ kV/cm and $\varepsilon_F = 0.6$ eV.

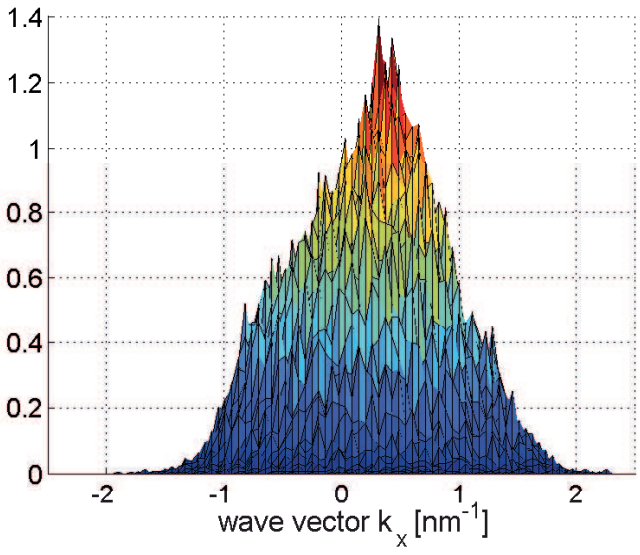

Fig. 2.27 Distribution function section along the field direction with variant 4 when $E = 20$ kV/cm and $\varepsilon_F = 0.6$ eV.

2.2.3 The space-dependent case

In this case the electric field is usually no longer constant and must be self-consistently evaluated by coupling the transport equation with the Poisson equation for the electrostatic potential. For example this problem arises when one has a variable Fermi energy or, as happens for conventional semiconductors, a non uniform doping. A similar problem has also

been tackled in [41] for the simulation of compressible inviscid flows by using a particle method with a procedure having several analogies with that proposed here.

There is a relevant difference, with respect to the space-homogeneous case, in the calculation of the distribution function f for fixed time and space. Now, we must find the distribution in an finite suitable set of points in the real space. To this scope, we initially introduce a partition of the space domain D, which is assumed compact, and we denote by D_a the generic cell of the partition. The initial partition of the domain D is introduced according to the following requirements. Every cell contains, at the initial time, a sufficiently large number of particles to guarantee a reasonable statistic, which is necessary to estimate f and its moments. This partition, introduced at the initial time, will not be changed in the sequel, and it is used to evaluate macroscopic quantities, as density or energy, by means of the standard procedure to perform the statistic.

We choose a partition of the $\mathbf{k}$-domain $[-k_{xmax}, k_{xmax}] \times [-k_{ymax}, k_{ymax}]$ in every cell D_a and we denote by C_{ij}^a the generic cell of the partition in the $\mathbf{k}$-space, coupled to the cell D_a.

Now, in the non-homogeneous case, we must find the occupation number in each set $D_a \times C_{ij}^a$ for all a and (i, j), and check the validity of the Pauli's exclusion principle in every set $D_a \times C_{ij}^a$.

As initial conditions we arrange the particles in each cell according to the value of the doping or equivalently according to the value of the Fermi energy in the cell.

The solution at the time $t_n + \Delta t$ is obtained by splitting the transport equation into three steps:

1. solve
$$\frac{\partial f(t,\mathbf{x},\mathbf{k})}{\partial t} - \frac{e}{\hbar}\mathbf{E}\cdot\nabla_{\mathbf{k}} f(t,\mathbf{x},\mathbf{k}) = 0 \tag{2.20}$$
with initial data $f(t_n,\mathbf{x},\mathbf{k})$;

2. solve
$$\frac{\partial f(t,\mathbf{x},\mathbf{k})}{\partial t} = \frac{df}{dt}(t,\mathbf{x},\mathbf{k})\bigg|_{e-ph}, \tag{2.21}$$
taking as initial condition the solution of Eq. (2.20);

3. solve
$$\frac{\partial f(t,\mathbf{x},\mathbf{k})}{\partial t} + \mathbf{v}\cdot\nabla_{\mathbf{x}} f(t,\mathbf{x},\mathbf{k}) = 0, \quad t \in [t_n, t_n + \Delta t] \tag{2.22}$$
taking as initial condition the solution of Eq.(2.21).

The global procedure gives a numerical approximation of $f(t_n + \Delta t, \mathbf{x}, \mathbf{k})$ up to first order in Δt.

Let us see the previous steps from a DSMC point of view. The first and the second step are performed in a way, which is very similar to the previous space-homogeneous case. We only use a piecewise constant approximation of the electric field, such that in each cell D_a the electric field $\mathbf{E}$ is a constant. The position of the particles in the physical space remains unchanged. We remark that, after these two steps, for every cell D_a, the coupled grid in $\mathbf{k}$-space moves, according to the value of the electric field, in a non uniform way.

Now, we consider the last step. In the DSMC scheme, it corresponds to the equation

$$\dot{\mathbf{x}} = \frac{v_F}{|\mathbf{k}|}\mathbf{k}. \tag{2.23}$$

We solve this equation as in the standard DSMC method. Since, now, Pauli's exclusion principle is not guaranteed in all the sets $D_a \times C_{ij}^a$, we can use the exact solution of Eq. (2.22), which gives

$$f(t_n + \Delta t, \mathbf{x}, \mathbf{k}) = f(t_n, \mathbf{x} - \mathbf{v}\, t_n, \mathbf{k}) \tag{2.24}$$

as a corrector. In fact, in every $D_a \times C_{ij}^a$ where Pauli's exclusion principle is not satisfied, we simply replace the simulated particles belonging to $D_a \times C_{ij}^a$ by the same number of new particles created according the exact distribution (2.24), which of course is less than one.

Chapter 3

The Discontinuous Galerkin method

3.1 Basic assumptions

Lately several efficient numerical schemes have been applied for getting deterministic solutions of the Boltzmann equation for charge transport in semiconductors. Several works based on WENO schemes can be found in the literature about simulation of silicon and gallium arsenide electron devices [50, 51] and recently also for suspended monolayer graphene [38]. Here we use an alternative method for solving the kinetic model, i.e. for discretizing Eq. (2.10), based on the discontinuous Galerkin method [52].

The electron distribution function $f(t,\cdot)$ must belong to $L^1(\mathbb{R}^2)$, then, for each $t > 0$, firstly the space of the wave-vector is approximated by a bounded domain $\Omega \subset \mathbb{R}^2$ such that $f(t,\mathbf{k}) \approx 0$ for every $\mathbf{k} \notin \Omega$ and $t > 0$. We expect an exponential decay of the distribution function as $|\mathbf{k}| \to \infty$. This is proved, under suitable conditions, for the classical Boltzmann equation of rarefied monatomic gases. In our simulations, we check if, after each time step, the values of f at the boundary of the domain Ω are sufficiently low; otherwise, we enlarge the domain Ω and repeat the integration starting from the initial time.

We introduce a finite decomposition $\{C_\alpha\}$ of Ω, with C_α appropriate open sets, such that

$$C_\alpha \cap C_\beta = \emptyset \quad \text{if } \alpha \neq \beta, \text{ and } \quad \bigcup_{\alpha=1}^{N} \overline{C_\alpha} = \Omega .$$

We assume that the distribution function f is constant in each cell C_α. If we denote by $\chi_\alpha(\mathbf{k})$ the characteristic function relative to the cell C_α, then

$$f(t,\mathbf{k}) \approx f^\alpha(t) \quad \forall \mathbf{k} \in C_\alpha \iff f(t,\mathbf{k}) \approx \sum_{\alpha=1}^{N} f^\alpha(t)\,\chi_\alpha(\mathbf{k}) \quad \forall \mathbf{k} \in \bigcup_{\alpha=1}^{N} C_\alpha .$$

This assumption replaces the unknown f, which depends on the two variables t and $\mathbf{k}$, with a set of N unknowns f^α, which depend only on time t. In order to obtain a set of N equations for the new unknowns f^α, we integrate the Boltzmann equation with respect to $\mathbf{k}$ over every cell C_α and replace f with its approximation. Up the truncation error, one gets

$$M_\alpha \frac{d f^\alpha(t)}{dt} - \frac{e}{\hbar}\mathbf{E}\cdot\int_{\partial C_\alpha} f(t,\mathbf{k})\,\mathbf{n}\,d\sigma$$
$$= \sum_{\beta=1}^{N}\Big[A^{\beta,\alpha}\big(1-f^\alpha(t)\big)f^\beta(t) - A^{\alpha,\beta}f^\alpha(t)\big(1-f^\beta(t)\big)\Big] \tag{3.1}$$

where

$$A^{\alpha,\beta} = \int_{C_\alpha}\left[\int_{C_\beta} S(\mathbf{k},\mathbf{k}')\,d\mathbf{k}'\right]d\mathbf{k}\,, \tag{3.2}$$

M_α is the measure of the cell C_α and $\mathbf{n}$ is the external unit normal to the boundary ∂C_α of the cell C_α. If a suitable discretization of the drift and collision term is performed, it is clear that the numerical method yields a system of ordinary differential equations. This latter can be numerically integrated by using a total variation diminishing (TVD) Runge-Kutta scheme [54] in order to avoid the introduction of spurious oscillations.

3.2 Discretization of the drift term

Since, due to the Galerkin method, the approximation of f is not defined on the boundary of the cells, we must introduce a *numerical flux*, that furnishes reasonable values of f on every ∂C_α, depending on the values of the approximation of f in the nearest neighborhoods of the cell C_α and on the sign of $\mathbf{E}\cdot\mathbf{n}$.

We use a zero flux condition at the boundary of Ω which guarantees the conservation of the total charge. For the interior boundaries, a simple approach is given by *upwind rule* between the nearest adjacent cells.

On account of the symmetry of the $\mathbf{k}$-domain, we approximate it by the circle $|\mathbf{k}| \le k_{max}$ and introduce the regular decomposition of Fig. 3.1, where k_{max} is a fixed maximum value such that f is negligible for all $|\mathbf{k}| > k_{max}$.

Since our unknowns are defined only in the open cell C_α, an approximation of f must be defined on the boundary of the generic cell, which now, see Fig.3.2, consists in four simple arcs.

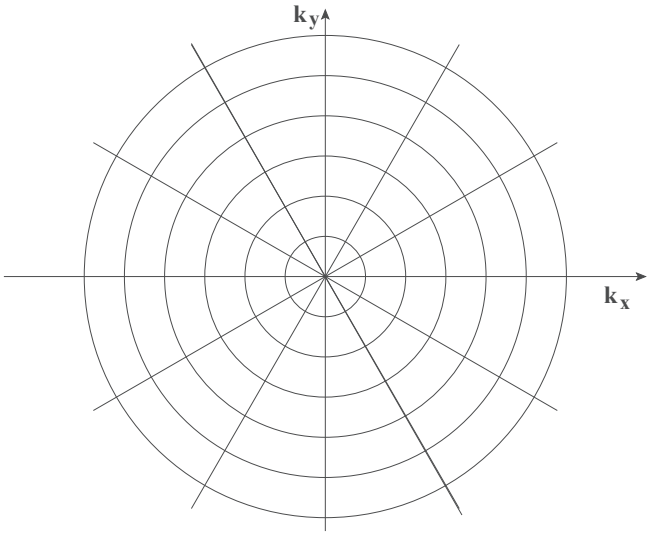

Fig. 3.1 Grid in polar coordinates used for the discretization of the **k**-domain.

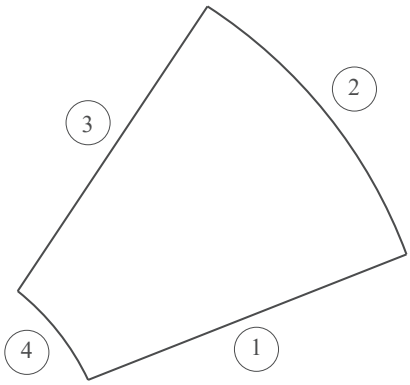

Fig. 3.2 Numbering of the edges of each cell for the evaluation of the flux across it.

Let us fix an arc γ of C_α. If we denote by $C_{\alpha'}$ the cell adiacent to C_α along the considered arc, in the simplest version, the upwind scheme leads to the following algorithm

$$\forall z \in \gamma : \text{if} \quad -e\mathbf{E}\cdot\mathbf{n} \geq 0 \quad \text{then} \quad f(z) = f^{\alpha} \quad \text{else} \quad f(z) = f^{\alpha'}. \tag{3.3}$$

In other words f on the arc is approximated by the interior value of the adiacent cell according to the component of the drift force along the outer normal $\mathbf{n}$. We remark that if the grid is chosen in a way that each cell belongs only to a single quadrant, e.g. as in Fig. 3.1, then in each arc of the cell boundary $\mathbf{E}\cdot\mathbf{n}$ has a constant sign.

A more elaborate approach is based on the Min-Mod slope limiter [55]. In order to make clear the algorithm, first we consider the following case. Let z_1, z_2, $\cdots$, z_N be a set of grid points, which represent a partition of the interval $[z_1, z_N]$, and let $g : [z_1, z_N] \to \mathbb{R}$ be a smooth function. We look for an approximation of the value $g(z_{n+\frac{1}{2}})$ when the following piecewise approximation of $g(z)$ is known: $g(z) \approx g(z_k) := g_k$ in the open interval $]z_{k-\frac{1}{2}}, z_{k+\frac{1}{2}}[$, $k = n-1, n, n+1, n+2$.
We denote $z_{n+\frac{1}{2}} - z_{n-\frac{1}{2}}$ by Δz_n for every n.

Taking into account the hyperbolic character of the equations, if we define the *wind velocity* $a = -e\mathbf{E}\cdot\mathbf{n}$, a simple Taylor expansion gives

$$g_{n+\frac{1}{2}} \approx \begin{cases} g_n + \dfrac{\Delta z_n}{2} g'_n & \text{if } a > 0 \\ \\ g_{n+1} - \dfrac{\Delta z_{n+1}}{2} g'_{n+1} & \text{if } a < 0 \end{cases}, \tag{3.4}$$

where, only in this section, a prime denotes partial derivatives with respect to z. Of course, the case of vanishing a need not be considered. Eq. (3.4) allows us to replace the function $g_{n+\frac{1}{2}}$ with an approximation containing g_n or g_{n+1}, but also one derivative. Now, we define for $a > 0$

$$d_- = 2\,\frac{g_n - g_{n-1}}{\Delta z_{n-1} + \Delta z_n}, \quad d_+ = 2\,\frac{g_{n+1} - g_n}{\Delta z_n + \Delta z_{n+1}}$$

and approximate the sought derivative according to

$$g'_n \approx \begin{cases} \min\{|d_-|, |d_+|\}\,\mathrm{sgn}(d_-) & \text{if } d_- d_+ > 0 \\ 0 & \text{otherwise} \end{cases}.$$

For $a < 0$, a similar formula holds.

On account of the geometry of the decomposition, it is more convenient to employ polar coordinates r and ϑ. Let us denote with $\mathbf{i}$ and $\mathbf{j}$ the unit vectors of the x and y axes. Moreover, for regularity reasons, let us introduce also the variable $s = r^2$. In the coordinates s and ϑ

each cell C_α is now expressed as

$$C_\alpha = \{(s,\vartheta) \in [0,s_{max}] \times [0,2\pi] : s_{k-\frac{1}{2}} \le s \le s_{k+\frac{1}{2}}, \vartheta_{n-\frac{1}{2}} \le \vartheta \le \vartheta_{n+\frac{1}{2}}\}$$

for suitable index n and k depending on α, where $s_{-1/2} = 0 < s_{1/2} < s_{3/2} < \cdots < s_{N+1/2} = s_{max}$ is a partition of $[0,s_{max}]$ and $0 = \vartheta_{-1/2} < \vartheta_{1/2} < \cdots < \vartheta_{M+1/2} = 2\pi$ is a partition of $[0,2\pi]$.

Since

$$\nabla u = \frac{\partial u}{\partial r}\,\mathbf{e}_r + \frac{1}{r}\,\frac{\partial u}{\partial \vartheta}\,\mathbf{e}_\vartheta = 2\sqrt{s}\,\frac{\partial u}{\partial s}\,\mathbf{e}_r + \frac{1}{\sqrt{s}}\,\frac{\partial u}{\partial \vartheta}\,\mathbf{e}_\vartheta\,, \tag{3.5}$$

where $\mathbf{e}_r = \cos\vartheta\,\mathbf{i} + \sin\vartheta\,\mathbf{j}$ and $\mathbf{e}_\vartheta = -\sin\vartheta\,\mathbf{i} + \cos\vartheta\,\mathbf{j}$, set $g(s,\vartheta) = f(\sqrt{s}\cos\vartheta, \sqrt{s}\sin\vartheta)$, one has

$$\begin{aligned}
\mathbf{E}\cdot\int_{C_\alpha}\nabla_{\mathbf{k}}\,g\,d\mathbf{k} &= \mathbf{E}\cdot\int_{s_{k-\frac{1}{2}}}^{s_{k+\frac{1}{2}}} ds\int_{\vartheta_{n-\frac{1}{2}}}^{\vartheta_{n+\frac{1}{2}}} d\vartheta\left[\left(\sqrt{s}\cos\vartheta\,\frac{\partial g}{\partial s} - \frac{1}{2\sqrt{s}}\sin\vartheta\,\frac{\partial g}{\partial\vartheta}\right)\mathbf{i}\right.\\
&\qquad\left. + \left(\sqrt{s}\sin\vartheta\,\frac{\partial g}{\partial s} + \frac{1}{2\sqrt{s}}\cos\vartheta\,\frac{\partial g}{\partial\vartheta}\right)\mathbf{j}\right]\\
&= (\mathbf{E}\cdot\mathbf{i})\left\{\int_{\vartheta_{n-\frac{1}{2}}}^{\vartheta_{n+\frac{1}{2}}}\cos\vartheta\left[\sqrt{s_{k+\frac{1}{2}}}\,g(s_{k+\frac{1}{2}},\vartheta) - \sqrt{s_{k-\frac{1}{2}}}\,g(s_{k-\frac{1}{2}},\vartheta)\right]d\vartheta\right.\\
&\qquad\left. - \int_{s_{k-\frac{1}{2}}}^{s_{k+\frac{1}{2}}}\frac{1}{2\sqrt{s}}\left[\sin\vartheta_{n+\frac{1}{2}}\,g(s,\vartheta_{n+\frac{1}{2}}) - \sin\vartheta_{n-\frac{1}{2}}\,g(s,\vartheta_{n-\frac{1}{2}})\right]ds\right\}\\
&\quad + (\mathbf{E}\cdot\mathbf{j})\left\{\int_{\vartheta_{n-\frac{1}{2}}}^{\vartheta_{n+\frac{1}{2}}}\sin\vartheta\left[\sqrt{s_{k+\frac{1}{2}}}\,g(s_{k+\frac{1}{2}},\vartheta) - \sqrt{s_{k-\frac{1}{2}}}\,g(s_{k-\frac{1}{2}},\vartheta)\right]d\vartheta\right.\\
&\qquad\left. - \int_{s_{k-\frac{1}{2}}}^{s_{k+\frac{1}{2}}}\frac{1}{2\sqrt{s}}\left[\cos\vartheta_{n+\frac{1}{2}}\,g(s,\vartheta_{n+\frac{1}{2}}) + \cos\vartheta_{n-\frac{1}{2}}\,g(s,\vartheta_{n-\frac{1}{2}})\right]ds\right\}\\
&\approx (\mathbf{E}\cdot\mathbf{i})\left\{\left[\sqrt{s_{k+\frac{1}{2}}}\,g_{k+\frac{1}{2},n} - \sqrt{s_{k-\frac{1}{2}}}\,g_{k-\frac{1}{2},n}\right]\int_{\vartheta_{n-\frac{1}{2}}}^{\vartheta_{n+\frac{1}{2}}}\cos\vartheta\,d\vartheta\right.\\
&\qquad\left. - \left[\sin\vartheta_{n+\frac{1}{2}}\,g_{k,n+\frac{1}{2}} - \sin\vartheta_{n-\frac{1}{2}}\,g_{k,n-\frac{1}{2}}\right]\int_{s_{k-\frac{1}{2}}}^{s_{k+\frac{1}{2}}}\frac{1}{2\sqrt{s}}\,ds\right\}
\end{aligned}$$

$$+(\mathbf{E}\cdot\mathbf{j})\left\{\left[\sqrt{s_{k+\frac{1}{2}}}\,g_{k+\frac{1}{2},n}-\sqrt{s_{k-\frac{1}{2}}}\,g_{k-\frac{1}{2},n}\right]\int_{\vartheta_{n-\frac{1}{2}}}^{\vartheta_{n+\frac{1}{2}}}\sin\vartheta\,d\vartheta\right.$$
$$\left.-\left[\cos\vartheta_{n+\frac{1}{2}}\,g_{k,n+\frac{1}{2}}+\cos\vartheta_{n-\frac{1}{2}}\,g_{k,n-\frac{1}{2}}\right]\int_{s_{k-\frac{1}{2}}}^{s_{k+\frac{1}{2}}}\frac{1}{2\sqrt{s}}\,ds\right\}.$$

The discretization is completed by approximating the terms $g_{k+\frac{1}{2},n}$ with the Min-Mod slope limiter along $\vartheta=$ constant and and by approximating the terms $g_{k,n+\frac{1}{2}}$ with the Min-Mod slope limiter along $s=$ constant.

3.3 Discretization of the collision term

We need to evaluate the coefficients (3.2). They are a sum of integrals of this kind

$$\int_{\vartheta_a'}^{\vartheta_b'}d\vartheta'\int_{\vartheta_a}^{\vartheta_b}d\vartheta\int_{s_a'}^{s_b'}ds'\int_{s_a}^{s_b}ds\,\frac{1}{4}\left[A+B\cos(\vartheta-\vartheta')\right]\left[\delta\left(\varepsilon(\mathbf{k}')-\varepsilon(\mathbf{k})+\hbar\,\omega_{\mathbf{q}}^{(\nu)}\right)\right.$$
$$\left.\left(n_{\mathbf{q}}^{(\nu)}+1\right)+\delta\left(\varepsilon(\mathbf{k}')-\varepsilon(\mathbf{k})-\hbar\,\omega_{\mathbf{q}}^{(\nu)}\right)n_{\mathbf{q}}^{(\nu)}\right],$$

where A and B are constant and the factor $\frac{1}{4}$ is the product of the Jacobian of the transformations $r=\sqrt{s}$ and $r'=\sqrt{s'}$.

We have taken into account that the function $\cos(\vartheta_{\mathbf{k},\mathbf{k}'-\mathbf{k}}+\vartheta_{\mathbf{k}',\mathbf{k}'-\mathbf{k}})$, which appears both in the longitudinal and transversal optical scattering, is canceled when the sum of the scattering terms is performed.

The previous integral can be factorized as the product of twofold integrals. If we introduce the parameter $\xi=\left(\hbar\,\omega_{\mathbf{q}}^{(\nu)}\right)/(\hbar\,v_F)$ and the characteristic function $\chi_{[a,b]}(z)$ relative to the interval $[a,b]$, one has

$$\int_{\vartheta_a'}^{\vartheta_b'}d\vartheta'\int_{\vartheta_a}^{\vartheta_b}d\vartheta\left[A+B\cos(\vartheta-\vartheta')\right]=A\left(\vartheta_b'-\vartheta_a'\right)\left(\vartheta_b-\vartheta_a\right)+B$$
$$\times 4\sin\left(\frac{\vartheta_b'-\vartheta_a'}{2}\right)\cos\left(\frac{\vartheta_a+\vartheta_b}{2}-\frac{\vartheta_a'+\vartheta_b'}{2}\right)\sin\left(\frac{\vartheta_b-\vartheta_a}{2}\right),$$

$$
\begin{aligned}
&\frac{1}{4}\int_{s'_a}^{s'_b} ds' \int_{s_a}^{s_b} ds \left[\delta\left(\varepsilon(\mathbf{k}')-\varepsilon(\mathbf{k})+\hbar\,\omega_{\mathbf{q}}^{(\nu)}\right)\left(n_{\mathbf{q}}^{(\nu)}+1\right)+\delta\left(\varepsilon(\mathbf{k}')-\varepsilon(\mathbf{k})-\hbar\,\omega_{\mathbf{q}}^{(\nu)}\right)n_{\mathbf{q}}^{(\nu)}\right]\\
&\quad=\frac{1}{4}\frac{1}{|\hbar\, v_F|}\int_{s'_a}^{s'_b} ds' \int_{s_a}^{s_b} ds\times\left[\left(n_{\mathbf{q}}^{(\nu)}+1\right)\delta\left(|\mathbf{k}'|-|\mathbf{k}|+\xi\right)+n_{\mathbf{q}}^{(\nu)}\,\delta\left(|\mathbf{k}'|-|\mathbf{k}|-\xi\right)\right]\\
&\quad=\frac{1}{2}\frac{1}{|\hbar\, v_F|}\int_{s_a}^{s_b} ds \int_{\sqrt{s'_a}}^{\sqrt{s'_b}} dr'\left[\left(n_{\mathbf{q}}^{(\nu)}+1\right)\delta\left(|\mathbf{k}'|-|\mathbf{k}|+\xi\right)+n_{\mathbf{q}}^{(\nu)}\,\delta\left(|\mathbf{k}'|-|\mathbf{k}|-\xi\right)\right]r'\\
&\quad=\frac{1}{2}\frac{1}{|\hbar\, v_F|}\int_{s_a}^{s_b} ds \int_{\mathbb{R}} dr'\left[\left(n_{\mathbf{q}}^{(\nu)}+1\right)\times\delta\left(r'-|\mathbf{k}|+\xi\right)\right.\\
&\quad\left.+\,n_{\mathbf{q}}^{(\nu)}\,\delta\left(r'-|\mathbf{k}|-\xi\right)\right]\chi_{\left[\sqrt{s'_a},\sqrt{s'_b}\right]}(r')\,r'\\
&\quad=\frac{1}{2}\frac{1}{|\hbar\, v_F|}\int_{s_a}^{s_b} ds\left[\left(n_{\mathbf{q}}^{(\nu)}+1\right)\chi_{\left[\sqrt{s'_a},\sqrt{s'_b}\right]}(|\mathbf{k}|-\xi)\,(|\mathbf{k}|-\xi)\right.\\
&\quad\left.+\,n_{\mathbf{q}}^{(\nu)}\chi_{\left[\sqrt{s'_a},\sqrt{s'_b}\right]}(|\mathbf{k}|+\xi)\,(|\mathbf{k}|+\xi)\right]\\
&\quad=\frac{1}{2}\frac{1}{|\hbar\, v_F|}\int_{s_a}^{s_b} ds\left[\left(n_{\mathbf{q}}^{(\nu)}+1\right)\chi_{\left[\sqrt{s'_a},\sqrt{s'_b}\right]}(\sqrt{s}-\xi)\,(\sqrt{s}-\xi)\right.\\
&\quad\left.+\,n_{\mathbf{q}}^{(\nu)}\chi_{\left[\sqrt{s'_a},\sqrt{s'_b}\right]}(\sqrt{s}+\xi)\,(\sqrt{s}+\xi)\right]\\
&\quad=\frac{1}{|\hbar\, v_F|}\int_{\sqrt{s_a}}^{\sqrt{s_b}} dr\left[\left(n_{\mathbf{q}}^{(\nu)}+1\right)\times\chi_{\left[\sqrt{s'_a},\sqrt{s'_b}\right]}(r-\xi)\,(r-\xi)\right.\\
&\quad\left.+\,n_{\mathbf{q}}^{(\nu)}\chi_{\left[\sqrt{s'_a},\sqrt{s'_b}\right]}(r+\xi)\,(r+\xi)\right]r\\
&\quad=\frac{n_{\mathbf{q}}^{(\nu)}+1}{|\hbar\, v_F|}\int_{\left[\sqrt{s_a},\sqrt{s_b}\right]\cap\left[\sqrt{s'_a}+\xi,\sqrt{s'_b}+\xi\right]}(r-\xi)\,r\,dr\\
&\quad+\frac{n_{\mathbf{q}}^{(\nu)}}{|\hbar\, v_F|}\int_{\left[\sqrt{s_a},\sqrt{s_b}\right]\cap\left[\sqrt{s'_a}-\xi,\sqrt{s'_b}-\xi\right]}(r+\xi)\,r\,dr\\
&\quad=\frac{n_{\mathbf{q}}^{(\nu)}+1}{|\hbar\, v_F|}\left[\frac{1}{3}r^3-\frac{1}{2}\xi\,r^2\right]_{\left[\sqrt{s_a},\sqrt{s_b}\right]\cap\left[\sqrt{s'_a}+\xi,\sqrt{s'_b}+\xi\right]}\\
&\quad+\frac{n_{\mathbf{q}}^{(\nu)}}{|\hbar\, v_F|}\left[\frac{1}{3}r^3+\frac{1}{2}\xi\,r^2\right]_{\left[\sqrt{s_a},\sqrt{s_b}\right]\cap\left[\sqrt{s'_a}-\xi,\sqrt{s'_b}-\xi\right]}.
\end{aligned}
$$

As the numerical results confirm, the DG approach guarantees that the distribution function never exceed the unit. To understand such an outcome, we observe that by using the simple splitting the overall DG scheme can be formulated, at first order in the time step, given $t = t_n$,

as the numerical discretization of

$$M_\alpha \frac{d f^\alpha(t)}{dt} - \frac{e}{\hbar} \mathbf{E} \cdot \int_{\partial C_\alpha} f(t,\mathbf{k}) \, \mathbf{n} \, d\sigma = 0 \,, \qquad t_n \leq t \leq t_{n+1} \,,$$

followed by the numerical discretization of

$$M_\alpha \frac{d f^\alpha(t)}{dt} = \sum_{\beta=1}^{N} \left[A^{\beta,\alpha} \left(1 - f^\alpha(t)\right) f^\beta(t) - A^{\alpha,\beta} \, f^\alpha(t) \left(1 - f^\beta(t)\right) \right] , \qquad t_n \leq t \leq t_{n+1} \,.$$

The first equation is solved by taking as initial condition the solution at $t = t_n$. The second equation is solved by taking as initial condition the solution of the drift equation. The drift part is an advection equation. The use of the Min-Mod slope limiter prevents the formation of spurious oscillations [56] and does not allow to increase the maximum values of the distribution function or decrease the minimum one. Moreover, the DG scheme preserves as the dissipative character of the collision term as well. Therefore, at first order in the time step, the numerical solution remains bounded by the extrema of the initial data.

Chapter 4

Monolayer graphene on substrates

In [57, 58], a study of the charge transport in a monolayer of graphene on substrates (Fig.4.1) is performed in order to investigate the degradation effects due to the substrate in the electron velocity and then in the total current and mobility. We also compared different substrates in order to identify the better one and we checked the effect of the randomness of the distribution of the substrate impurities.

4.1 Monolayer graphene on SiO_2

Regarding the kinetic model, we use the same Boltzmann equations as in the previous chapters but we need to add also the effects of the remote phonons and the impurities of the substrate. We start considering a SiO_2 substrate. Quantum effects has also been included in the literature but for Fermi energies high enough, as those we considered, the interband tunneling effect is practically negligible and the semiclassical approach still reveals satisfactory [59].

The scattering rate between the electrons and the phonons of the substrate has the same form of that of the suspended case; the remote optical phonons of the substrate are assumed to have an energy equal to 55 meV and a deformation potential $D_f = 5.14 \cdot 10^7$ eV/cm. The interaction with the impurities adds noticeable additional difficulties, mainly due to the rather involved expression of the dielectric function which is itself a source of theoretical debates [60, 61].

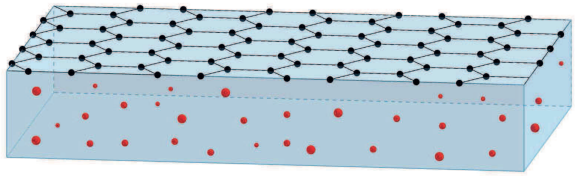

Fig. 4.1 The graphene sheet over a substrate. The spheres represents the impurities.

We will assume the model proposed in [61] for the charge-impurities scattering and consider the following additional transition rate

$$S^{(imp)}(\mathbf{k},\mathbf{k}') = \frac{2\pi}{\hbar}\frac{n_i}{(2\pi)^2}\left|\frac{V_i(|\mathbf{k}-\mathbf{k}'|,d)}{\varepsilon(|\mathbf{k}-\mathbf{k}'|)}\right|^2 \frac{\left(1+\cos\vartheta_{\mathbf{k},\mathbf{k}'}\right)}{2}\delta\left(\varepsilon(\mathbf{k}')-\varepsilon(\mathbf{k})\right), \tag{4.1}$$

where

a) n_i is the number of impurities per unit area.

b) $V_i(|\mathbf{k}-\mathbf{k}'|,d) = 2\pi e^2 \dfrac{\exp(-d\,|\mathbf{k}-\mathbf{k}'|)}{\tilde{\kappa}\,|\mathbf{k}-\mathbf{k}'|}$

- d is the location of the charged impurity measured from the graphene sheet
- $\tilde{\kappa}$ is the effective dielectric constant, defined by $4\pi\times\varepsilon_0\times(\kappa_{top}+\kappa_{bottom})/2$, where ε_0 is the vacuum dielectric constant and κ_{top} and κ_{bottom} are the relative dielectric constants of the medium above and below the graphene layer. For example, if the materials are SiO_2 and air, $\tilde{\kappa} = 4\pi\times\varepsilon_0\times(1+\kappa_{SiO_2})/2 \approx 4\pi\times 2.45\,\varepsilon_0$.

c) $\varepsilon(|\mathbf{k}-\mathbf{k}'|) = \begin{cases} 1+\dfrac{q_s}{|\mathbf{k}-\mathbf{k}'|}-\dfrac{\pi q_s}{8k_F} & \text{if } |\mathbf{k}-\mathbf{k}'|<2k_F \\ 1+\dfrac{q_s}{|\mathbf{k}-\mathbf{k}'|}-\dfrac{q_s\sqrt{|\mathbf{k}-\mathbf{k}'|^2-4k_F^2}}{2|\mathbf{k}-\mathbf{k}'|^2}-\dfrac{q_s}{4k_F}\operatorname{asin}\left(\dfrac{2k_F}{|\mathbf{k}-\mathbf{k}'|}\right) & \text{otherwise} \end{cases}$

is the 2D finite temperature static RPA dielectric (screening) function appropriate for graphene;

- $q_s = \dfrac{4e^2k_F}{\tilde{\kappa}\hbar v_F}$ is the effective Thomas-Fermi wave-vector for graphene; it can be rewritten in terms of the dimensionless Wigner-Seitz radius as $q_s = 4r_S k_F$;
- $k_F = \dfrac{\varepsilon_F}{\hbar v_F}$ is the Fermi wave-vector.

With a standard correction [62, 63] we have the following additional scattering rate for the substrate impurities

$$\Gamma_{imp}(\mathbf{k}) = \int S^{(imp)}(\mathbf{k},\mathbf{k}')\left(1-\cos\vartheta_{\mathbf{k},\mathbf{k}'}\right) d\mathbf{k}'. \tag{4.2}$$

We also investigated the influence of the distance from the substrate that, as we would have expected, is very effective. We consider a surface impurity density of $n_i = 2.5\times10^{11}$ cm^{-2} and several values of the distance d between the graphene sheet and the remote impurities. d should of the order of few angstroms. In the literature a range from 0 to 1 nm is considered. The simulations are performed at several values of the electric field and Fermi energy. The parameter r_S is set equal to 0.8.

The physical parameters for the scattering rates are summarized in Table 4.1. In the

Table 4.1 Physical parameters for the scattering rates.

v_F	10^8 cm/s	v_p	2×10^6 cm/s
σ_m	7.6×10^{-8} g/cm^2	D_{ac}	6.8 eV
$\hbar\omega_O$	164.6 meV	D_O	10^9 eV/cm
$\hbar\omega_K$	124 meV	D_K	3.5×10^8 eV/cm
$\hbar\omega_{op-ac}$	55 meV	D_f	5.14×10^7 eV/cm

DSMC 10^4 particles have been used. Fig.4.2 shows the distribution function f in the stationary regime in the case of an applied electric field equal to 4 kV/cm. In Figs 4.3-4.5, we show the numerical results of the average velocity $\mathbf{v}$ and the average energy W, defined as

$$\mathbf{v}(t) = \frac{2}{(2\pi)^2\rho}\int f(t,\mathbf{k})\frac{1}{\hbar}\nabla_{\mathbf{k}}\varepsilon(\mathbf{k})\,d\mathbf{k}, \quad W(t) = \frac{2}{(2\pi)^2\rho}\int f(t,\mathbf{k})\,\varepsilon(\mathbf{k})\,d\mathbf{k}. \tag{4.3}$$

There is an excellent agreement, of course within the unavoidable stochastic noise of the DCMS data, between the deterministic solutions obtained with the DG method and the stochastic ones in all the considered cases. Since the theoretical basis of the two simulation approaches are radically different, the results represent a strong evidence of the accuracy and validity of the obtained solutions.

We can observe that the values of the average velocity and energy, in the case of graphene on substrate, become lower by reducing the distance d from the impurities in the oxide, confirming the degradation of the mobility due to the substrate as a direct consequence of the additional scatterings with the remote impurities. The simulations are in a qualitative

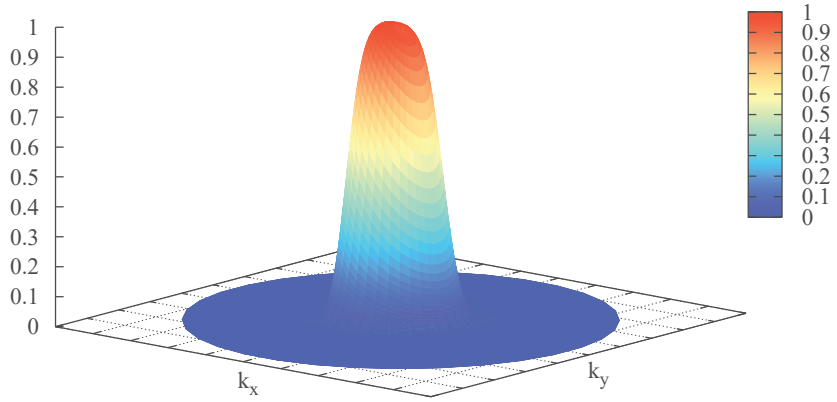

Fig. 4.2 The steady state distribution function in the case of an applied electric field of 4 kV/cm.

agreement with the theoretical expectations and are crucial for the determination of the characteristic curves in graphene on a substrate.

4.2 High filed mobility: comparison between different substrates

Two different substrates are investigated: SiO_2 and hexagonal boron nitride (h-BN). We confirm, as in [64], where only the low-field mobility has been investigated, that h-BN is one of the most promising substrate also for the high-field mobility on account of the reduced degradation of the velocity due to the remote impurities. Here we take into account the randomness of the impurities location, related also to the roughness of the interface of the oxide, by considering d a random variable. Various distributions have been analyzed: uniform and Gamma with several values of parameters. In [64] HfO_2 has also been considered but the analysis at low fields reveals that it is not an adequate material because of the strong degradation of the mobilities. Our analysis confirms that the h-BN is a better material than SiO_2 on account of the reduced degradation of the mobility and the stability with respect to the fluctuations of the parameter d, even if significant quantitative differences are found with

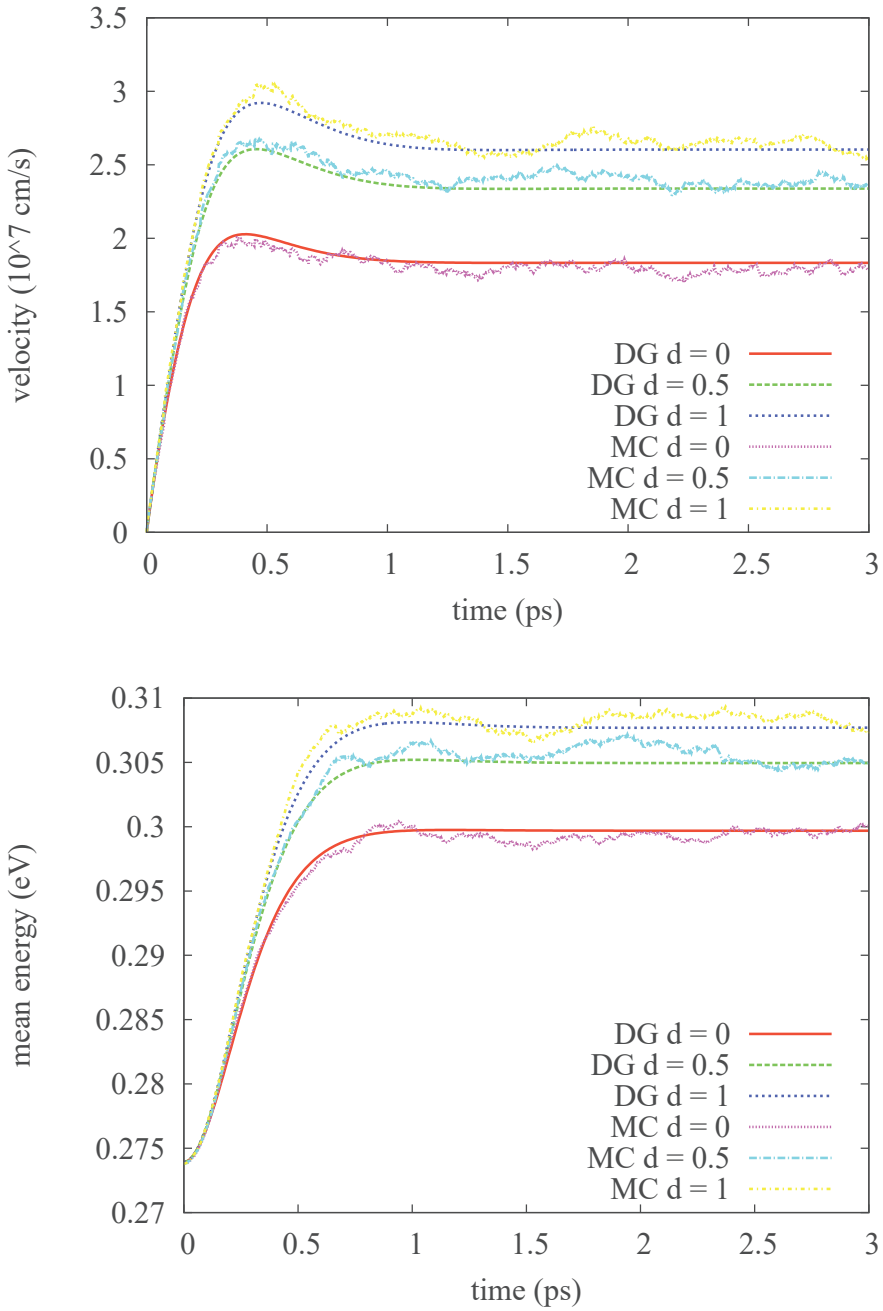

Fig. 4.3 Comparison of the average velocity (top) and average energy (bottom) versus time for $d = 0, 0.5, 1$ nm in the case of an applied electric field of 5 kV/cm and Fermi energy $\varepsilon_F = 0.4$ eV.

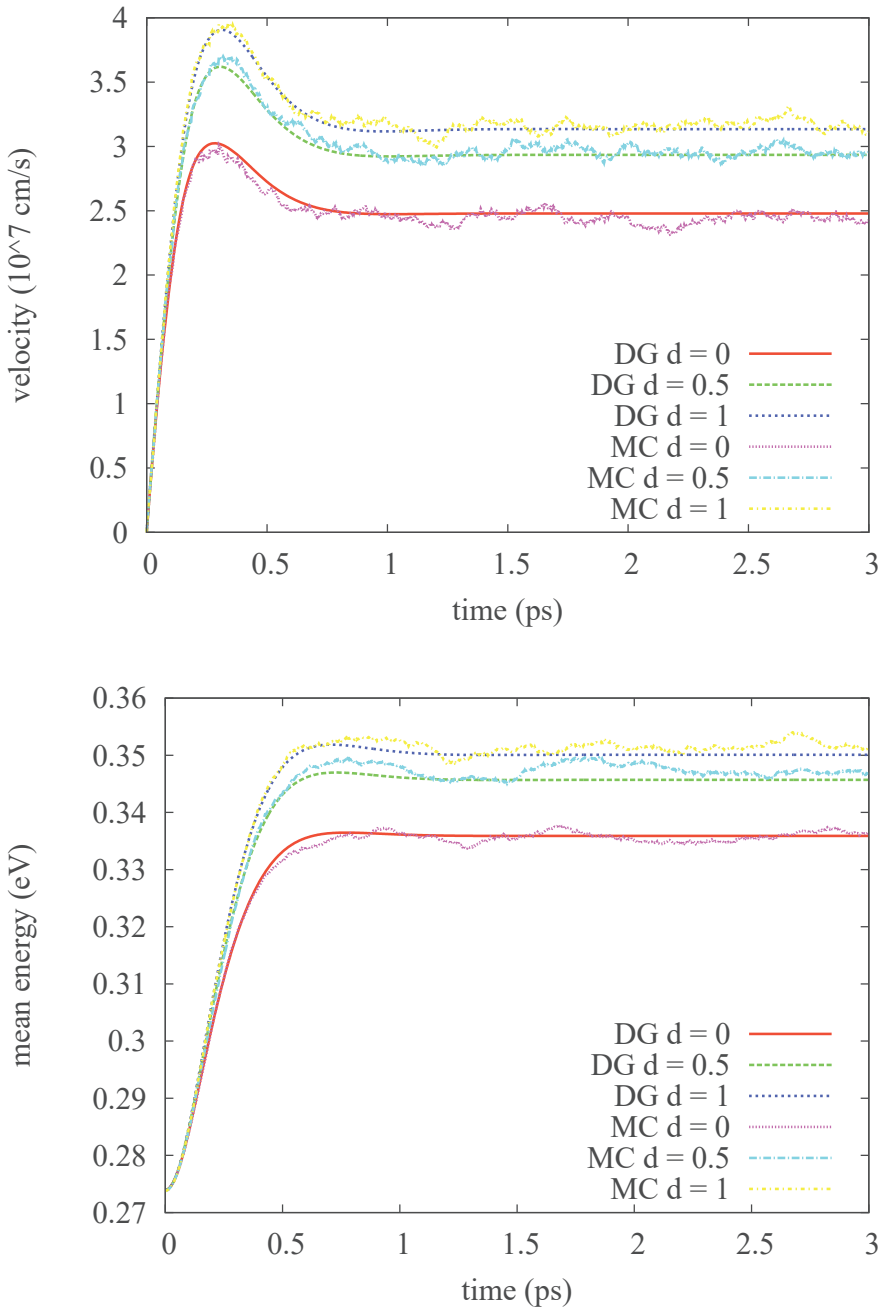

Fig. 4.4 Comparison of the average velocity (top) and average energy (bottom) versus time for $d = 0, 0.5, 1$ nm in the case of an applied electric field of 10 kV/cm and Fermi energy $\varepsilon_F = 0.4$ eV.

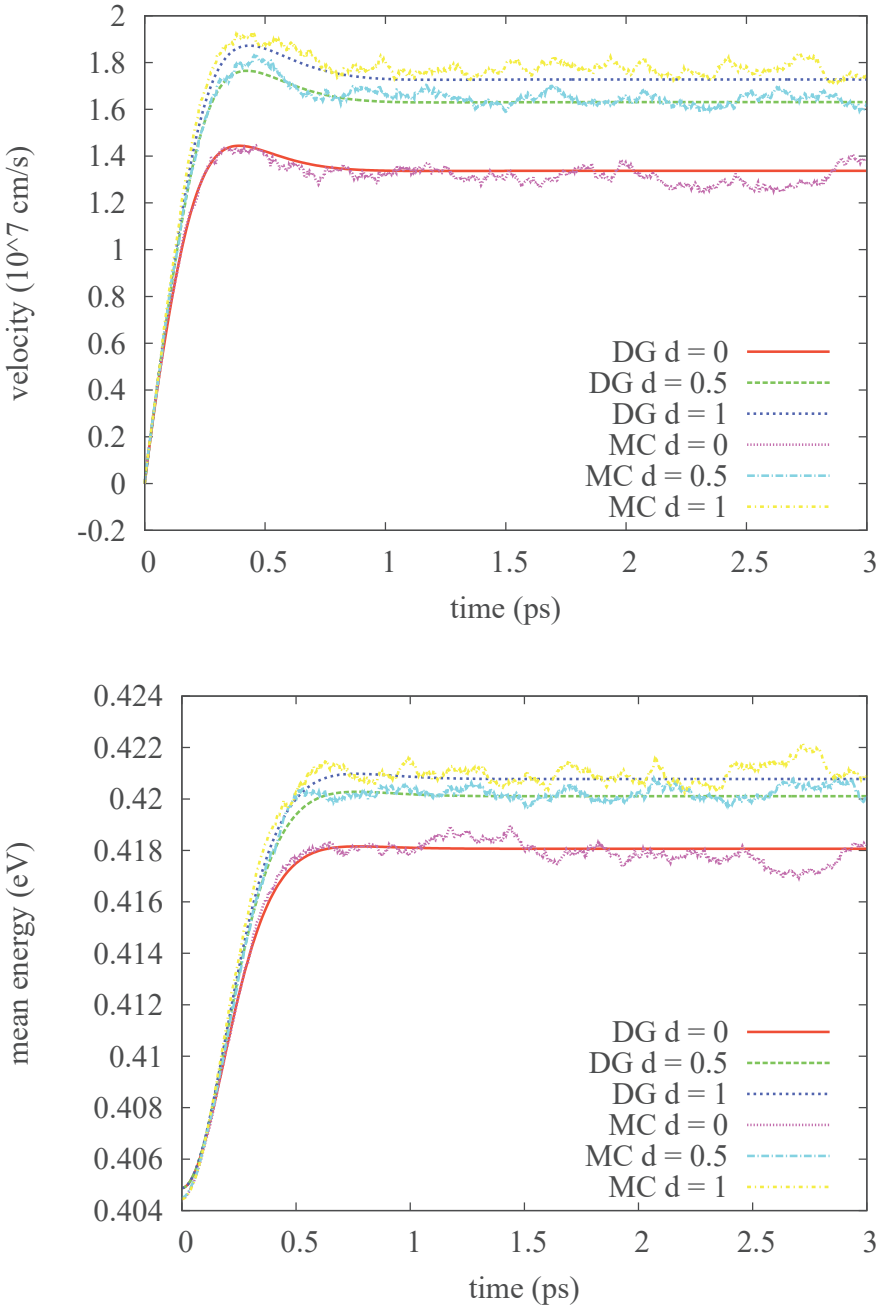

Fig. 4.5 Comparison of the average velocity (top) and average energy (bottom) versus time for $d = 0, 0.5, 1$ nm in the case of an applied electric field of 5 kV/cm and Fermi energy $\varepsilon_F = 0.6$ eV.

respect to [64]. h-BN assures the higher mobility and its performance is robust with respect to the randomness of d. The physical parameters for the substrates are summerized in Table 4.2.

Table 4.2 Physical parameters for the scattering rates related to the substrates.

	SiO_2	h-BN
$\hbar\omega_{op-ac}$	55 meV	200 meV
D_f	5.14×10^7 eV/cm	1.29×10^9 eV/cm
n_i	2.5×10^{11} cm^{-2}	2.5×10^{10} cm^{-2}
κ_{bottom}	3.9	3

We consider a surface impurities density according to Table 4.2. The simulations are performed at several values of the electric field and Fermi energy. In the simulations, whenever a scattering with impurities occurs d is generated according to the chosen distribution. For comparison, the cases with fixed d are also shown along with the solutions obtained by the DG method. 10^5 particles have been used for the DSMC. In Figs 4.6-4.8, we show the numerical results of the average velocity. The velocity is related to the current $\mathbf{J}$ by the relation

$$\mathbf{J} = -e\rho\mathbf{v}$$

and, in turn, $\mathbf{v}$ is related to the mobility $\mu(\mathbf{E})$ as follows

$$\mathbf{v} = \mu(\mathbf{E})\mathbf{E}.$$

Therefore, from the analysis of the average velocity it is possible to estimate the effect of the impurities on the mobility. It is expected that the scattering with the remote impurities leads to a degradation of the mobility depending on the specific material. First we have assessed the general performance of the different materials, by a comparison of the average velocity for three different values of d kept constant. We can observe that the values of the average velocity and energy become lower by reducing the distance d from the impurities in the oxide, confirming the degradation of the mobility due to the substrate as a direct consequence of the additional scatterings with the remote impurities. For the higher value of d, which is very close to the pristine case, both SiO_2 and h-BN produce of course the same effect with a comparable electron velocity. For the intermediate value of d h-BN performs better than SiO_2 and this behaviour is even more evident for $d = 1$. Therefore, h-BN gives a better high-field mobility, in qualitative agreement with the low field analysis in [64].

The previous results, however, do not take into account the intrinsic noise in the location of the impurities. In order to assess its effect on the high-field mobility, we have performed some

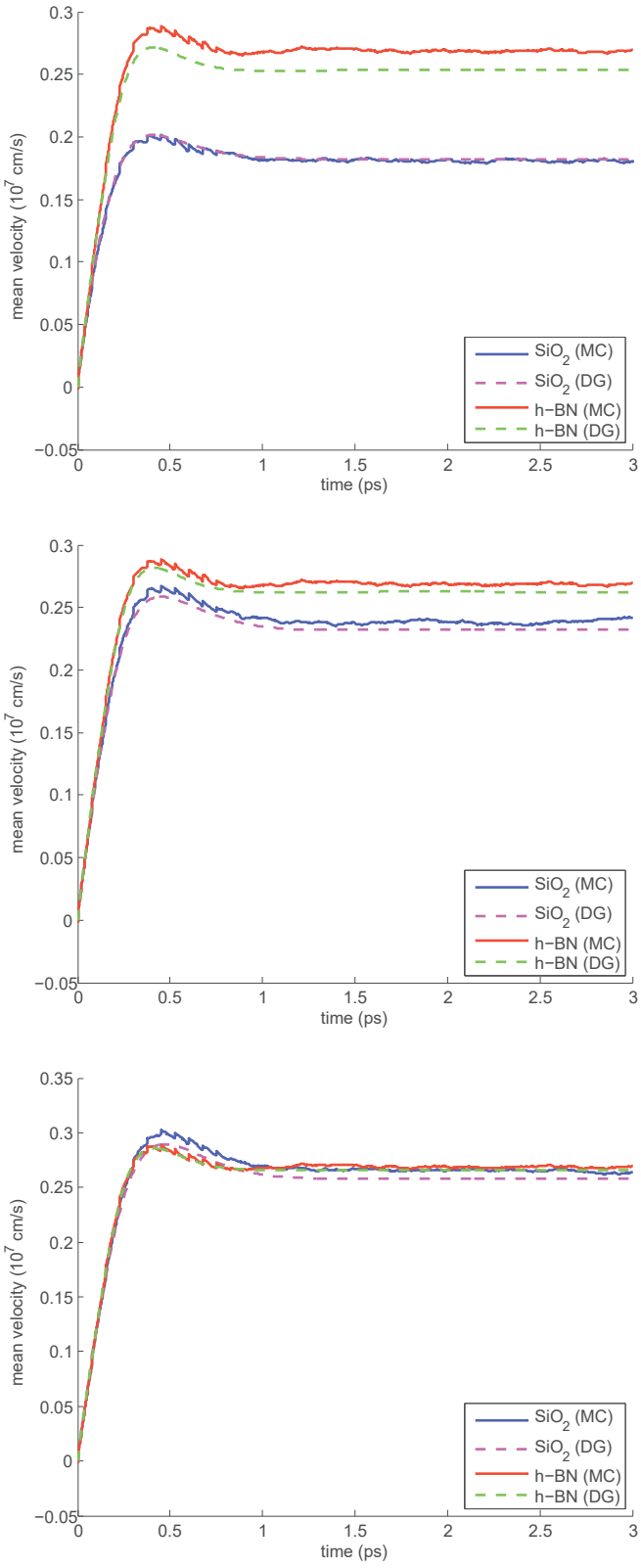

Fig. 4.6 Comparison of the average velocity versus time for $d = 0$ (top) , 0.5, 1 (bottom) nm in the case of an applied electric field of 5 kV/cm and Fermi energy $\varepsilon_F = 0.4$ eV.

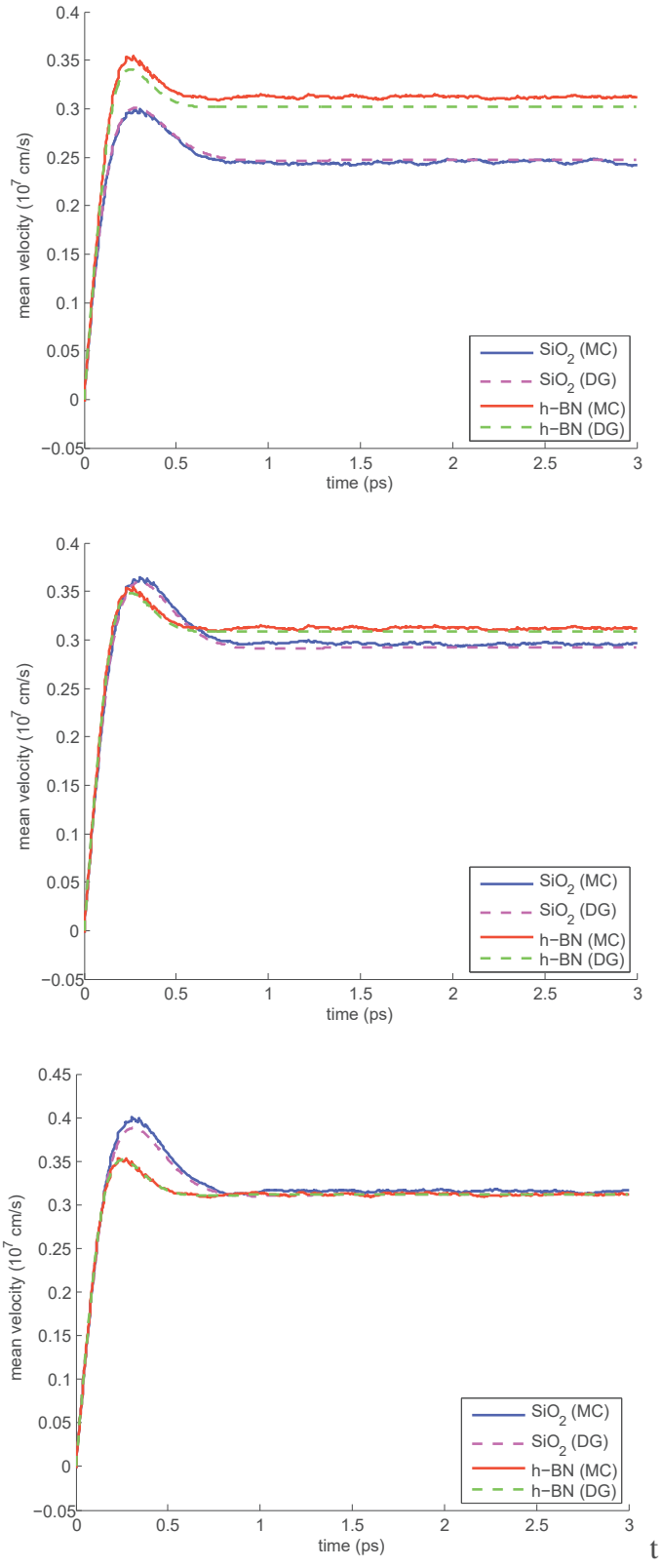

Fig. 4.7 Comparison of the average velocity versus time for $d = 0$ (top) , 0.5, 1 (bottom) nm in the case of an applied electric field of 10 kV/cm and Fermi energy $\varepsilon_F = 0.4$ eV.

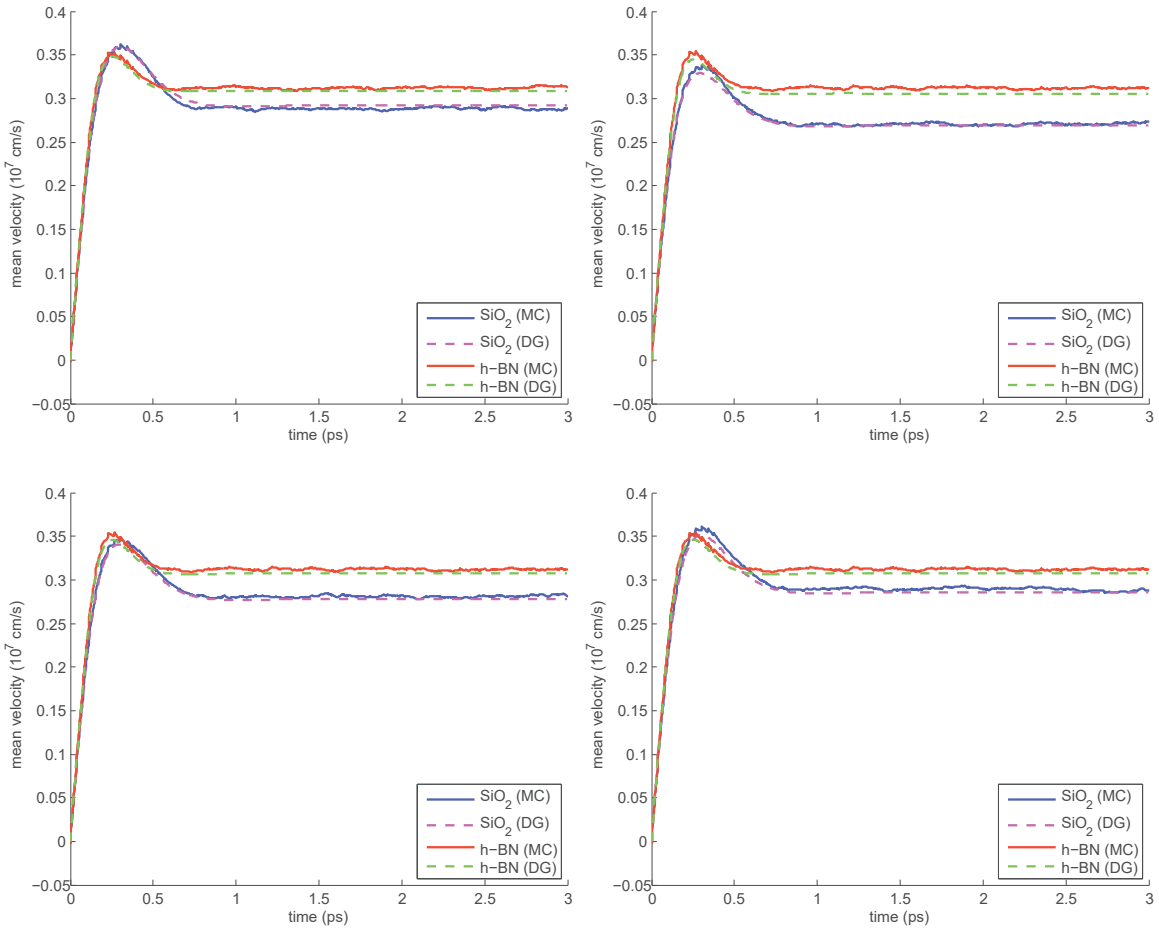

Fig. 4.8 Comparison of the average velocity versus time in the case of an applied electric field of 10 kV/cm and Fermi energy $\varepsilon_F = 0.4$ eV by considering different distribution for d: uniform (top left), $\Gamma(2, 0.5)$ (top right), $\Gamma(3, 0.5)$ (bottom left), $\Gamma(4, 0.5)$ (bottom right). In the results obtained with the discontinuous Galerkin methods (DG) we have assumed d equal to the mean values of the corresponding distribution rescaled by the factor 0.2 nm.

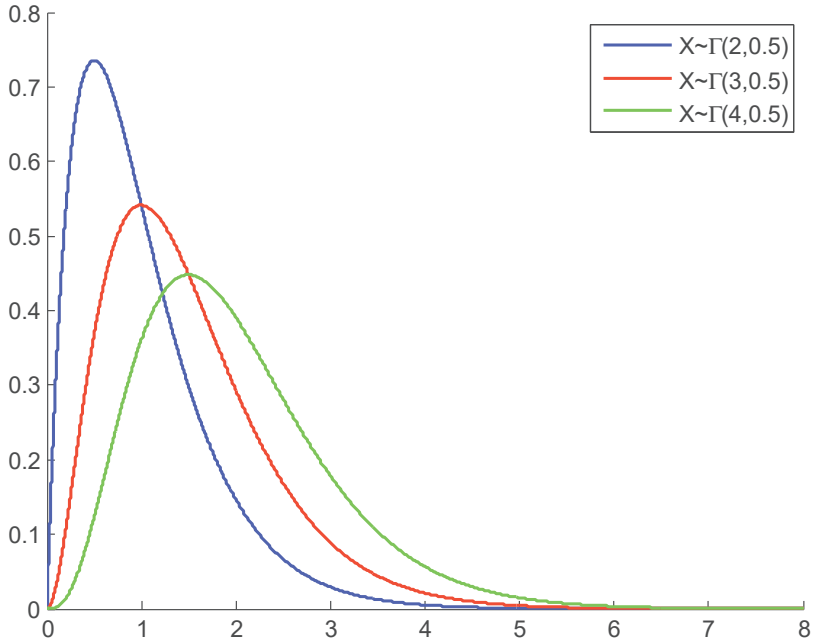

Fig. 4.9 Plot of the $\Gamma(\alpha,\lambda)$ distribution with $\lambda = 0.5$ and $\alpha = 2,3,4$. Note that the probability to generate a number greater than 5 is practically zero.

simulations with a random d generated, in each scattering involving impurities, according to a prescribed probability distribution (see Fig. 4.8). First we have considered a uniform distribution in the interval $[0,1]$ (in nm). The results are similar to the case with constant $d = 0.5$ nm and this can be explained by observing that 0.5 is the expectation value. Then we have considered a $\Gamma(\alpha,\lambda)$ distribution

$$f(x) = \begin{cases} \dfrac{1}{\lambda\Gamma(\alpha)} x^{\alpha-1} e^{x/\lambda} & x > 0 \\ 0 & x \leq 0 \end{cases}$$

where $\Gamma(\alpha)$ is the Euler gamma function. We have used the values $\lambda = 0.5$ and $\alpha = 2,3,4$ (see Fig. 4.9) and rescaled d by a factor 0.5 nm to have a value less than 1 with very high probability, as confirmed by the simulation.

In order to validate our findings, the results are compared with those obtained by using the DG method but with values of d set equal to the mean values of the considered distribution ($\alpha\lambda$ for the $\Gamma(\alpha,\lambda)$ one) rescaled by the factor 0.2 nm. The agreement is still excellent.

We would like to conclude by observing that both the materials seem only slightly influenced by the stochastic effect related to the randomness of the impurity positions.

Chapter 5

Thermal effects and heating rate in monolayer graphene

5.1 Introduction

In [65, 66], we studied the thermal effects in graphene. Some of the most important improvements with respect to results in the literature are the following:

- acoustic phonons aren't at a thermal bath and we don't use any empirical formula for their heating;
- all the phonon populations are considered, then also the flexural acoustic *ZA* and optical *ZO* in addition to the planar ones; they don't give any contribution in the interactions with electrons but are important in the determination of the heating evolution; for the *ZA* we use a quadratic dispersion relation and not the linear approximation;
- the phonon distribution function is not approximated by an equivalent Bose-Einstein one;
- we define a global temperature for the crystal lattice;
- we are able to find a formula to predict the heating for any time and any value of the applied electrical field and of the Fermi level.

Charge transport in graphene has been investigated in several papers, e.g. see [36, 17, 26, 44, 49, 48], but in the most part the thermal effects of the crystal lattice are neglected. Here, we include also the lattice temperature as dynamical variable. Indeed, self-heating is a major issue in nano-electronics and an efficient power removing system requires a good modeling

of the behaviour of the lattice temperature related to the charge transport under an applied electric field.

Thermal effects in monolayer graphene due to an electron flow are investigated with a Direct Simulation Monte Carlo (DSMC) analysis. The crystal heating is described by simulating the phonon dynamics of the several relevant branches, acoustic, optical, K and Z phonons. The contribution of each type of phonon is highlighted. In particular, it is shown that the Z phonons, although they do not enter the scattering with electrons, play a non negligible role in the determination of the crystal temperature.

The phonon distributions are evaluated by counting the emission and absorption processes during the MC simulation. The rate of rise in the crystal temperature is obtained for several applied electric fields and for several positive Fermi energies. The latters produce the effect of a kind of n-doping in the graphene layer. Critical temperatures can be reached in few tens of picoseconds posing significant issues regarding the cooling system in view of a possible application of graphene in semiconductor devices. On the contrary, it is observed only a slight influence of the lattice temperature on the characteristic curves confirming graphene rather robust as regards the electrical performance.

A similar problem has been tackled in [67, 38] with an accurate numerical method based on the WENO scheme but retaining the acoustic phonons at equilibrium or by changing their temperature with an empirical formula. Moreover, the Z-phonons have been neglected.

5.2 The mathematical model

The complete model consists of the semiclassical Boltzmann equations for charges as shown in Chapter 1 and for each species of phonons (acoustic, optical, K and Z). The transport equation is solved by the Direct Simulation Monte Carlo (DSMC) scheme developed in Chapter 2 which properly takes into account the Pauli exclusion principle. Here, we consider the in plane optical phonons as two distinct branches and not an equivalent one as done before in this thesis. We remind that the general form of the scattering rate is

$$\begin{aligned} S_{\ell',s',\ell,s}(\mathbf{k}',\mathbf{k}) \;=\; & \sum_A \left| G^{(A)}_{\ell',s',\ell,s}(\mathbf{k}',\mathbf{k}) \right|^2 \left[\left(g_A^- + 1\right) \delta\left(\varepsilon_{\ell,s}(\mathbf{k}) - \varepsilon_{\ell',s'}(\mathbf{k}') + \hbar\,\omega_A\right) \right. \\ & \left. + g_A^+ \, \delta\left(\varepsilon_{\ell,s}(\mathbf{k}) - \varepsilon_{\ell',s'}(\mathbf{k}') - \hbar\,\omega_A\right) \right]. \end{aligned}$$

The index A labels the Ath phonon mode. The $\left| G^{(A)}_{\ell',s',\ell,s}(\mathbf{k}',\mathbf{k}) \right|^2$'s are the electron-phonon coupling matrix elements, which describe the interaction mechanism of an electron with the Ath phonon, from the state of wave-vector $\mathbf{k}'$ belonging to the valley ℓ' and band s' to the state $\mathbf{k}$ belonging to the valley ℓ and band s. The symbol δ denotes the Dirac distribution, ω_A

is the Ath phonon frequency, $g_A(\mathbf{q})$ is the phonon distribution for the A-type phonons with $\mathbf{q}$ the phonon wave-vector belonging to B. In (5.1) $g_A^{\pm} = g_A(\mathbf{q}^{\pm})$, where $\mathbf{q}^{\pm} = \pm(\mathbf{k}' - \mathbf{k})$, stemming from the momentum conservation.

For acoustic phonons, we assume the elastic approximation according to which the transition rate reads

$$\frac{1}{(2\pi)^2} \frac{\pi D_{ac}^2 k_B T}{2\hbar \sigma_m v_s^2} \left(1 + \cos \vartheta_{\mathbf{k},\mathbf{k}'}\right) \delta\left(\varepsilon(\mathbf{k}') - \varepsilon(\mathbf{k})\right), \tag{5.1}$$

where D_{ac} is the acoustic phonon coupling constant, v_p is the sound speed in graphene, σ_m is the graphene density, and $\vartheta_{\mathbf{k},\mathbf{k}'}$ is the convex angle between $\mathbf{k}$ and $\mathbf{k}'$.
The electron-phonon coupling matrix elements of the longitudinal optical (LO), the transversal optical (TO) and the K phonons are (see for example [38])

$$\left|G^{(LO)}(\mathbf{k}',\mathbf{k})\right|^2 = \frac{1}{(2\pi)^2} \frac{\pi D_O^2}{\sigma_m \omega_O} \left(1 - \cos(\vartheta_{\mathbf{k},\mathbf{k}'-\mathbf{k}} + \vartheta_{\mathbf{k}',\mathbf{k}'-\mathbf{k}})\right) \tag{5.2}$$

$$\left|G^{(TO)}(\mathbf{k}',\mathbf{k})\right|^2 = \frac{1}{(2\pi)^2} \frac{\pi D_O^2}{\sigma_m \omega_O} \left(1 + \cos(\vartheta_{\mathbf{k},\mathbf{k}'-\mathbf{k}} + \vartheta_{\mathbf{k}',\mathbf{k}'-\mathbf{k}})\right) \tag{5.3}$$

$$\left|G^{(K)}(\mathbf{k}',\mathbf{k})\right|^2 = \frac{1}{(2\pi)^2} \frac{2\pi D_K^2}{\sigma_m \omega_K} \left(1 - \cos \vartheta_{\mathbf{k},\mathbf{k}'}\right), \tag{5.4}$$

where D_O is the optical phonon coupling constant, ω_O the optical phonon frequency, D_K is the K phonon coupling constant and ω_K the K phonon frequency. The angles $\vartheta_{\mathbf{k},\mathbf{k}'-\mathbf{k}}$ and $\vartheta_{\mathbf{k}',\mathbf{k}'-\mathbf{k}}$ denote the convex angles between $\mathbf{k}$ and $\mathbf{k}' - \mathbf{k}$ and between $\mathbf{k}'$ and $\mathbf{k}' - \mathbf{k}$, respectively.

In the sequel we will consider only cases of high values of the Fermi energy, which are equivalent for conventional semiconductors to a n-type doping. Under such a condition the dynamics of the electrons belonging to the valence band can be neglected.

Acoustic phonon scattering is intra-valley and intra-band. Optical phonon scattering is intra-valley and can be longitudinal optical (LO) and transversal optical (TO); it can be intra-band, leaving the electrons in the same band, or inter-band, pushing the electrons from the initial band toward another one. Scattering with phonons of K type pushes electrons from a valley to a nearby one (inter-valley scattering). Regarding the optical and K phonons we will assume the Einstein approximation: $\hbar\omega_\eta$ is constant, $\eta = LO, TO, K$. Instead for the in plane (LA, TA) acoustic phonons the Debye approximation will be assumed, $\hbar\omega_{ac} = \hbar v_s q$ with v_s the sound speed in graphene, and the Brillouin zone will be consistently extended to $\mathbb{R}^2$.

For the simulation we use the same parameter of the previous chapters.

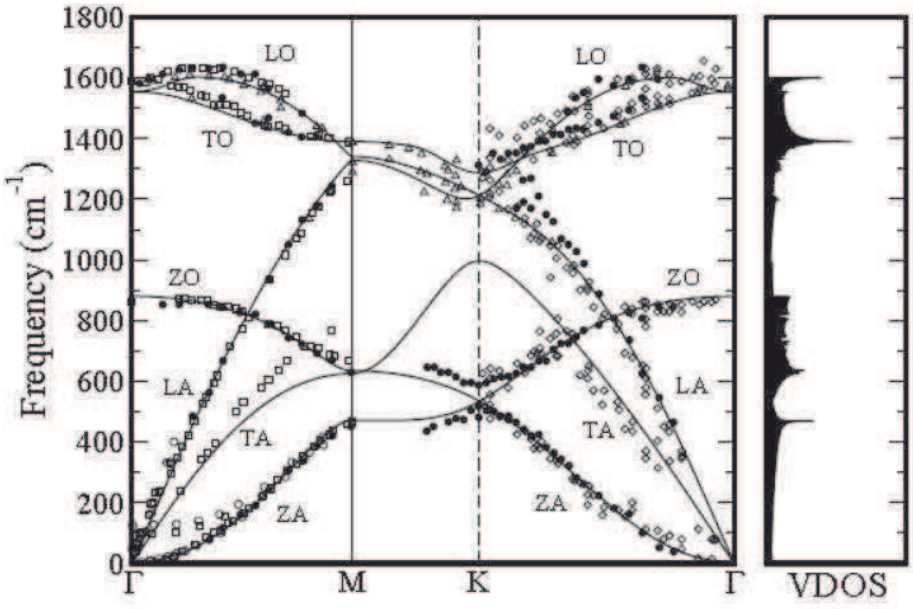

Fig. 5.1 Phonon dispersion for graphene(solid lines) and experimental data for graphite, reported from [71].

The evolution of the phonon distributions is governed by the following Boltzmann equations

$$\frac{g_\eta}{\partial t} = C_\eta\,, \quad \eta = LO, TO, ZO, K \tag{5.5}$$

$$\frac{g_{ac}}{\partial t} + \mathbf{c}_{ac} \cdot \nabla_{\mathbf{x}} g_{ac} = C_{ac}\,, \quad ac = (LA + TA), ZA \tag{5.6}$$

with $\mathbf{c}_{ac} = \nabla_{\mathbf{q}} \omega_{ac}$ the acoustic group velocity (on account of the Einstein approximation, the group velocity of the other phonons is negligible). The collision terms C_η and C_{ac} describe the interaction of the phonons with the electrons and the other phonons. It is worth to stress that we consider also ZO (transversal optical), and ZA (tranversal acoustic) phonons in addition to the transversal (TA) and longitudinal (LA) acoustic ones, that are considered here as a unique in-plane population. The Z-phonons don't give any contribution to the electron-phonon interactions but they are important for the phonon-phonon ones and, therefore, for an accurate description of the time evolution of the lattice temperature.

For the energy of ZA phonons we use a quadratic dispersion relation $\hbar\omega_{ZA} = \hbar\alpha\,|\mathbf{q}|^2$, where $\alpha = 6.2 \cdot 10^{-7}\mathrm{m}^2/\mathrm{s}$ (see for example [69, 70]). In Fig 5.1 the phonon dispersion curves are reported.

The phonon-phonon collision term is very complicated and represents a formidable task from a numerical point of view. For these reasons, in the applications the Bhatnagar-Gross-

Krook (BGK) approximation is usually employed. It gives a simple way to describe the tendency of each species of phonon to an equilibrium distribution. We adopt the same approach in [72], modeling the phonon-phonon interaction by requiring that each type of phonon branch relaxes to a local equilibrium given by a Bose-Einstein distribution evaluated, for all the phonons species, with a common local equilibrium temperature T_{LE}, determined by the procedure we will specify below. Therefore we split the phonon collision terms as follows

$$C_\eta = C_{\eta-e} - \frac{g_\eta - g_\eta^{LE}}{\tau_\eta}\,, \tag{5.7}$$

$$C_{ac} = C_{ac-e} - \frac{g_{ac} - g_{ac}^{LE}}{\tau_{ac}}\,, \tag{5.8}$$

where $C_{\eta-e}$ and C_{ac-e} describe the phonon-electron collisions and are equal to zero for ZO and ZA, τ_η and τ_{ac} are the phonon relaxation times, g_η^{LE} and g_{ac}^{LE} are the local equilibrium phonon distributions given by

$$g_\eta^{LE} = \left[e^{\hbar\omega_\eta/k_B T_{LE}} - 1\right]^{-1}\,, \tag{5.9}$$

$$g_{ac}^{LE} = \left[e^{\hbar c_{ac} q/k_B T_{LE}} - 1\right]^{-1}\,. \tag{5.10}$$

The average phonon energies are given by

$$W_\eta = \frac{y_{ph}}{(2\pi)^2}\int_B \hbar\omega_\eta\, g_\eta\, d\mathbf{q}\,, \quad \eta = LO, TO, ZO, K \tag{5.11}$$

$$W_{ac} = \frac{y_{ph}}{(2\pi)^2}\int_{\mathbb{R}^2} \hbar\omega_{ac}\, g_{ac}\, d\mathbf{q}\,. \quad ac = (LA+TA), ZA. \tag{5.12}$$

Note that the phonon density of state is $1/(2\pi)^2$ and the degeneracy factor y_{ph} is equal to two for $(LA+TA)$, equal to one otherwise. g_η and g_{ac} are the current phonons distribution, updated during the emission and absorption processes counted in the Monte Carlo simulation, and not the Bose-Einstein ones.

By multiplying, for each species, the phonon Boltzmann equation by the phonon energies and integrating with respect to the wave-vector $\mathbf{q}$, one gets the following macroscopic balance equations for the average phonon energies

$$\frac{\partial W_\eta}{\partial t} = C_{W_\eta}\,, \tag{5.13}$$

$$\frac{\partial W_{ac}}{\partial t} + \nabla_{\mathbf{x}}\cdot\mathbf{Q}_{ac} = C_{W_{ac}}\,, \tag{5.14}$$

where $\mathbf{Q}_{ac}$ is the phonon energy-flux, defined as

$$\mathbf{Q}_{ac} = \frac{y_{ph}}{(2\pi)^2} \int_{\mathbb{R}^2} \hbar \omega_{ac} \mathbf{c}_{ac}\, g_{ac}\, d\mathbf{q}\,, \tag{5.15}$$

and

$$C_{W_\eta} = C^{p-e}_{W_\eta} - \frac{W_\eta - W^{LE}_\eta}{\tau_\eta}\,, \tag{5.16}$$

$$C_{W_{ac}} = C^{p-e}_{W_{ac}} - \frac{W_{ac} - W^{LE}_{ac}}{\tau_{ac}} \tag{5.17}$$

are the energy-production terms. Here

$$W^{LE}_\eta = \frac{y_{ph}}{(2\pi)^2} \int_B \hbar \omega_\eta \left[e^{\hbar\omega_\eta / k_B T_{LE}} - 1 \right]^{-1} d\mathbf{q}\,, \quad \eta = LO, TO, ZO, K \tag{5.18}$$

$$W^{LE}_{LA+TA} = \frac{y_{ph}}{(2\pi)^2} \int_B \hbar \omega_{LA+TA} \left[e^{\hbar\omega_{LA+TA} / k_B T_{LE}} - 1 \right]^{-1} d\mathbf{q}\,, \tag{5.19}$$

$$W^{LE}_{ZA} = \frac{y_{ph}}{(2\pi)^2} \int_B \hbar \omega_{ZA} \left[e^{\hbar\omega_{ZA} / k_B T_{LE}} - 1 \right]^{-1} d\mathbf{q} \tag{5.20}$$

are the average energies at the local equilibrium, while $C^{p-e}_{W_\eta}$ and $C^{p-e}_{W_{ac}}$ are the contributions arising from the phonon-electron interactions, equal to zero for ZO and ZA phonons. They satisfy the relationships

$$C^{e-p}_{W_\eta} + C^{p-e}_{W_\eta} = 0\,, \tag{5.21}$$

$$C^{e-p}_{W_{ac}} + C^{p-e}_{W_{ac}} = 0\,. \tag{5.22}$$

We remark that, since the electron flow does not influence the phonon-phonon scatterings, the conservation of the total phonon energy in absence of external field implies

$$\sum_\eta \frac{W_\eta - W^{LE}_\eta}{\tau_\eta} + \sum_{ac} \frac{W_{ac} - W^{LE}_{ac}}{\tau_{ac}} = 0\,. \tag{5.23}$$

Now we turn to give the definition of the local equilibrium temperature according to [72].

Definition 5.2.1 *T_{LE} is the common temperature we must assign to each species in order to have*

$$\sum_\eta W_\eta + \sum_{ac} W_{ac} = \sum_\eta W^{LE}_\eta + \sum_{ac} W^{LE}_{ac}\,. \tag{5.24}$$

In other words, T_{LE} is the common temperature each phonon species should have if they would be at thermodynamic equilibrium in order to preserve the total energy.

We assume that follows in order to define the temperature for each specie of phonons.

Assumption 5.2.1 *The phonon distributions are locally equivalent to a Bose-Einstein one*

$$g_\eta = \left[e^{\hbar\omega_\eta/k_BT_\eta} - 1\right]^{-1}, \quad g_{ac} = \left[e^{\hbar\omega_{ac}/k_BT_{ac}} - 1\right]^{-1}.$$

As consequence the temperatures of the phonon species are related to the respective average energies according to

$$\int_B \hbar\omega_\eta \left[e^{\hbar\omega_\eta/k_BT_\eta} - 1\right]^{-1} d\mathbf{q} = \int_B \hbar\omega_\eta g_\eta(\mathbf{q})\, d\mathbf{q}, \quad \eta = LO, TO, ZO, K \tag{5.25}$$

$$\int_B \hbar\omega_{ac} \left[e^{\hbar\omega_{ac}/k_BT_{ac}} - 1\right]^{-1} d\mathbf{q} = \int_B \hbar\omega_{ac} g_{ac}(\mathbf{q})\, d\mathbf{q}. \quad ac = (LA+TA), ZA \tag{5.26}$$

The current temperature at each time step for each phonon population is calculated solving the previous equations by the standard numerical methods. The Eq. (5.26) for $(LA+TA)$ phonons can be solved analytically by extending the first Brillouin zone to all $\mathbb{R}^2$. One obtains

$$W_{ac} = (k_BT_{ac})^3 \cdot \left(\frac{4y_{ph}\pi\zeta(3)}{(2\pi)^2(\hbar\omega_{ac}/q)^2}\right), \tag{5.27}$$

where $\zeta(s)$ is the zeta function and $A = \frac{8\sqrt{3}\pi^2}{9a_0^2}$ is the area of the first Brillouin zone, with $a_0 = 0.142$ nm the interatomic distance.

By taking into account the assumption 5.2.1 and the expressions (5.18) - (5.20), we find that T_{LE} must satisfy the nonlinear equation

$$\begin{aligned} h(T_{LE}) &= \sum_\eta y_{ph} \frac{\hbar\omega_\eta A}{(2\pi)^2} \left[e^{\hbar\omega_\eta/k_BT_{LE}} - 1\right]^{-1} \\ &+ \sum_{ac} \frac{y_{ph}}{(2\pi)^2} \int_B \hbar\omega_{ac} \left[e^{\hbar\omega_{ac}/k_BT_{LE}} - 1\right]^{-1} d\mathbf{q} = \sum_\eta W_\eta + \sum_{ac} W_{ac} \end{aligned} \tag{5.28}$$

with W_η and W_{ac} the current values of the average phonon energies.

We observe that

$$h'(T_{LE}) = \sum_{\eta} A \cdot \frac{y_{ph}}{(2\pi)^2} \frac{(\hbar\omega_\eta)^2}{k_B T_{LE}^2} \left[e^{\hbar\omega_\eta / k_B T_{LE}} - 1 \right]^{-2} + \sum_{ac} \frac{y_{ph}}{(2\pi)^2} \int_B \frac{(\hbar\omega_{ac})^2 \cdot e^{\hbar\omega_{ac}/k_B T_{LE}}}{k_B T_{LE}^2} \left[e^{\hbar\omega_{ac}/k_B T_{LE}} - 1 \right]^{-2} d\mathbf{q} > 0 \quad \forall T_{LE} > 0 \quad ,$$

$$\lim_{T \mapsto +\infty} h(T) = +\infty, \quad \lim_{T \mapsto 0^+} h(T) = 0,$$

and therefore Eq. (5.28) admits an unique solution for assigned positive W_η's and W_{ac}'s.

By taking into account the definition of T_{LE}, a simple way to satisfy Eq. (5.23) is to take

$$\tau_\eta = \tau_{ac} = \tau. \tag{5.29}$$

In the sequel the phonon relaxation times will considered as equal.

5.3 Simulation strategy

For a homogeneous monolayer graphene under a constant electric field **E**, the only significative components of the evolution equations are those parallel to the field and there is not dependence on the spatial variables. By choosing a reference frame in the plane of the graphene sheet with the x-axis parallel to **E**, the complete model consists of the following equations

$$\frac{\partial f(t,\mathbf{k})}{\partial t} - \frac{e}{\hbar}\mathbf{E}\frac{\partial f(t,\mathbf{k})}{\partial k_x} = \int S(\mathbf{k}',\mathbf{k})\, f(t,\mathbf{k}')\,(1 - f(t,\mathbf{k}))\, d\mathbf{k}' - \int S(\mathbf{k},\mathbf{k}')\, f(t,\mathbf{k})\left(1 - f(t,\mathbf{k}')\right) d\mathbf{k}', \tag{5.30}$$

$$\frac{\partial g_\eta(t,\mathbf{q})}{\partial t} = C_{\eta-e}(\mathbf{q}) - \frac{g_\eta - g_\eta^{LE}}{\tau_\eta}, \tag{5.31}$$

$$\frac{\partial g_{ac}(t,\mathbf{q})}{\partial t} = C_{ac-e}(\mathbf{q}) - \frac{g_{ac} - g_{ac}^{LE}}{\tau_{ac}}, \tag{5.32}$$

$$W_\eta = \frac{y_{ph}}{(2\pi)^2} \int_B \hbar\omega_\eta\, g_\eta(\mathbf{q})\, d\mathbf{q}, \quad \eta = LO, TO, ZO, K \tag{5.33}$$

$$W_{ac} = \frac{y_{ph}}{(2\pi)^2} \int_{\mathbb{R}^2} \hbar\omega_{ac}\, g_{ac}(\mathbf{q})\, d\mathbf{q}. \quad ac = (LA+TA), ZA. \tag{5.34}$$

Similar equations hold for the K' valley. As initial condition for the electrons we take the Fermi-Dirac distribution

$$f(0,\mathbf{k}) = \frac{1}{1+\exp\left(\dfrac{\varepsilon(\mathbf{k})-\varepsilon_F}{k_B T_0}\right)},$$

where T_0 is the room temperature (300 K) and ε_F is the Fermi energy, which is related to the initial charge density by

$$\rho(0) = \frac{4}{(2\pi)^2}\int f(0,\mathbf{k})\, d\mathbf{k}\,. \tag{5.35}$$

As said, in (5.35) the factor 4 arises because we are considering both the two states of spin and the degeneracy (equal to 2) of the valley. As alternative one can consider the population of a single valley, and put equal to one the valley degeneracy and take in (5.35) $\rho(0)/2$ for the electron density. Note that in the unipolar case ρ remains constant, $\rho(t) = \rho(0)$, as a consequence of the charge conservation.

Regarding the phonons, we assume that initially all the phonons are at the room temperature T_0 and described by Bose-Einstein distributions. Therefore the initial conditions for the phonon average energies are given by (5.18)-(5.20) with $T_{LE} = T_0$.

Let us introduce an uniform time-step Δt and denote by t_n the nth time level. For each interval $[t_n, t_n + \Delta t]$ we solve Eq. (5.30) by the Direct Simulation Monte Carlo scheme by freezing the phonon temperatures to the values they have at $t = t_n$.

By discretizing the Eq.s (5.31)-(5.32) with the explicit Euler method, we obtain the current values of the phonon distributions g_{ac} and g_η and numerically calculate the energy densities by means of Eq.s (5.33)-(5.34). T_{LE} is evaluated at the time step t_n by taking into account Eq.s (5.24)-(5.26).

The Brillouin zone is approximated by a square grid centered at the Γ point. The approximation with a square grid doesn't introduce appreciable errors because the values of the phonons distributions are close to zero far from the Γ point.

The phonons distribution is a Bose-Einstein one for $t = 0$ and it is updated at each time step using the scatterings dynamics. For this purpose, we need to know the production terms of Eq.s (5.31)-(5.32), $C_{\eta-e}(\mathbf{q})$ and $C_{ac-e}(\mathbf{q})$, that represent the rate of variation of the phonon populations per unit time and are proportional to the difference between the number of emission and absorption processes, $n^+(\mathbf{q})$ and $n^-(\mathbf{q})$ respectively, due to the electron-phonon scatterings. These are evaluated using the intermediate results of the DSMC part, counting them in each time window $[t_{n-1}, t_n]$ and in each elementary cell of the grid in the $\mathbf{q}$-space. In the acoustic transition rate, under the elastic approximation, the number of emission scatterings balances exactly that of absorption ones leading to a zero net energy

production. Moreover, there aren't scattering events with the out of plane ZA and ZO phonons; therefore, $C_{ac-e} = C_{ZO-e} = 0$ and the only relevant contributions come from the LO, TO and K phonons.

For each scattering event, we consider whether is an absorption or an emission one and calculate the wave-vector $\mathbf{q}$ and the cell to be updated taking into account the momentum conservation $\mathbf{q}^{\pm} = \pm(\mathbf{k}' - \mathbf{k})$. The values of the phonons distributions in the cell the wave-vector belong to is updated by augmenting or decreasing the number of phonons per unit cell by using the values $n^-$and n^+ obtained from the MC simulation as follows.

The crucial point is to define the suitable statistical weight, β_{scatt}, for each phonon, in order to estimate the correct values of the production terms as $C_{\eta-e}(\mathbf{q}) = \beta_{scatt}\left(n^+(\mathbf{q}) - n^-(\mathbf{q})\right)$.

As known in the literature [76, 78], the global phonon energy production term is given by

$$C_W^{p-e} = \frac{\rho}{N_P \Delta t} \hbar\omega_\eta \left(C_{tot}^+ - C_{tot}^-\right), \tag{5.36}$$

where ρ is the electron density, N_P the number of (super)-particles used for electrons in the DSMC, C_{tot}^+ and C_{tot}^- are the total number of emission and absorption process in the whole Brillouin zone. This is the density energy variation per unit time due to the phonon distribution variation $\Delta g_\eta(\mathbf{q})$ associated with scattering events that on account of the Einstein approximation for $\hbar\omega_\eta$ can be written as

$$C_W^{p-e} = \frac{1}{(2\pi)^2} \int_B \hbar\omega_\eta \Delta g_\eta(\mathbf{q}) d\mathbf{q} = \frac{\hbar\omega_\eta}{(2\pi)^2} \int_B C_{\eta-e}(\mathbf{q}) d\mathbf{q}. \tag{5.37}$$

If we denote the generic cell of the grid by C_α, by comparing (5.36) and (5.37), and performing numerically the integration by the middle point formula, one has

$$\begin{aligned} \int_B C_{\eta-e}(\mathbf{q}) d\mathbf{q} &\approx \frac{(2\pi)^2 \rho}{N_P \Delta t} \left(C_{tot}^+ - C_{tot}^-\right) = \frac{(2\pi)^2 \rho}{N_P \Delta t} \sum_\alpha \int_{C_\alpha} \left(C^+(\mathbf{q}) - C^-(\mathbf{q})\right) d\mathbf{q} \\ &\approx \frac{(2\pi)^2 \rho}{N_P \Delta t} \sum_\alpha \frac{n^+(\mathbf{q}) - n^-(\mathbf{q})}{(\Delta q)^2} (\Delta q)^2 \end{aligned} \tag{5.38}$$

where $C^{\pm}(\mathbf{q})$ is the pure number of processes in each cell per unit area, that is $C^{\pm}(\mathbf{q}) = n^{\pm}(\mathbf{q})/(\Delta q)^2$. Therefore, the average value of $C_{\eta-e}$ in each cell, $\bar{C}_{\eta-e}$, is given by

$$\bar{C}_{\eta-e} \approx \frac{(2\pi)^2 \rho}{N_P \Delta t} \frac{n^+(\mathbf{q}) - n^-(\mathbf{q})}{(\Delta q)^2}. \tag{5.39}$$

This implies that the statistical weight associated at each emission and absorption event, or equivalently at the numbers $n^{\pm}(\mathbf{q})$, used to update the phonon distribution at each time step

is equal to

$$\beta_{scatt} = \frac{(2\pi)^2 \rho}{N_P \Delta t (\Delta q)^2}\,. \tag{5.40}$$

5.4 Simulation results

Lattice heating due to the electron flow is considerably important in graphene. It can influence the electrical characteristics but can also create hot spots with rather high temperatures and the possibility of damaging the material. The main aim of our simulations is to evaluate the heating rate of a monolayer graphene induced by charge carriers under a constant electric field.

$N_P = 10^4$ particles have been used. The time step has been set as $\Delta t = 2.5$ fs and a constant phonon relaxation time has been adopted, $\tau = 5$ ps which is a values of the order of those already used in the literature [73]. In [38] a phonon relaxation time depending on the temperature has been adopted but it is strictly valid only for low electric fields. Indeed, more accurate expressions are still lacking and represent an open problem.

Several Fermi energies have been considered in order to investigate the dependence of the rise in temperature also on the electron density and not only on the applied field. The shift of the Fermi level from the Dirac point inside the conduction band cone can be obtained in suspended graphene with gate contacts [79]. In graphene over a SiC substrate it is due to chemical effects (see for example [80] where other cases are discussed as well).

In Fig. 5.2 the evolution of the temperatures of each type of phonons along with T_{LE} is plotted. The latter can be identified as the temperature of the crystal lattice and can therefore be directly related to the measurements. The most energetic phonons are the optical ones while the least energetic phonons are the acoustic ones. Note that the LO, TO and K phonons have different temperatures while the $(LA+TA)$, ZA, ZO phonons have practically the same temperature. One observes that the raise rate of the temperature, as experimentally expected [74], increases with the electric field, roughly speaking, in a linear way.

In order to study the influence of the heating effects on the electron transport and, therefore, the influence of the crystal heating on the characteristic curves, we have also performed a comparison with the case when the phonons are kept at equilibrium with the room temperature. In Fig. 5.3, a comparison of the average electron velocity and energy is shown between the case with the lattice heating and that with the phonons kept at room temperature. The differences in the average energy and velocity are negligible and this is a sign of goodly stable electrical properties of graphene with respect to thermal disturbances. The slight variation in the shape of the electron distribution function, as shown in Fig. 5.4, does not affect in a sizable way the expectation values, in particular the velocity and therefore

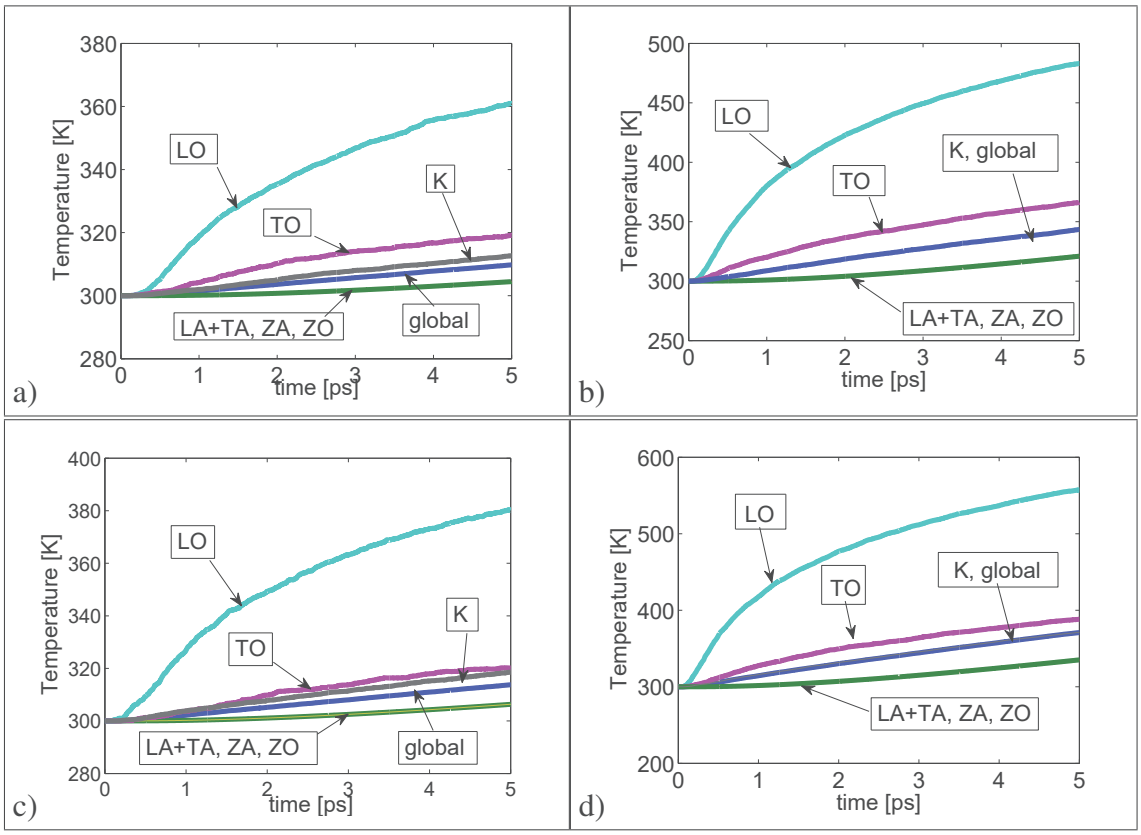

Fig. 5.2 Phonon temperatures and local equilibrium temperature T_{LE} versus time in the case $\varepsilon_F = 0.4$ eV when $E = 5$ kV/cm (a), $E = 20$ kV/cm (b), and in the case $\varepsilon_F = 0.6$ eV when $E = 5$ kV/cm (c) and $E = 20$ kV/cm (d).

the electric current $\mathbf{J} = -ne\mathbf{V}$. This implies that the use of the characteristic curves obtained with the phonons as a thermal bath are rather accurate and can be used in the engineering applications, at least for low and moderate electric fields.

If the Z phonons are neglected as in [65], at high fields one observes a lowering of the velocity by increasing the electric field. The effect disappears when the Z phonons are included in the simulations (see Fig. 5.5).

Regarding the phonons distributions, in Figs (5.6)-(5.7)-(5.8) we show the comparisons between the initial (the Bose-Einstein ones) and the final distributions. The most important difference is located at the centre of the Brillouin zone.

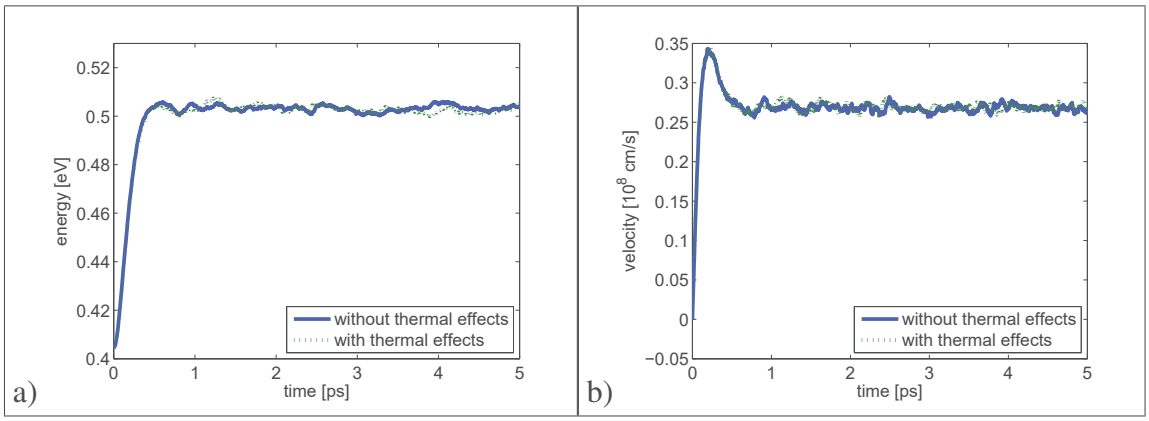

Fig. 5.3 Comparison of energy a) and velocity b) versus time without and with thermal effects in the case $\varepsilon_F = 0.6$ eV and $E = 20$ kV/cm .

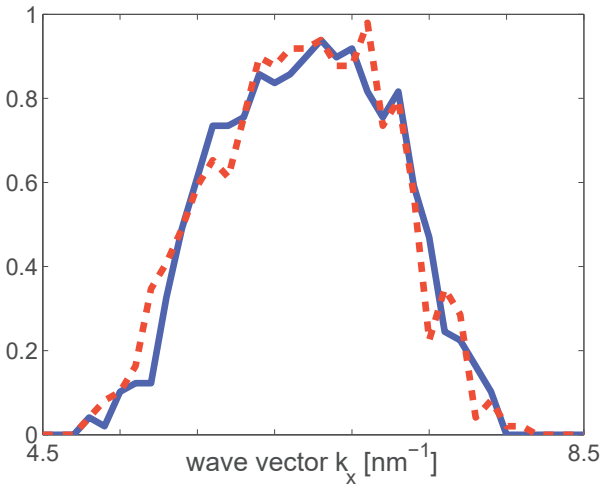

Fig. 5.4 Comparison of distribution functions with (dashed line) and without (continuous line) thermal effects with $E = 20$ kV/cm and $\varepsilon_F = 0.6$ eV after 10 ps.

5.5 Heating rate

Now, we focus our attention on the behaviour of the global equilibrium temperature versus time in order to deduce an analytical formula for the heating rate depending on the Fermi energy (or equivalently on the electron density) and the electric field. As shown in Figs 5.9-5.10, a linear dependence with respect to time is a good approximation, with only a very small error for times very close to $t = 0$ (Fig. 5.11)

$$T_{LE} = T_0 + mt. \tag{5.41}$$

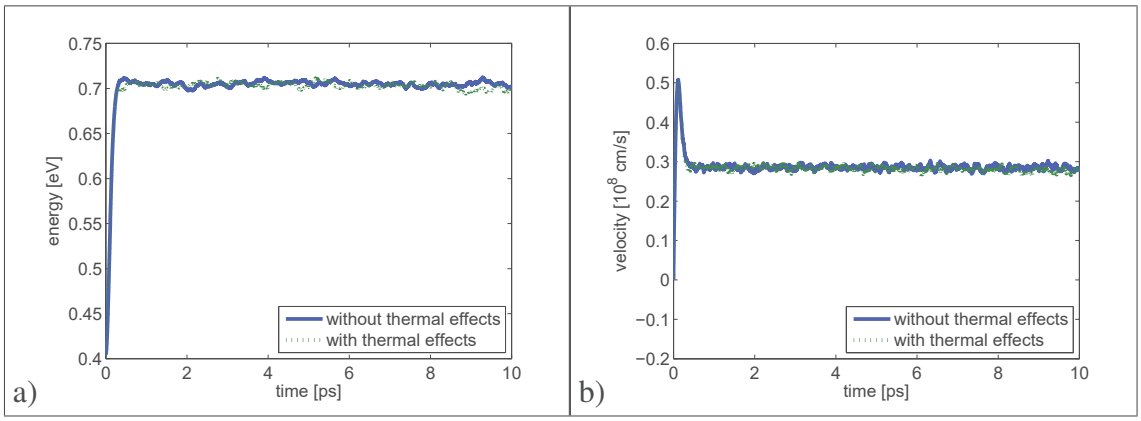

Fig. 5.5 Average electron energy and velocity versus time in the case $\varepsilon_F = 0.6$ eV, $E = 50$ kV/cm.

Taking into account the slope of each time-temperature curve, we look for a fitting of the angular coefficient m with respect both to the Fermi level and the applied electric field. In Fig. 5.12 m as a function of the electric field and the Fermi level is shown.

We seek for a polynomial fitting of the type

$$m = (a_0 + a_1 \cdot E + a_2 \cdot E^2 + \ldots + a_p \cdot E^p) \cdot (b_0 + b_1 \cdot \varepsilon_F + b_2 \cdot \varepsilon_F^2 + \ldots + b_q \cdot \varepsilon_F^q) \qquad (5.42)$$

a_i, b_j and p, q are parameters to be determined via a regression analysis of the data obtained with the simulations. A very good agreement is obtained with $p = 4$ and $q = 3$, as the statistical parameters of Tab. 5.1 indicate. In this table R_{pq} represents the determination coefficient varying the degree of the polynomials in the fitting formula. For the sake of completeness the adjusted determination coefficient is reported as well. Although there are good results even with lower values of p and q, the statistical model is well explained only with $p > 3$ and $q > 2$; this is clear comparing the residuals distributions with respect to the response function, Fig. 5.13, and with respect to the electric field, Fig. 5.14, and to the Fermi levels with those of other cases, for examples Figs 5.15-5.18. Only in the case with $p = 4$ and $q = 3$, the residual distributions don't show any strong correlation between the independent variable and the predictor.

Therefore, we have

$$m = (a_0 + a_1 \cdot E + a_2 \cdot E^2 + a_3 \cdot E^3 + a_4 \cdot E^4) \cdot (b_0 + b_1 \cdot \varepsilon_F + b_2 \cdot \varepsilon_F^2 + b_3 \cdot \varepsilon_F^3) = \sum_{i,j} \gamma_{ij} E^i \cdot \varepsilon_F^j. \qquad (5.43)$$

The fitting parameters are listed in Table 5.2.

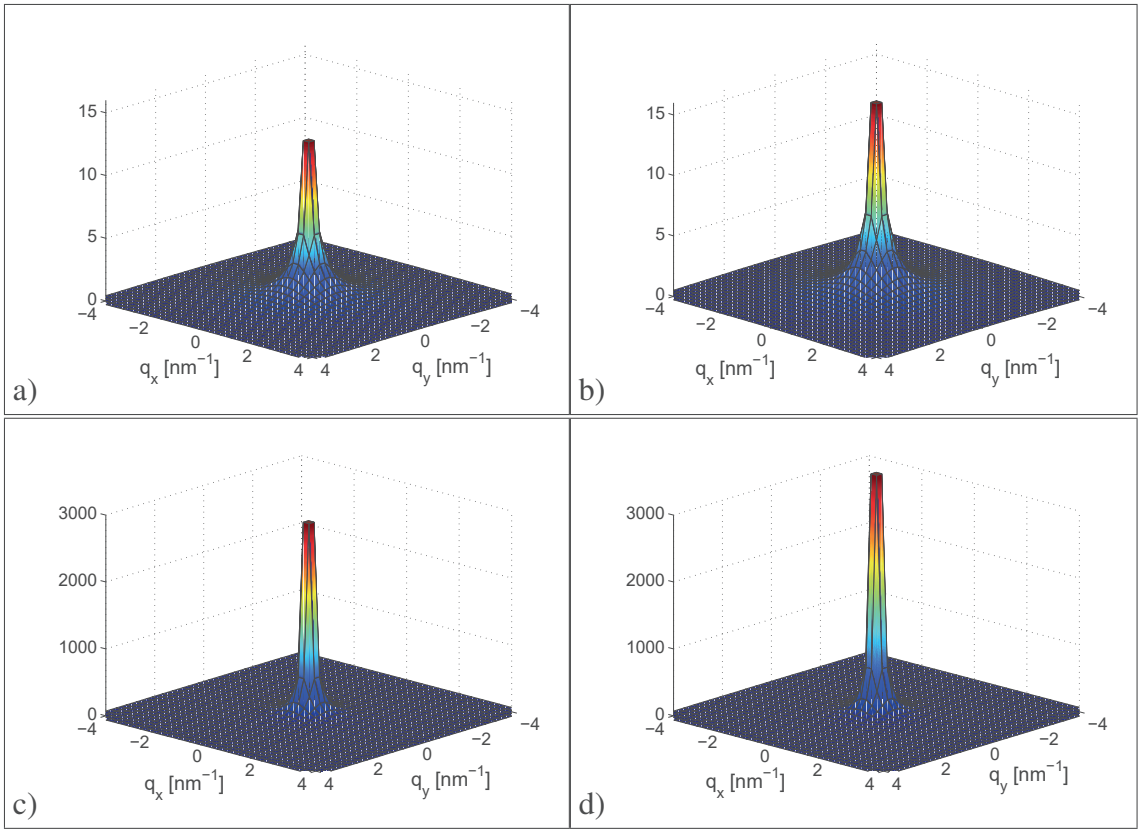

Fig. 5.6 initial $(LA+TA)$ distribution (a), final $(LA+TA)$ distribution after 10 ps (b), initial ZA distribution (c), final ZA distribution after 10 ps (d), in the case $\varepsilon_F = 0.6$ eV and $E = 20$ kV/cm.

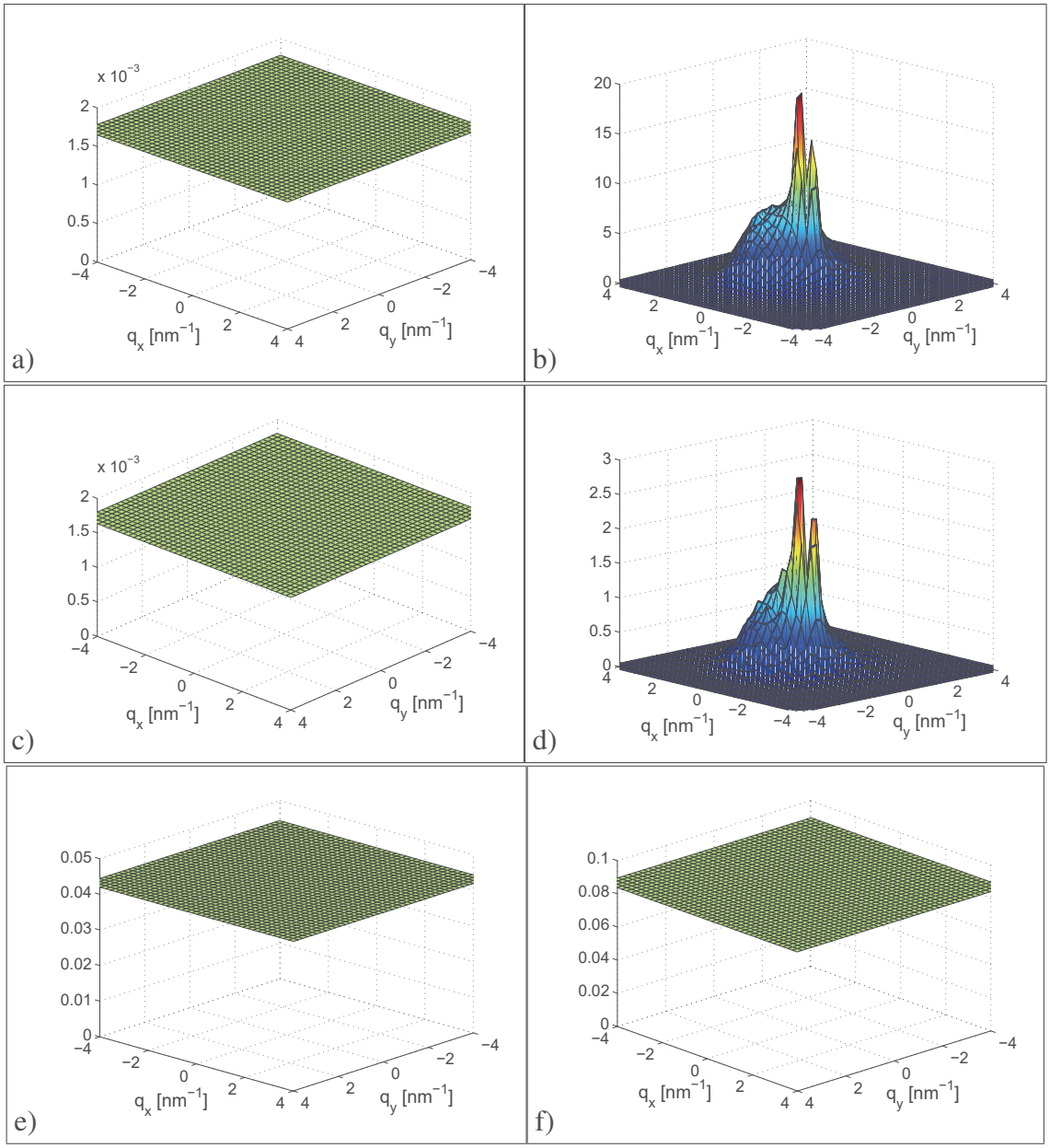

Fig. 5.7 initial LO distribution (a), final LO distribution after 10 ps (b), initial TO distribution (c), final TO distribution after 10 ps (d), initial ZO distribution (e), final ZO distribution after 10 ps (f), in the case $\varepsilon_F = 0.6$ eV and $E = 20$ kV/cm.

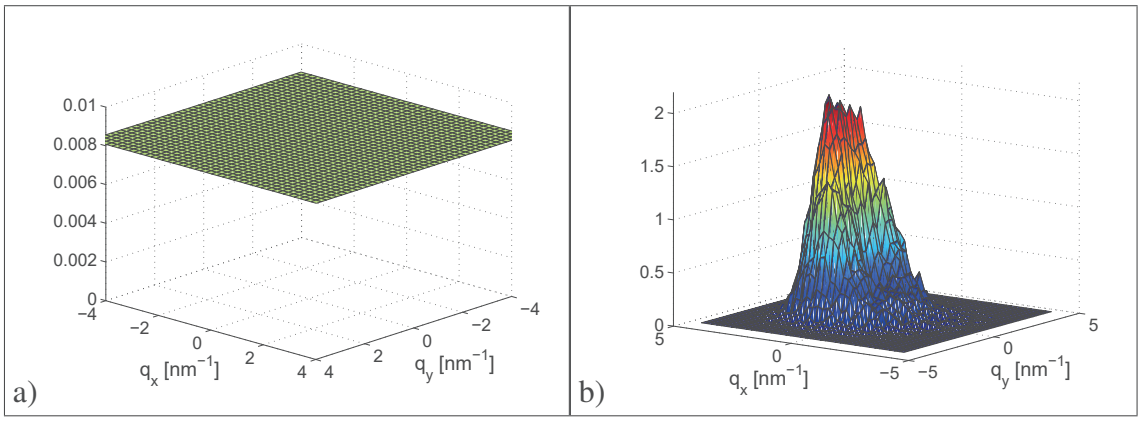

Fig. 5.8 initial K phonons distribution (a), final K phonons distribution after 10 ps (b), in the case $\varepsilon_F = 0.6$ eV and $E = 20$ kV/cm.

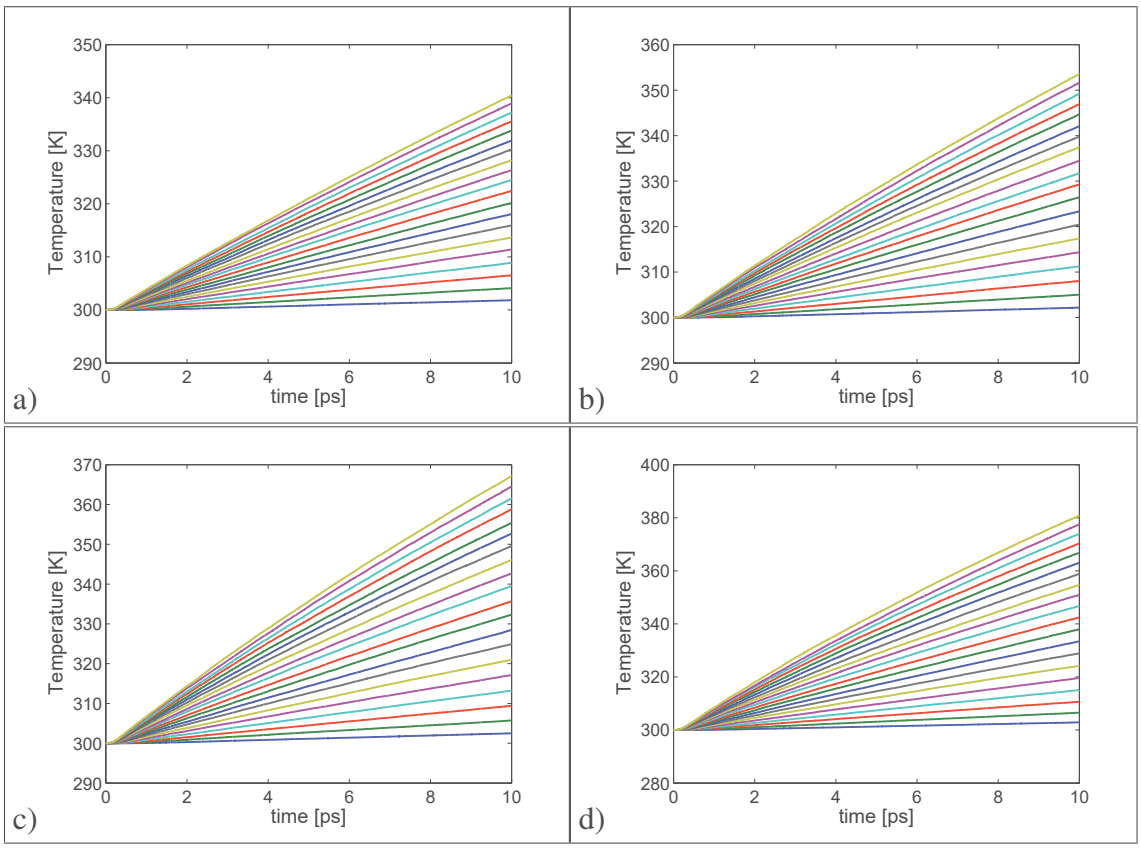

Fig. 5.9 Equilibrium temperature versus time, the electric field varying from 1 kV/cm to 20 kV/cm; from bottom to top: $\varepsilon_F = 0.25$ eV (a), $\varepsilon_F = 0.3$ eV (b), $\varepsilon_F = 0.35$ eV (c), $\varepsilon_F = 0.4$ eV (d).

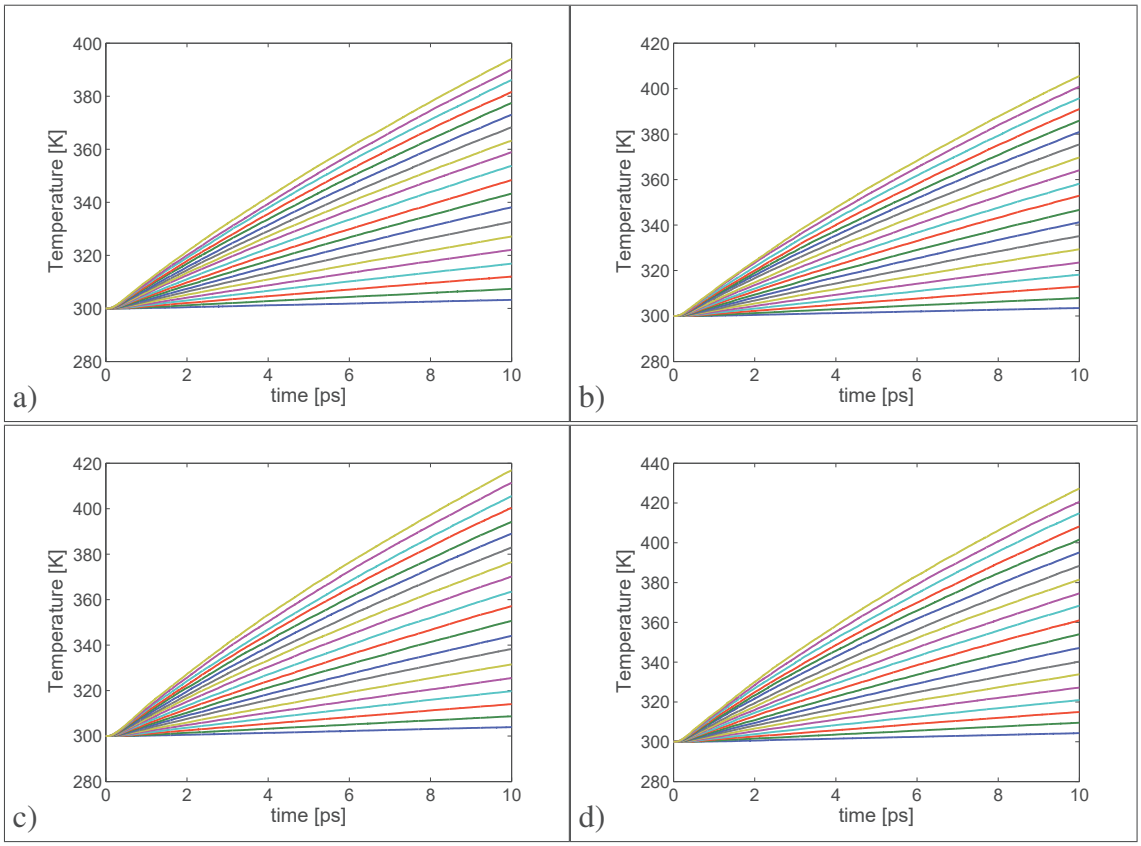

Fig. 5.10 Equilibrium temperature versus time, the electric field varying from 1 kV/cm to 20 kV/cm; from bottom to top: $\varepsilon_F = 0.45$ eV (a), $\varepsilon_F = 0.5$ eV (b), $\varepsilon_F = 0.55$ eV (c), $\varepsilon_F = 0.6$ eV (d).

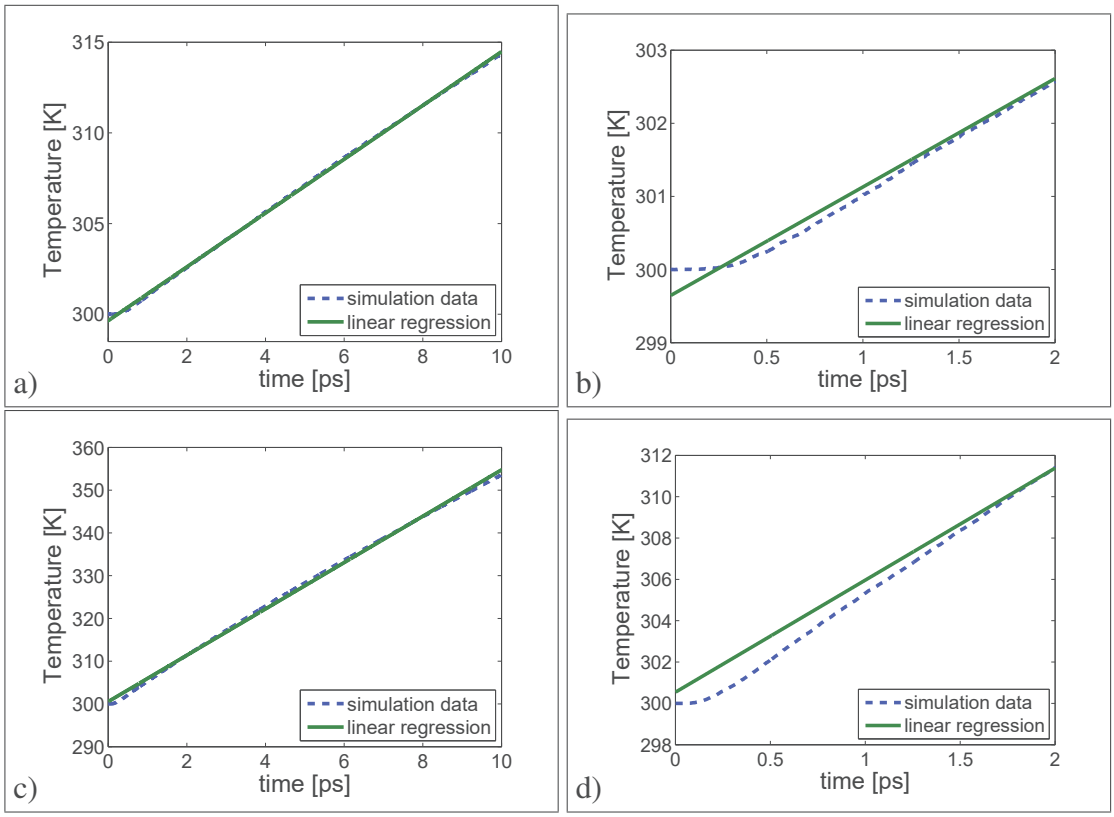

Fig. 5.11 Equilibrium temperature versus time, with $E = 5$ kV/cm and $\varepsilon_F = 0.3$ eV (a), zoom near $t = 0$ ps (b), and with $E = 20$ kV/cm and $\varepsilon_F = 0.3$ eV (c), zoom near $t = 0$ ps (d).

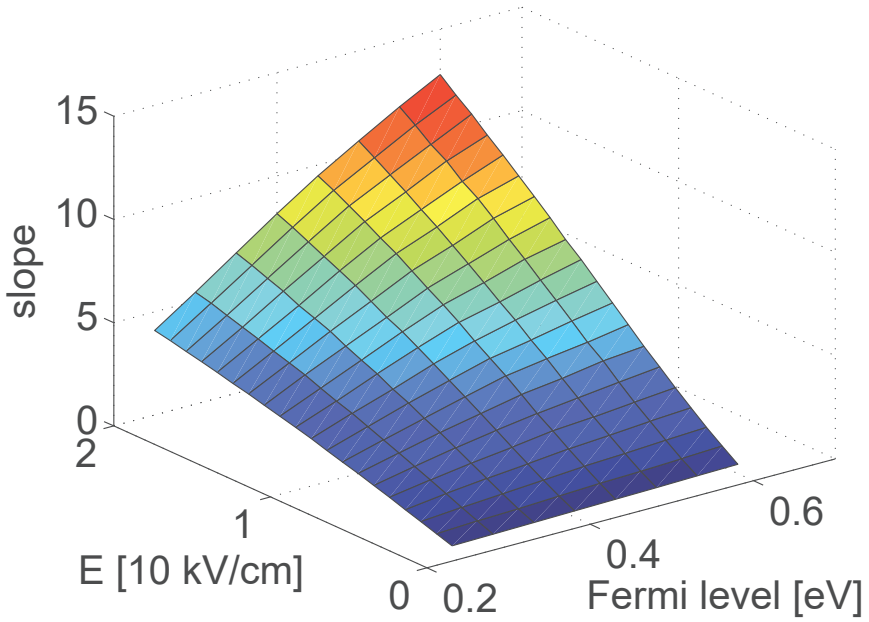

Fig. 5.12 Slope versus Fermi level and electric field.

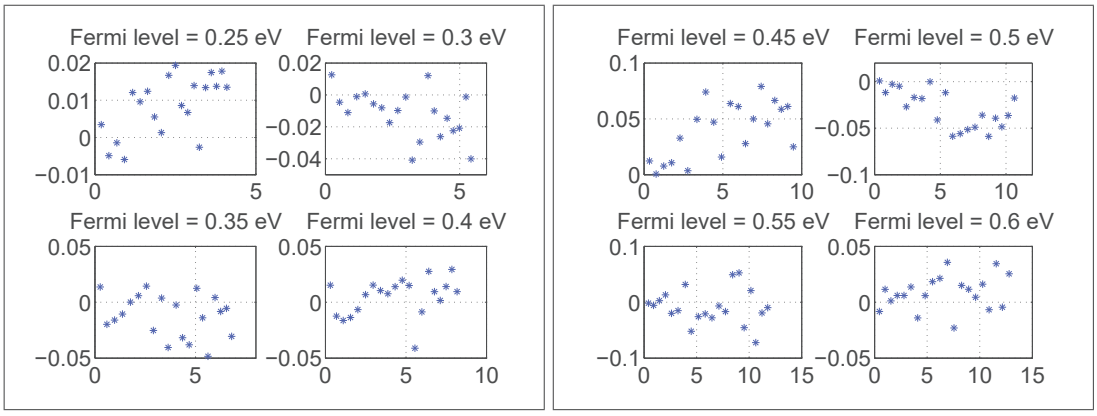

Fig. 5.13 Residual plot with respect to the response data in case p=4, q=3.

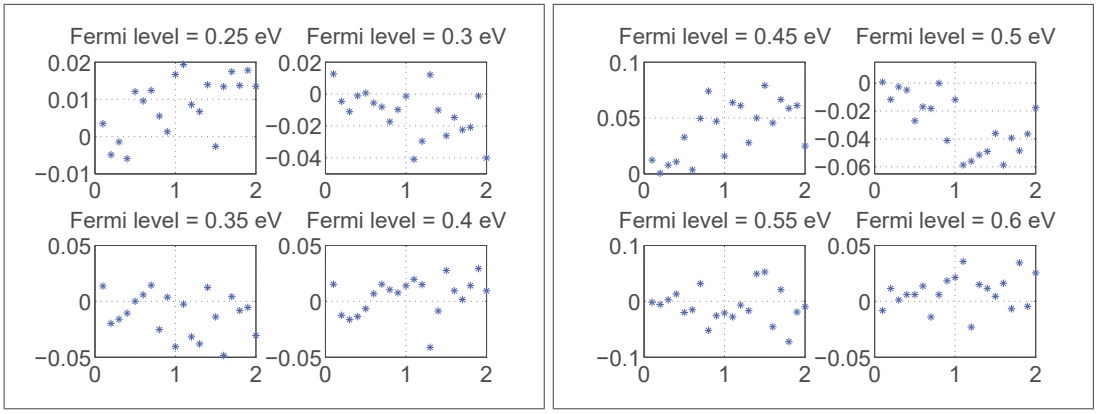

Fig. 5.14 Residual plot with respect to the electric field in case $p = 4$, $q = 3$.

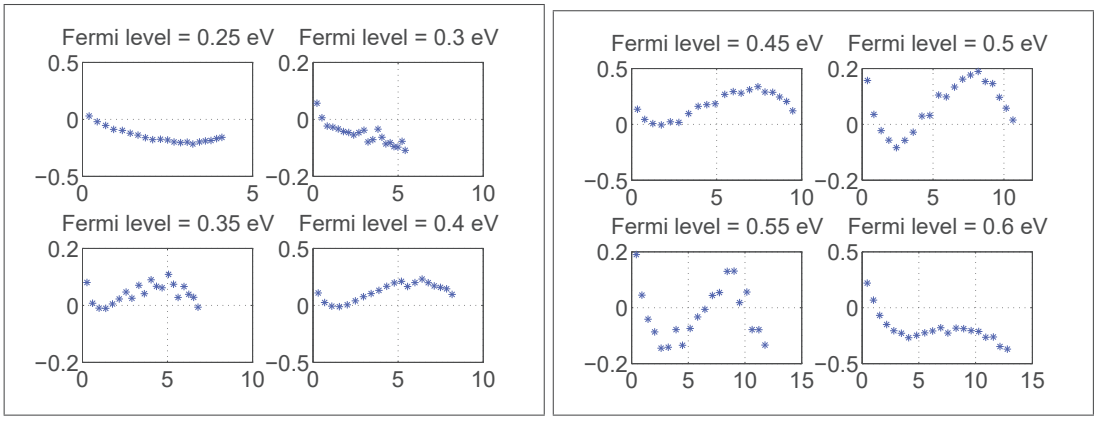

Fig. 5.15 Residual plot with respect to the response data in case $p = 2$, q =1.

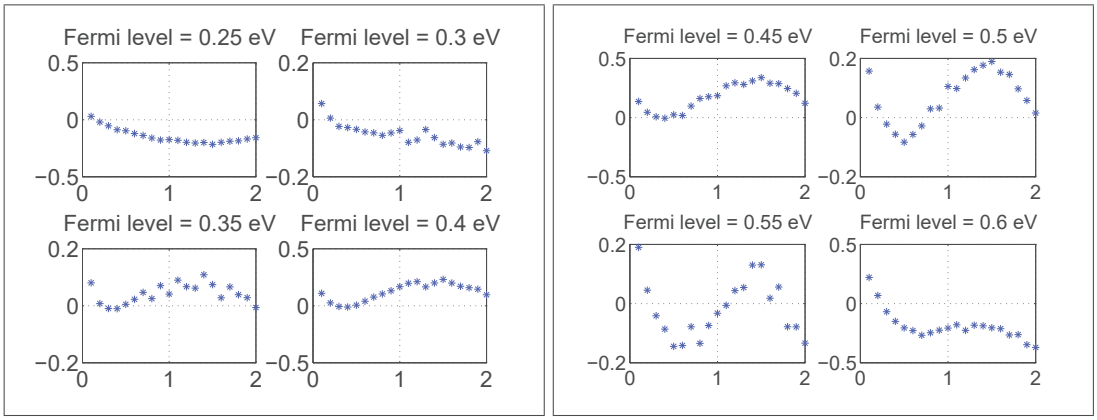

Fig. 5.16 Residual plot with respect to the electric field in case p =2, q =1.

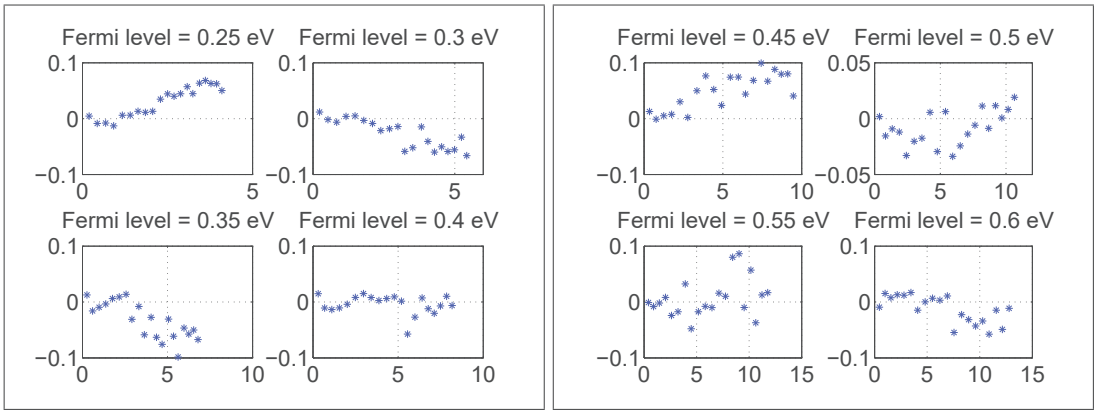

Fig. 5.17 Residual plot with respect to the response data in case $p = 4$, $q = 2$.

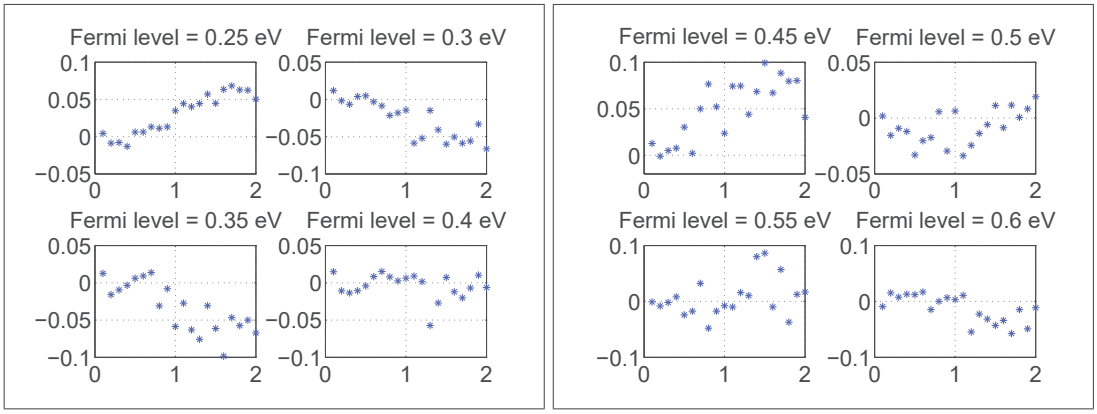

Fig. 5.18 Residual plot with respect to the electric field in case $p = 4$, $q = 2$.

Table 5.1 Determination and adjusted determination coefficients.

$R11$	$R11_{adj}$	$R12$	$R12_{adj}$	$R21$	$R21_{adj}$
0.9972	0.9971	0.9988	0.9988	0.9978	0.9977
$R22$	$R22_{adj}$	$R42$	$R42_{adj}$	$R43$	$R43_{adj}$
0.9995	0.9970	0.9999	0.9998	0.9999	0.9999

Table 5.2 Fitting parameters.

γ_{00}	γ_{01}	γ_{02}	γ_{03}	γ_{10}
0.5565	-4.4479	9.5689	-6.1728	-4.2305
γ_{11}	γ_{12}	γ_{13}	γ_{20}	γ_{21}
45.2239	-89.3014	62.9967	1.0312	-23.6548
γ_{22}	γ_{23}	γ_{30}	γ_{31}	γ_{32}
100.8034	-92.5045	2.1011	-8.7135	-5.1857
γ_{33}	γ_{40}	γ_{41}	γ_{42}	γ_{43}
15.8855	-0.9526	6.2162	-10.5929	5.9443

We predict that the crystal temperature reaches the melting point after about few hundreds of picoseconds.

5.6 Summary

An analysis of the thermal effects in graphene induced by a charge flow under a bias voltage has been performed. All the phonons modes have been taken into account, both in plane and out of plane. The importance of the Z phonons is highlighted and the rate of the temperature rise with respect to time is determined. This latter can be very useful in devising electron devices based on graphene. It furnishes a theoretical basis for design an efficient cooling system for removing the heat produced by the energy transferred by electrons to the lattice via the scattering interactions with the phonon modes.

5.7 A simplified model

In this section, a simplified model for thermal analysis in graphene will be shown; the main important approximations are: the in plane optical phonons populations, LO and TO, are considered as an unique population with the same energy, the out of plane phonon populations are neglected and the phonon distributions are approximated by means of equivalent Bose-Einstein ones at the current temperature. For taking into account the two in plane polarizations

states for optical phonons and the three total polarizations for acoustic ones, in the evaluation of the densities of energy, we consider a density of states equal to $\frac{2}{2\pi}$ and $\frac{3}{2\pi}$, respectively. We would also evaluate the error introduced by such an approximation with respect the previous complete model. The scattering matrix elements and the physical parameters are the same as in the previous sections.

The average phonon energies are

$$W_{LO+TO} = \frac{2}{(2\pi)^2}\int_B \hbar\omega_{LO/TO}\, g_{LO/TO}\, d\mathbf{q}\,, \tag{5.44}$$

$$W_K = \frac{1}{(2\pi)^2}\int_B \hbar\omega_K\, g_K\, d\mathbf{q}\,, \tag{5.45}$$

$$W_{ac} = \frac{3}{(2\pi)^2}\int_{\mathbb{R}^2} \hbar\omega_{ac}\, g_{ac}\, d\mathbf{q}\,. \tag{5.46}$$

By multiplying, for each species, the phonon Boltzmann equation with the phonon energy and by integrating with respect to the wave-vector $\mathbf{q}$, one gets the following macroscopic balance equations for the average phonon energies

$$\frac{\partial W_{LO+TO}}{\partial t} = C_{W_{LO+TO}}\,, \quad \frac{\partial W_K}{\partial t} = C_{W_K}\,, \tag{5.47}$$

$$\frac{\partial W_{ac}}{\partial t} = -\nabla_{\mathbf{x}}\cdot\mathbf{Q}_{ac} + C_{W_{ac}}\,, \tag{5.48}$$

where $\mathbf{Q}_{ac}$ is the phonon energy-flux defined as

$$\mathbf{Q}_{ac} = \frac{3}{(2\pi)^2}\int_{\mathbb{R}^2} \hbar\omega_{ac}\mathbf{c}_{ac}\, g_{ac}\, d\mathbf{q}\,, \tag{5.49}$$

and

$$C_{W_{LO+TO}} = C^{p-e}_{W_{LO+TO}} - \frac{W_{LO+TO} - W^{LE}_{LO+TO}}{\tau_{LO+TO}}\,, \tag{5.50}$$

$$C_{W_K} = C^{p-e}_{W_K} - \frac{W_K - W^{LE}_K}{\tau_K}\,, \tag{5.51}$$

$$C_{W_{ac}} = C^{p-e}_{W_{ac}} - \frac{W_{ac} - W^{LE}_{ac}}{\tau_{ac}} \tag{5.52}$$

are the energy-production terms, with

$$W_{LO+TO}^{LE} = \frac{2}{(2\pi)^2}\int_B \hbar\omega_{LO/TO}\left[e^{\hbar\omega_\eta/k_BT_{LE}}-1\right]^{-1} d\mathbf{q}\,, \tag{5.53}$$

$$W_K^{LE} = \frac{1}{(2\pi)^2}\int_B \hbar\omega_K\left[e^{\hbar\omega_\eta/k_BT_{LE}}-1\right]^{-1} d\mathbf{q}\,, \tag{5.54}$$

$$W_{ac}^{LE} = \frac{3}{(2\pi)^2}\int_B \hbar\omega_{ac}\left[e^{\hbar v_p q/k_BT_{LE}}-1\right]^{-1} d\mathbf{q} \tag{5.55}$$

the average energies in local equilibrium, while $C_{W_{LO+TO}}^{p-e}$, $C_{W_K}^{p-e}$ and $C_{W_{ac}}^{p-e}$ are the contributions arising from the phonon-electron interactions. Due to energy conservation, these satisfy the relationships

$$C_{W_{LO+TO}}^{e-p} + C_{W_{LO+TO}}^{p-e} = 0\,, \tag{5.56}$$

$$C_{W_K}^{e-p} + C_{W_K}^{p-e} = 0\,, \tag{5.57}$$

$$C_{W_{ac}}^{e-p} + C_{W_{ac}}^{p-e} = 0\,, \tag{5.58}$$

where $C_{W_{LO+TO}}^{e-p}$ and $C_{W_{ac}}^{e-p}$ are the energy production terms for electrons.

The non linear equation for finding the common equilibrium temperature reads as

$$\begin{aligned} h(T_{LE}) :=& \frac{2\hbar\omega_{LO/TO}A}{(2\pi)^2}\left[e^{\hbar\omega_{LO/TO}/k_BT_{LE}}-1\right]^{-1} + \frac{\hbar\omega_K A}{(2\pi)^2}\left[e^{\hbar\omega_K/k_BT_{LE}}-1\right]^{-1} \\ &+ (k_BT_{LE})^3\,\frac{3\,\zeta(3)}{\pi\hbar^2 v_p^2} = W_{LO+TO} + W_K + W_{ac}\,, \end{aligned} \tag{5.59}$$

where $\zeta(s)$ is the zeta function and $A = \frac{8\sqrt{3}\pi^2}{9a_0^2}$ is the area of the first Brillouin zone, with $a_0 = 0.142$ nm. In (5.59) W_{LO+TO}, W_K and W_{ac} are the current values of the average phonon energies.

Considering the phonon distributions as a sum of even and odd parts and these last ones of Bose-Einstein type, each phonon temperature is related to its energy density by

$$k_B T_{LO/TO} = \frac{\hbar\omega_{LO/TO}}{\ln\left(1+\dfrac{2A\hbar\omega_{LO/TO}}{(2\pi)^2 W_{LO+TO}}\right)}, \tag{5.60}$$

$$k_B T_K = \frac{\hbar\omega_K}{\ln\left(1+\dfrac{A\hbar\omega_K}{(2\pi)^2 W_K}\right)}, \tag{5.61}$$

$$k_B T_{ac} = W_{ac}^{1/3}\left(\frac{3\,\zeta(3)}{\pi\hbar^2 v_p^2}\right)^{-1/3}. \tag{5.62}$$

We recall the assumption for the phonons relaxation times

$$\tau_{LO+TO} = \tau_K = \tau_{ac} = \tau\,. \tag{5.63}$$

Now, the model consists of the following equations

$$\begin{aligned}\frac{\partial f(t,\mathbf{k})}{\partial t} - \frac{e}{\hbar}E\,\frac{\partial f(t,\mathbf{k})}{\partial k_x} &= \int S(\mathbf{k}',\mathbf{k})\,f(t,\mathbf{k}')\,(1-f(t,\mathbf{k}))\,d\mathbf{k}' \\ &\quad - \int S(\mathbf{k},\mathbf{k}')\,f(t,\mathbf{k})\left(1-f(t,\mathbf{k}')\right)d\mathbf{k}',\end{aligned} \tag{5.64}$$

$$\frac{dW_{LO+TO}(t)}{dt} = C^{p-e}_{W_{LO+TO}} - \frac{W_{LO+TO}-W^{LE}_{LO+TO}}{\tau}, \tag{5.65}$$

$$\frac{dW_K(t)}{dt} = C^{p-e}_{W_K} - \frac{W_K - W^{LE}_K}{\tau}, \tag{5.66}$$

$$\frac{dW_{ac}(t)}{dt} = C^{p-e}_{W_{ac}} - \frac{W_{ac}-W^{LE}_{ac}}{\tau}. \tag{5.67}$$

Similar equations hold for the K' valley. As initial condition for the electrons we take the Fermi-Dirac distribution

$$f(0,\mathbf{k}) = \frac{1}{1+\exp\left(\dfrac{\varepsilon(\mathbf{k})-\varepsilon_F}{k_B T_0}\right)},$$

where T_0 is the room temperature (300 K). Regarding the phonons, we assume that initially all the phonons are at the room temperature T_0. Therefore the initial conditions for the phonon average energies are given by (5.53)-(5.55) with $T_{LE} = T_0$.

Let us introduce a uniform time-step Δt and denote by t_n the nth time level. For each interval $[t_n, t_n + \Delta t]$ we solve Eq. (5.64) by the previous Direct Simulation Monte Carlo scheme by freezing the phonon temperatures at the values they have at $t = t_n$.

The remaining Eqs. (5.65)-(5.67) are discretized by an explicit Euler method with T_{LE} evaluated at the previous time step by solving the nonlinear relation (5.59).

In order to complete the numerical scheme we have to evaluate the production terms $C^{p-e}_{W_{LO+TO}}$, $C^{p-e}_{W_K}$ and $C^{p-e}_{W_{ac}}$. They represent the rate of variation of phonon energy per unit time and are proportional to the difference between the number of emission and absorption processes per unit time due to the electron-phonon scatterings. By taking the advantage of the intermediate results coming from the DSMC part, in each time window $[t_{n-1}, t_n]$ we count, for each phonon species, the number of emission scatterings C^+_η and absorption scatterings C^-_η, $\eta = LO+TO, K$. If N_p is the number of particles used in the MC method, each simulation particle has a statistical density weight given by ρ/N_P. Therefore we can estimate the phonon energy production term as

$$C^{p-e}_{W_\eta} = \frac{\rho}{N_P \Delta t} \hbar \omega_\eta \left(C^+_\eta - C^-_\eta \right), \tag{5.68}$$

similarly to the procedure adopted for the simulation of other semiconductors [76, 78].

As before, assuming the elastic approximation for the acoustic transition rate, $C^{p-e}_{W_{ac}} = 0$.

For the DSMC part, $N_P = 10^4$ particles have been used. The time step is set as $\Delta t = 2.5$ fs and a constant phonon relaxation time has been adopted, $\tau = 5$ ps, which is a value already used in the literature, also in consideration of the fact that only phonons which more strongly interact with electrons, having as said an almost constant frequency, are significantly brought out of local equilibrium. We have also performed a comparison with the case when all phonons are kept at equilibrium at the room temperature in order to analyze the influence of the crystal heating on the characteristic curves.

First we analyze the case with $\varepsilon_F = 0.3$ eV by considering several applied fields. In Fig.5.19 the evolution of the temperatures of each type of phonons along with T_{LE} is plotted. The most energetic phonons are the optical ones, while the least energetic phonons are the acoustic ones. One observes that in the first 5 ps the rise of the temperature increases, as expected, with the electric field. Roughly it seems that the maximum T_{LE} after 5 ps depends on the electric field in a linear way. In order to study also the influence of the heating effects on the electron transport, in Figs. 5.20, 5.21 a comparison of the average electron velocity and energy is shown between the case when the crystal heating is considered and that with the phonons kept at room temperature. The differences in the average electron energy and velocity are small up to fields of 20 kV/cm.

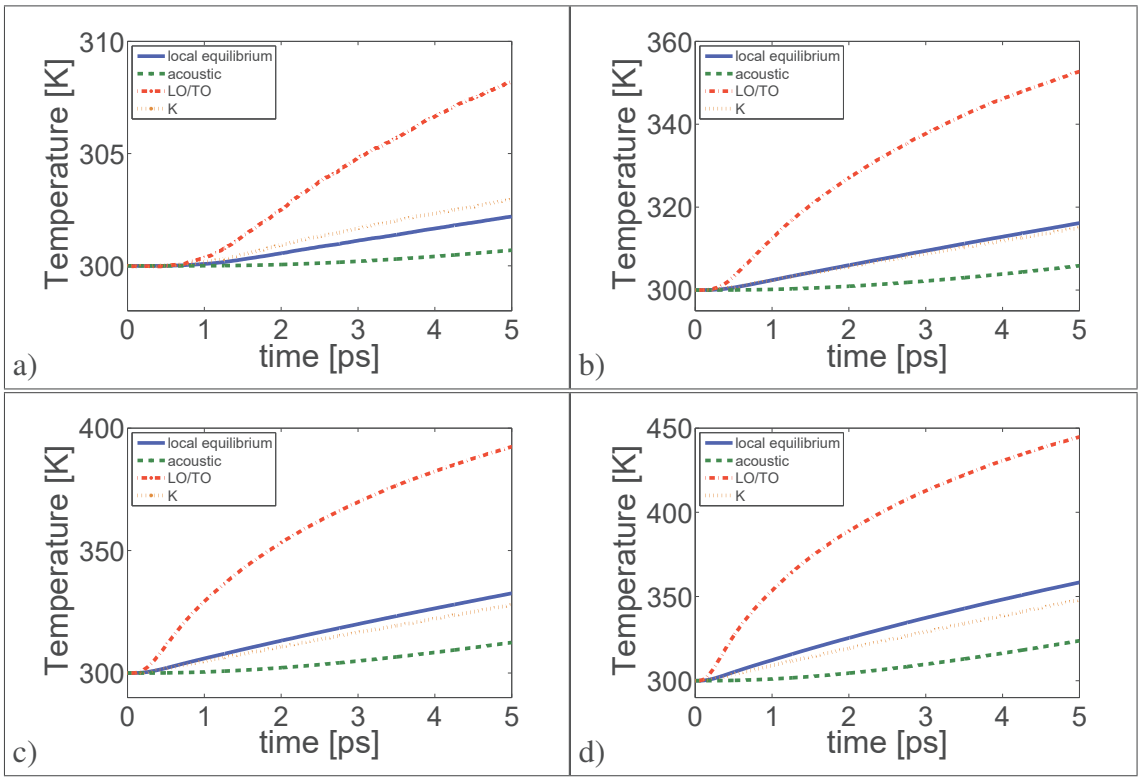

Fig. 5.19 Phonon temperatures and local equilibrium temperature T_{LE} versus time in the case $\varepsilon_F = 0.3$ eV, when $E = 1$ kV/cm (a), $E = 5$ kV/cm (b), $E = 10$ kV/cm (c) and $E = 20$ kV/cm (d).

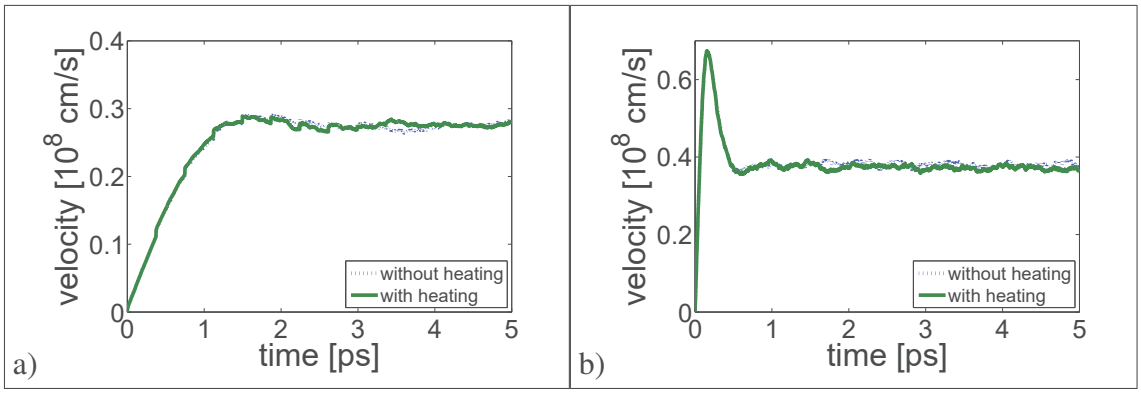

Fig. 5.20 Average electron velocity versus time in the case $\varepsilon_F = 0.3$ eV, when $E = 1$ kV/cm (a) and $E = 20$ kV/cm (b).

The previous cases have been also simulated with a higher Fermi energy $\varepsilon_F = 0.6$ eV. Now the heating effects are more evident due to the higher electron current and a consequent greater number of electron-phonon scatterings that transfer more energy to the lattice because

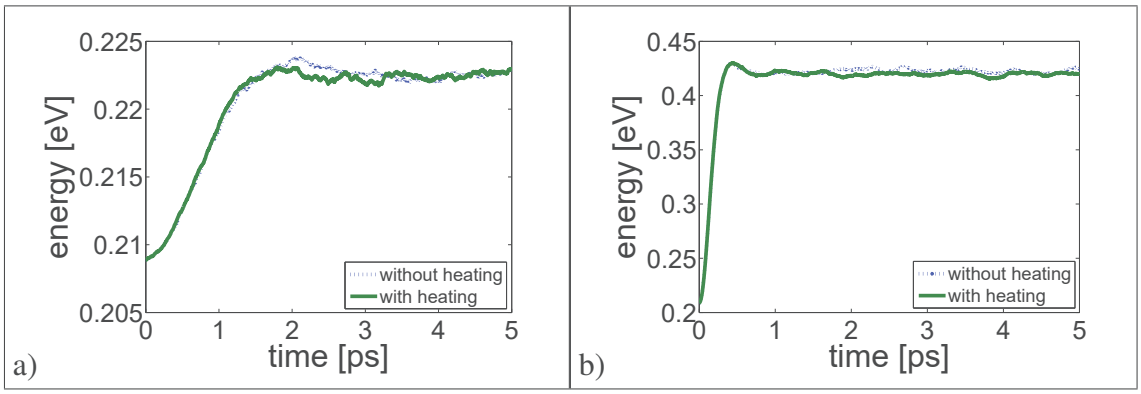

Fig. 5.21 Average electron energy versus time in the case $\varepsilon_F = 0.3$ eV, when $E = 1$ kV/cm (a) and $E = 20$ kV/cm (b).

the emission processes are dominant with respect to the absorption ones. The results are plotted in Figs. 5.22, 5.23, 5.24 and show a qualitative trend similar to those with $\varepsilon_F = 0.3$.

5.8 Summary

By using this simplified model, the temperature rises much more than in the previous complete model and this leads to an overestimation of the thermal effects. For example, there is a degradation in the characteristics curves at high fields, as comparison of Figs. 5.25 with 5.5 shows. This does not happen when the complete model is used.

Therefore, the inclusion of Z branches results very important for a right evaluation of thermal effects due to the charge flow.

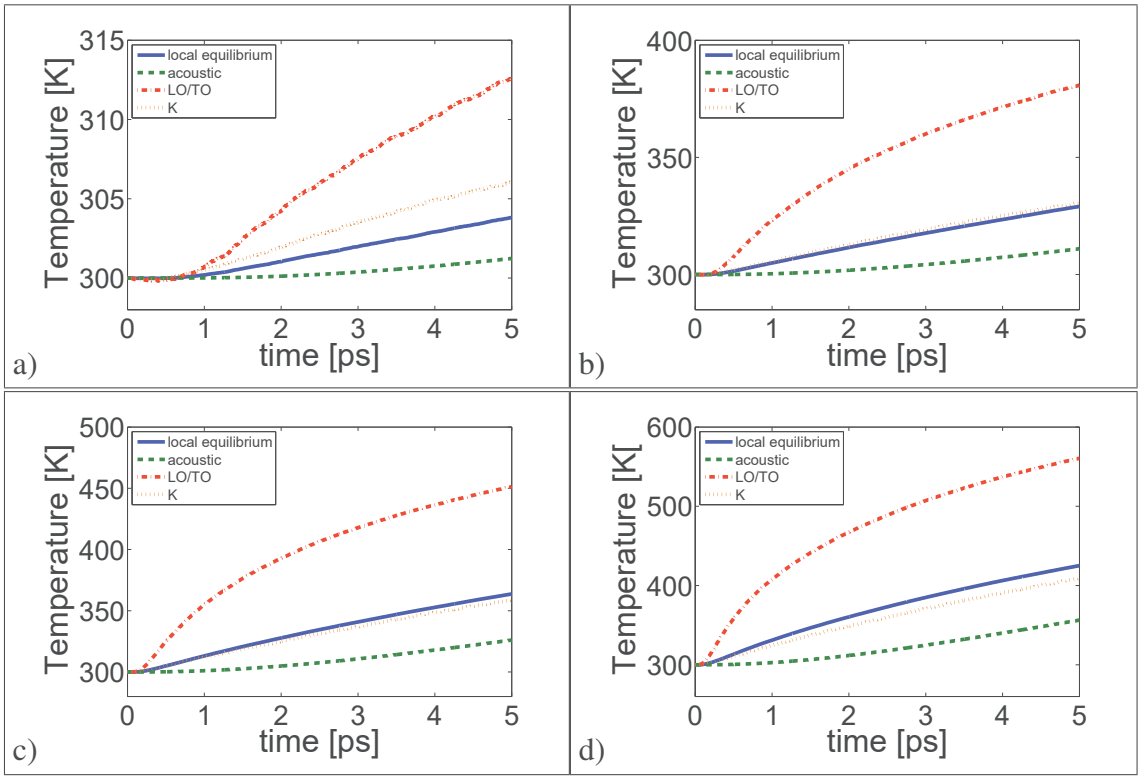

Fig. 5.22 Phonon temperatures and local equilibrium temperature T_{LE} versus time in the case $\varepsilon_F = 0.6$ eV, when $E = 1$ kV/cm (a), $E = 5$ kV/cm (b), $E = 10$ kV/cm (c) and $E = 20$ kV/cm (d).

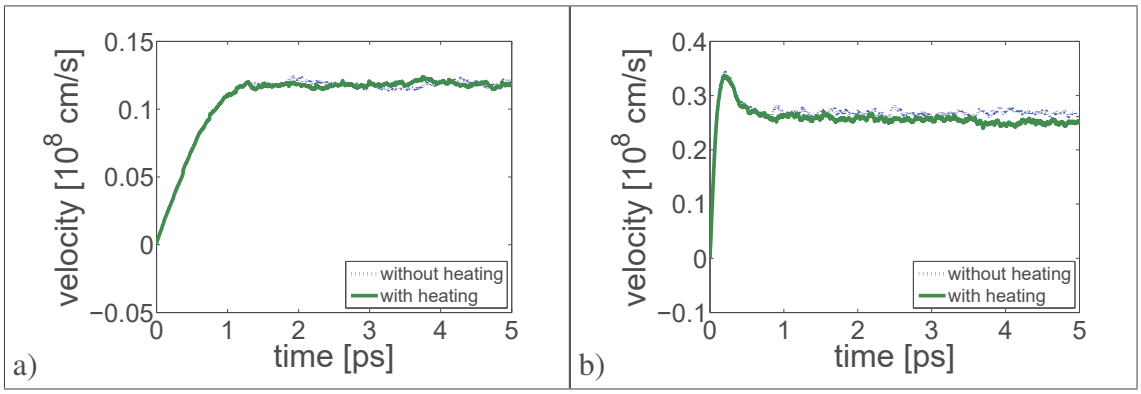

Fig. 5.23 Average electron velocity versus time in the case $\varepsilon_F = 0.6$ eV, when $E = 1$ kV/cm (a) and $E = 20$ kV/cm (b).

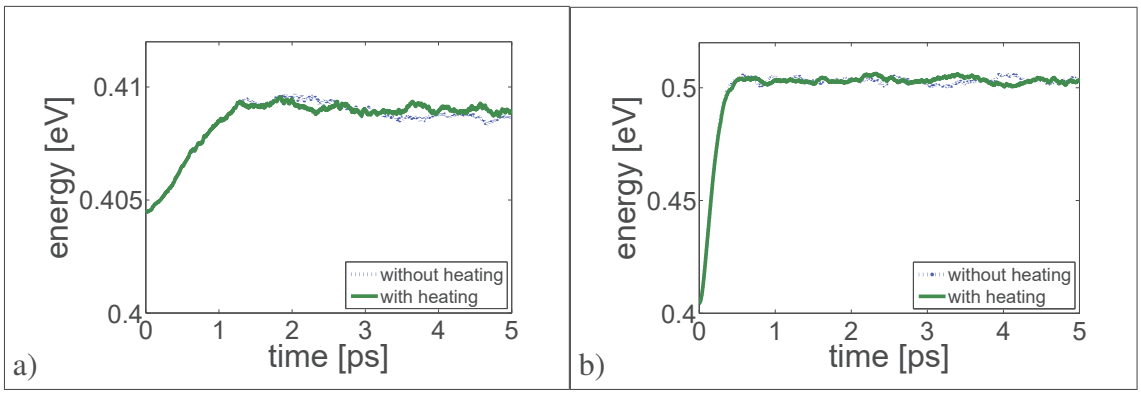

Fig. 5.24 Average electron energy versus time in the case $\varepsilon_F = 0.6$ eV, when $E = 1$ kV/cm (a) and $E = 20$ kV/cm (b).

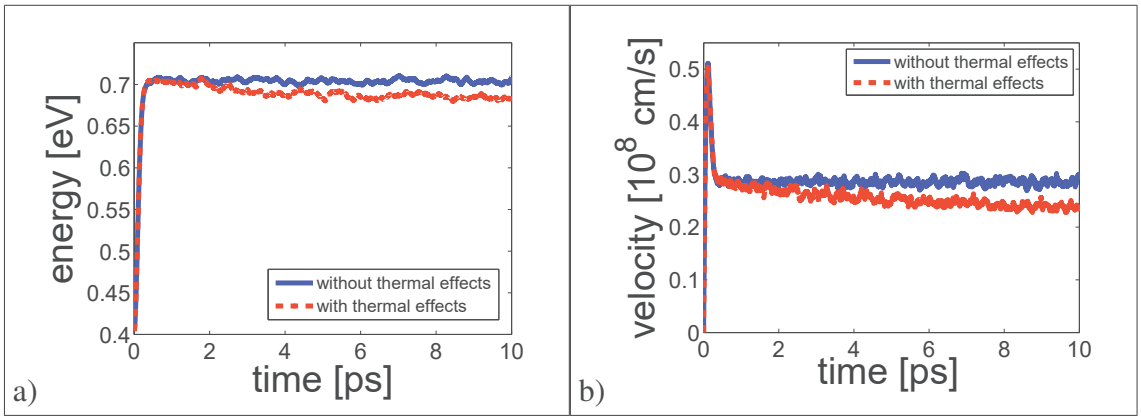

Fig. 5.25 Average electron energy and velocity versus time in the case $\varepsilon_F = 0.6$ eV, when $E = 50$ kV/cm.

Chapter 6

Macroscopic models

6.1 Introduction

The Boltzmann equation gives the advantage to focus on an ensemble of identical particles, so we have to deal only with the phase-space number density, which depends up seven variables, three space, three wave-vector coordinates and time. This is a great simplification but it remains a hard task to manage the Boltzmann equation, even with numerical method. To overcome such a difficulty and to have more immediate physical models, fluid dynamical models are obtained; the common feature is that the dependent variables can be interpreted as averages (*moments*) of the phase-space number density with respect to the wave-vector $\mathbf{k}$, and the variables reduce from seven to four. An approach is the Hilbert expansion based method; it is a perturbation argument that exploits the smallness of a dimensionless parameter, the scaled mean free path [98, 99].

With the *moments method* we are able to deduce balance equations for macroscopic quantities (avarage electron density, current, energy, etc) as moment equations of the Boltzmann equation [18]. It is required to state some physical assumptions and to resort to some phenomenological models, for example when the integrations are not analytically possible or when one needs physical parameters as the mobility, the diffusion coefficient or thermal conductivity.

The moment with respect a suitable weight function $\psi(\mathbf{k})$, with $\mathbf{k} \in \mathbb{R}^3_{\mathbf{k}}$, is defined as

$$M_\psi(\mathbf{x},t) = \int_B \psi(\mathbf{k}) f(\mathbf{x},\mathbf{k},t)\, d\mathbf{k}\,, \tag{6.1}$$

where f is the distribution function.

By multiplying the Boltzmann equation by the function $\psi(\mathbf{k})$, and with integration over B, one finds the moment equation

$$\partial_t M_\psi + \int_B \psi(\mathbf{k})\mathbf{v}(\mathbf{k})\cdot\nabla_{\mathbf{x}} f\, d\mathbf{k} - \frac{e}{\hbar}\mathbf{E}\int_B \psi(\mathbf{k})\cdot\nabla_{\mathbf{k}} f\, d\mathbf{k} = \int_B \psi(\mathbf{k})\, C[f]\, d\mathbf{k}\,, \tag{6.2}$$

where $\mathbf{E}$ is the force vector. Since

$$\int_B \psi(\mathbf{k})\nabla_{\mathbf{k}} f\, d\mathbf{k} = \int_{\partial B} \psi(\mathbf{k}) f\mathbf{n}\, d\sigma - \int_B f\nabla_{\mathbf{k}}\psi(\mathbf{k})\, d\mathbf{k}\,, \tag{6.3}$$

where $\mathbf{n}$ is the outward unit normal vector field on the boundary ∂B with surface element $d\sigma$, Eq.(6.2) becomes

$$\begin{aligned}\partial_t M_\psi + \nabla_{\mathbf{x}}\cdot\int_B f\psi(\mathbf{k})\mathbf{v}(\mathbf{k})d\mathbf{k} \quad &+ \quad \frac{e}{\hbar}\mathbf{E}\left[\int_B f\nabla_{\mathbf{k}}\psi(\mathbf{k})\, d\mathbf{k} - \int_{\partial B}\psi(\mathbf{k}) f\mathbf{n}\, d\sigma\right] = \\ &\int_B \psi(\mathbf{k})\, C[f]\, d\mathbf{k}\,.\end{aligned} \tag{6.4}$$

The last term on the l.h.s vanishes whit the assumption that f must decay sufficiently fast when $|\mathbf{k}|\to\infty$, or when B is compact and $\psi(\mathbf{k})$ is periodic and continuous on ∂B, a direct consequence of the periodicity of f on B and of the symmetry of B with respect to the origin. With different choices of the function $\psi(\mathbf{k})$, usually as power of $\mathbf{k}$, we obtain an infinite hierarchy of balance equations; any truncation of the hierarchy doesn't give a closed system because the moments are coupled and one always has more unknowns than equations.
Thus, one need suitable closure relations, for example resorting to the Maximum Entropy Principle [82–85, 25]. As an example, we consider the zero-order moment, with $\psi(\mathbf{k}) = 1$. We have

$$\int_B \frac{\partial}{\partial t} f(\mathbf{x},\mathbf{k},t)\, d\mathbf{k} + \nabla_{\mathbf{x}}\cdot\int_B f(\mathbf{x},\mathbf{k},t)\mathbf{v}(\mathbf{k})\, d\mathbf{k} = \int_B C[f]\, d\mathbf{k} = 0\,, \tag{6.5}$$

$$\frac{\partial}{\partial t}\int_B f(\mathbf{x},\mathbf{k},t)\, d\mathbf{k} + \nabla_{\mathbf{x}}\cdot\left[n(\mathbf{x},t)\,\mathbf{V}(\mathbf{x},t)\right] d\mathbf{k} = 0\,, \tag{6.6}$$

where $\mathbf{V}(\mathbf{x},t)$ is the average macroscopic velocity, and then the continuity equation for the charge spatial density n

$$\frac{\partial n(\mathbf{x},t)}{\partial t} + \nabla_{\mathbf{x}}\cdot\mathbf{J}(\mathbf{x},t) = 0\,, \tag{6.7}$$

where $\mathbf{J}(\mathbf{x},t) = n(\mathbf{x},t)\mathbf{V}(\mathbf{x},t)$ is the particle current density. By defining the charge current density as $\mathbf{J} = -en\mathbf{V}$, e being the elementary charge, we have the charge conservation equation

$$\frac{\partial n(\mathbf{x},t)}{\partial t} - \frac{1}{e}\nabla_{\mathbf{x}}\cdot\mathbf{J}(\mathbf{x},t) = 0\,. \tag{6.8}$$

In this example is clear that we have one equation but two unknowns, namely n and $\mathbf{J}$.

6.2 Comparison between DSMC and hydrodynamical results

Electrons which contribute to the charge transport in graphene are those in the conduction and valence band, and it is preferable to treat the latter as holes for insuring the integrability of the corresponding distribution function. Electrons and holes mostly populate the states near to the K and K' valleys. A reference frame centered in the K-point will be used.

We have a set of moment equations consisting of balance equations of the following quantities

$$\begin{aligned}
&\text{average density} \quad \rho_i = \frac{4}{(2\pi)^2}\int_{\mathbb{R}^2} f_i(t,\mathbf{x},\mathbf{k})\,d\mathbf{k}\,,\\
&\text{average velocity} \quad \rho_i\mathbf{V}_i = \frac{4}{(2\pi)^2}\int_{\mathbb{R}^2} f_i(t,\mathbf{x},\mathbf{k})\,\mathbf{v}\,d\mathbf{k}\,,\\
&\text{average energy} \quad \rho_i W_i = \frac{4}{(2\pi)^2}\int_{\mathbb{R}^2} f_i(t,\mathbf{x},\mathbf{k})\,\varepsilon\,d\mathbf{k}\,,\\
&\text{average energy-flux } \rho_i\mathbf{S}_i = \frac{4}{(2\pi)^2}\int_{\mathbb{R}^2} f_i(t,\mathbf{x},\mathbf{k})\,\varepsilon\mathbf{v}\,d\mathbf{k}\,,
\end{aligned}$$

(i = electron, hole), where the factor 4 arises from taking into account both the spin states and the two equivalent valleys.

By integrating the Boltzmann equations with respect to $\mathbf{k}$, one has the following balance equations for the above-defined macroscopic quantities

$$\frac{\partial}{\partial t}\rho_i + \nabla_{\mathbf{x}}\cdot(\rho_i\mathbf{V}_i) = \rho_i C_i\,, \tag{6.9}$$

$$\frac{\partial}{\partial t}(\rho_i\mathbf{V}_i) + \nabla_{\mathbf{x}}\cdot\left(\rho_i\mathbf{F}_i^{(0)}\right) + \mathsf{e}_i\rho_i\mathbf{G}_i^{(0)}\mathbf{E} = \rho_i C_{\mathbf{V}_i}\,, \tag{6.10}$$

$$\frac{\partial}{\partial t}(\rho_i W_i) + \nabla_{\mathbf{x}}\cdot(\rho_i\mathbf{S}_i) + \mathsf{e}_i\rho_i\mathbf{E}\cdot\mathbf{V}_i = \rho_i C_{W_i}\,, \tag{6.11}$$

$$\frac{\partial}{\partial t}(\rho_i\mathbf{S}_i) + \nabla_{\mathbf{x}}\cdot\left(\rho_i\mathbf{F}_i^{(1)}\right) + \mathsf{e}_i\rho_i\mathbf{G}_i^{(1)}\mathbf{E} = \rho_i C_{\mathbf{S}_i}\,, \tag{6.12}$$

where the G's and F's are extra-fluxes and the terms at the right hand sides are productions (the reader is referred to [44] for details) and e_i is equal to e for electrons and $-e$ for holes.

The extra fluxes and the production terms are additional unknown quantities. For them constitutive relations in terms of the fundamental variables are needed in order to get a closed system of balance equations. A well theoretically founded way to get the desired closure relations is to resort to the Maximum Entropy Principle (MEP) [22], according to which the electron and hole distribution functions can be estimated by the distributions $f_{e,MEP}$ and $f_{h,MEP}$ solving the following problem

$$(f_{e,MEP}, f_{h,MEP}) = \max_{f_e(t,\mathbf{x},\cdot), f_h(t,\mathbf{x},\cdot) \in \mathscr{F}(\mathbb{R}^2)} S[f_e, f_h],$$

under the constraints

$$\begin{pmatrix} \rho_i \\ \rho_i W_i \end{pmatrix} = \frac{4}{(2\pi)^2} \int_{\mathbb{R}^2} \begin{pmatrix} 1 \\ \varepsilon \end{pmatrix} f_i(t,\mathbf{x},\mathbf{k})\, d\mathbf{k},$$
$$\begin{pmatrix} \rho_i \mathbf{V}_i \\ \rho_i \mathbf{S}_i \end{pmatrix} = \frac{4}{(2\pi)^2} \int_{\mathbb{R}^2} f_i(t,\mathbf{x},\mathbf{k}) \begin{pmatrix} \mathbf{v} \\ \varepsilon \mathbf{v} \end{pmatrix} d\mathbf{k},$$

where $S[f_e, f_h]$ is the total entropy of the system (remind that the phonons are assumed to represent a thermal bath kept at constant temperature and therefore they add a constant contribution to the entropy) equal to

$$S[f_e, f_h] = -k_B \left\{ \frac{4}{(2\pi)^2} \int_{\mathbb{R}^2} \left[f^e \ln f^e + (1-f^e) \ln (1-f^e) \right] d\mathbf{k} + \frac{4}{(2\pi)^2} \int_{\mathbb{R}^2} \left[f^h \ln f^h + \left(1-f^h\right) \ln \left(1-f^h\right) \right] d\mathbf{k} \right\},$$

and $\mathscr{F}(\mathbb{R}^2)$ is the space of the distribution functions that admit the moments required as constraints.

By solving the above maximization problem we get

$$f_i = \frac{1}{1 + \exp\left(\lambda_i + \lambda_{W_i}\varepsilon + \mathbf{v} \cdot (\lambda_{\mathbf{V}_i} + \varepsilon \lambda_{\mathbf{S}_i})\right)},$$

where the λ's are Lagrange multipliers which have to be expressed as functions of the state variables by taking into account the constraints. As in [53], we linearize the distributions around their isotropic part, obtaining

$$f_i \approx \frac{1}{e^{\lambda_i + \lambda_{W_i}\varepsilon} + 1} \left[1 - \frac{e^{\lambda_i + \lambda_{W_i}\varepsilon}}{e^{\lambda_i + \lambda_{W_i}\varepsilon} - 1} \mathbf{v} \cdot (\lambda_{\mathbf{V}_i} + \varepsilon \lambda_{\mathbf{S}_i}) \right].$$

After that, these distributions are inserted into the kinetic definitions of the additional variables, so closing the system of the balance equations (see [44] for the details).

Even if macroscopic models are more suited for computer-aided design (CAD) purposes because they avoid a direct numerical solution of the Boltzmann equation, they introduce some approximation for the needed closure relation ([25, 44–49]).

We want to assess the validity of the MEP hydrodynamical model by a comparison with the solutions furnished by the new DSMC developed in this thesis. We consider the case of high values of Fermi energies, so that under such a condition electrons belonging to the conduction band do not move to the valence band and vice versa. Therefore, the hole dynamics is totally neglected.

The lattice temperature is kept constant and equal to 300 K and the physical parameter are the same as in chapter 2. The solutions do not depend on $\mathbf{x}$ and therefore we neglect the terms in divergence form in the balance equations (6.9)-(6.12), that become a system of ODEs. Moreover, only the component of the velocity and the energy-flux along the direction of the electric field, which we assume to be the x axis, is changing with time if we set the initial velocity equal to zero. Regarding the initial conditions of the other macroscopic variables, consistently with an initial Fermi-Dirac distribution, we assume zero energy-flux while the initial density and the average energy density are calculated from the initial Fermi-Dirac distribution. The Boltzmann equation and the system (6.9)-(6.12) have been solved for different values of the applied electric field and the results for the average velocity and the energy are shown in Figs 6.1, 6.2. In order to understand if the Fermi energy influences the accuracy of the MEP model, we have performed the same simulations with $\varepsilon_F = 0.4$ eV and $\varepsilon_F = 0.6$ eV.

Although the overall discrepancy is reasonable for the applications, it is likely that one needs to include some nonlinear terms in the velocity and the energy-flux or additional moments for improving more the hydrodynamical results.

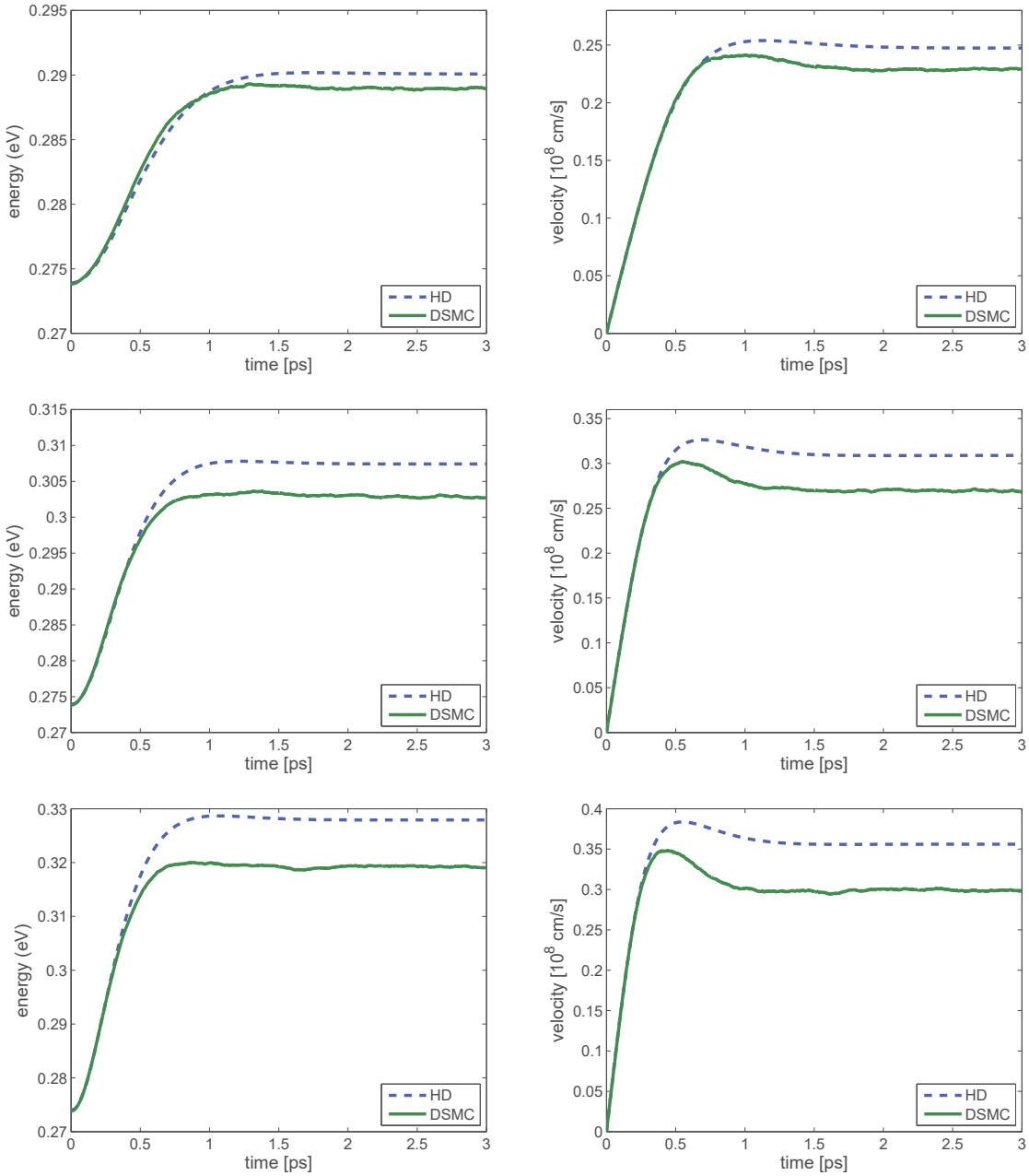

Fig. 6.1 Comparison of the energy and the velocity versus time obtained with DSMC and the MEP hydrodynamical model (HD) for the electric fields $E = 2$ kV/cm (top), $E = 4$ kV/cm, $E = 6$ kV/cm (bottom) and a Fermi energy equal to 0.4 eV.

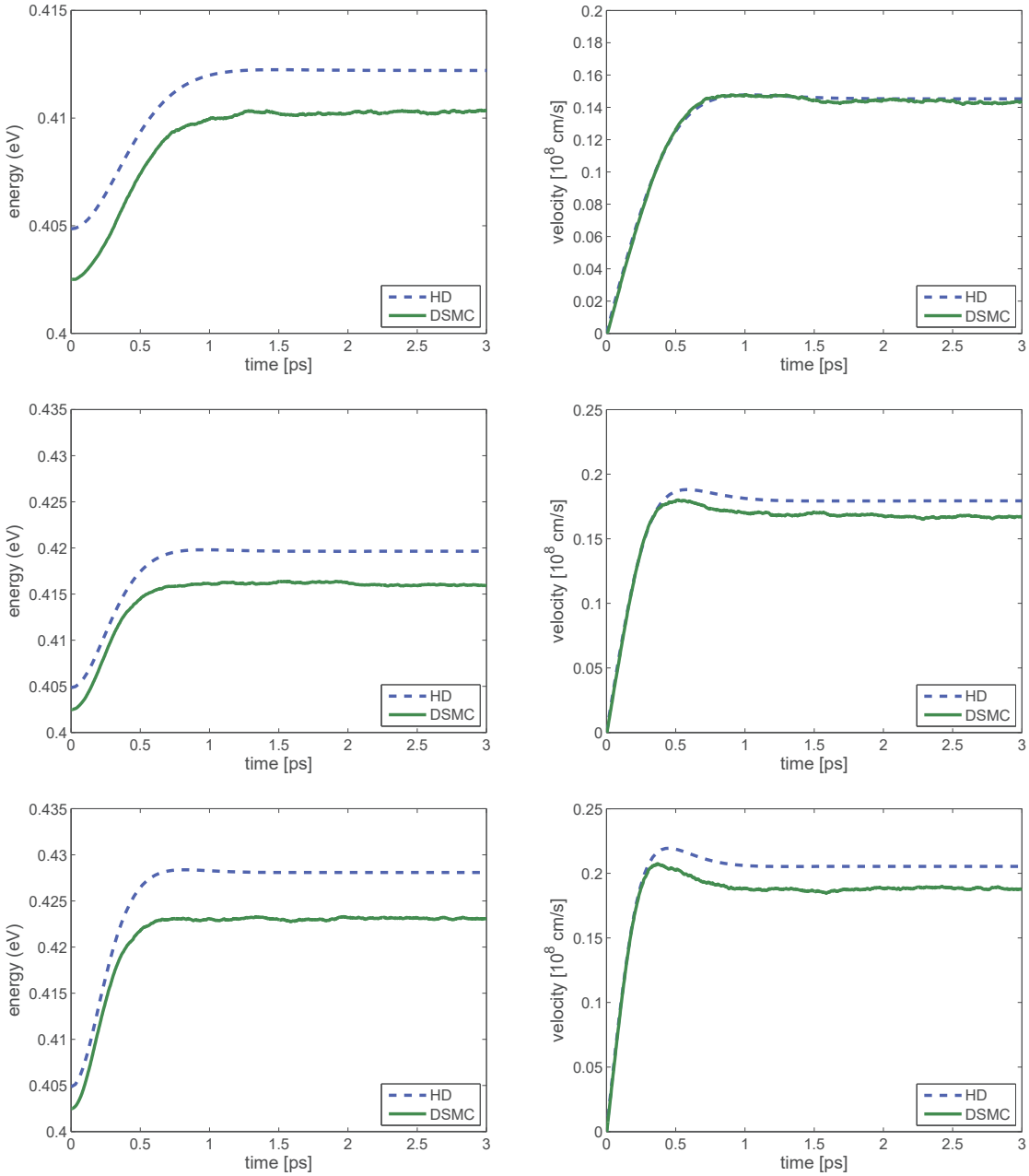

Fig. 6.2 Comparison of the energy and the velocity versus time obtained with DSMC and the MEP hydrodynamical model (HD) for the electric fields $E = 2$ kV/cm (top), $E = 4$ kV/cm, $E = 6$ kV/cm (bottom) and a Fermi energy equal to 0.6 eV.

Conclusions

In this thesis we have studied charge and phonon transport in graphene. We have considered values of Fermi energies high enough to neglect the dynamics of the valance band; this is equivalent to a n-type doping for traditional semiconductors.

The first aim was to develop a new Direct Simulation Monte Carlo strategy that properly takes into account the Pauli exclusion principle. This result is very important both from a theoretical point of view and for all practical applications when degeneracy effects are strongly effective. The proposed procedure gives correct results both for mean values and distribution functions.

The new DSMC procedure reveals very accurate and seems to respect the intrinsic nature of the Boltzmann equation and in particular the role of time. The l.h.s of the Boltzmann equation takes into account the time evolution while in the r.h.s the collisions are considered instantaneously, time is a frozen parameter. The coincidence that a numerical procedure that respects the nature of an equation also gives correct results could give important suggestions, at lest from a philosophical point of view, for example about the relationship between physical phenomena, their analytical models and numerical approximations. Is the previous result really a coincidence?

For a cross-validation of the results we have solved the Boltzmann equation also by means of a numerical scheme based on Discontinuous Galerkin method, already largely used for conventional semiconductors. The agreement between the stochastic and the deterministic solution is excellent and proves the accuracy of the new proposed DSMC strategy. Furthermore, the Discontinuous Galerkin solution preserves the positivity of the solution and, at first order in the time step, the numerical solution remains bounded by the extrema of the initial data, aspects strongly stressed in literature.

The new proposed DSMC strategy is able to investigate the transport properties in graphene and represents a basic framework to easily include additional scattering terms and other physical effects that could be important when one has to simulate real graphene-based devices.

Actually, we have applied the previous method to investigate the influence of different substrates on the transport properties of a graphene layer. The results are in perfect agreement with those obtained with the Discontinuous Galerkin method also in this case and respect the expected behaviour commonly found in literature, as the degradation of the mobilities and the effective influence of the distance between the graphene layer and the substrate.

Graphene is one of the most promising material for future electronic devices and the knowledge of its electro-thermal properties is of fundamental importance. In the last part of the thesis, phonon transport has been studied and the new DSMC scheme reveals again as a valid basic framework for further investigation of transport problems.

We have considered a complete phonon model, with all phonon branches, the in plane and the out of plane ones. These latter do not enter in the electron-phonon interactions but are important for a correct evaluation of thermal effects. We have introduced a global equilibrium temperature for the whole crystal lattice as a dynamical variable and we have deduced the rate in the rise in temperature of a graphene layer under the effect of an applied electric field. Moreover, the phonon populations have been described without any approximation with equivalent Bose-Einstein distributions. The contribution due to the phonon-electron interactions has been obtained by means of the intermediate results of the DSMC part, by counting the number of emission and absorption processes, with a suitable statistical weight that has to respect the density energy balance equation. The phonon-phonon interaction is still an open problem and it has been treated with a BGK approximation.

Furthermore, from the results of a statistical regression analysis, we have been able to predict the raise of the temperature for any value of the electric field and Fermi energy and that the crystal temperature reaches the melting point after about few hundreds of picoseconds.

We have compared the results with a simplified model, wherein the out of plane phonon branches are neglected and the phonon populations are approximated by Bose-Einstein distributions, and shown that the flexural modes are fundamental to avoid an overestimation of thermal effects in graphene.

Acknowledgements

First of all I want to thank my advisor Prof. Vittorio Romano for having accepted me as his PhD student, for his scientific competence and for his constant guidance during these important years.

I thank Prof. Armando Majorana from Universiy of Catania for the collaboration and discussions.

I thank Prof. Giovanni Mascali from University of Cosenza for his friendly kindness.

I am grateful to Prof. Andrea Ferrari from University of Cambridge for his precious inputs.

I thank Prof. Nicola Marzari from EPFL for having given me the possibility to be visiting student in his research group.

Appendix A

Derivation and properties of the Boltzmann transport equation

We have an ensemble of charged particles interacting with a driving force under the laws of classical mechanics [86]. To overcome the difficulty to know the initial state of all the particles, it is necessary to reformulate the problem from a probabilistic point of view obtaining the classical Liouville equation: it describes the trajectory of the ensemble of particles as a deterministic equation for its probability density in the position-momentum space. The motion of a single electron with position $\mathbf{x} \in \mathbb{R}^3_{\mathbf{x}}$ and velocity $\mathbf{v} \in \mathbb{R}^3_{\mathbf{v}}$, in position-velocity space, is described by the trajectory $w(t;\mathbf{x}_0,\mathbf{v}_0) = (\mathbf{x}(t),\mathbf{v}(t))$ obtained by the equations

$$\dot{\mathbf{x}} = \mathbf{v} \qquad\qquad \dot{\mathbf{v}} = -\frac{e}{m}\mathbf{E} \tag{A.1}$$

with the given initial state

$$\mathbf{x}(t=0) = \mathbf{x}_0\,, \qquad\qquad \mathbf{v}(t=0) = \mathbf{v}_0\,. \tag{A.2}$$

e is the elementary (positive) charge of the electron, m its mass and $\mathbf{E} = \mathbf{E}(\mathbf{x},t)$ is the electric field. Now, instead of the exact initial position and initial velocity of electron, $\mathbf{x}_0$ and $\mathbf{v}_0$, we consider the joint probability density $f_{in} = f_{in}(\mathbf{x},\mathbf{v})$ of the position and velocity of the single electron, that has the following properties:

$$f_{in}(\mathbf{x},\mathbf{v}) \geq 0, \int_{\mathbb{R}^3_{\mathbf{v}}}\int_{\mathbb{R}^3_{\mathbf{x}}} f_{in}(\mathbf{x},\mathbf{v})\,d\mathbf{x}\,d\mathbf{v} = 1\,. \tag{A.3}$$

The probability to find the electron in the subset A of the $(\mathbf{x},\mathbf{v})$ space at $t = 0$ is

$$P(A) := \int\int_A f_{in}(\mathbf{x},\mathbf{v})\,d\mathbf{x}\,d\mathbf{v}\,. \tag{A.4}$$

We look for a continuum equation for the probability density $f(\mathbf{x},\mathbf{v},t)$ with initial value $f_{in} = f(\mathbf{x},\mathbf{v},t=0)$. We postulate that f doesn't have any variation along the trajectories $w(t;\mathbf{x},\mathbf{v}) = (\mathbf{x}(t),\mathbf{v}(t))$:

$$f(w(t;\mathbf{x},\mathbf{v}),t) = f_{in}(\mathbf{x},\mathbf{v}), \qquad \forall \mathbf{x},\mathbf{v} \in \mathbb{R}^3,\ t \geq 0 \tag{A.5}$$

Differentiating (A.5) with respect to t,

$$\partial_t f + \dot{\mathbf{x}} \cdot \nabla_{\mathbf{x}} f + \dot{\mathbf{v}} \cdot \nabla_{\mathbf{v}} f = 0\,, \tag{A.6}$$

and with (A.1) we obtain the classical Liouville transport equation for the probability density f:

$$\partial_t f + \mathbf{v} \cdot \nabla_{\mathbf{x}} f - \frac{e}{m}\mathbf{E} \cdot \nabla_{\mathbf{v}} f = 0\,, \tag{A.7}$$

If we have an ensemble of M particles, the position and velocity vectors are $3M$-dimensional, $\mathbf{x} = (\mathbf{x}_1,\ldots,\mathbf{x}_M)$, $\mathbf{v} = (\mathbf{v}_1,\ldots,\mathbf{v}_M)$, where $\mathbf{x}_i$, $\mathbf{v}_i \in \mathbb{R}^3$, and the force field vector $\mathbf{F} = (\mathbf{F}_1,\ldots,\mathbf{F}_M)$ is a $3M$-dimensional vector depending on all $6M$ position and velocity coordinates and time. The classical ensemble Liouville equation is

$$\partial_t f + \mathbf{v} \cdot \nabla_{\mathbf{x}} f + \frac{1}{m}\mathbf{F} \cdot \nabla_{\mathbf{v}} f = 0\,. \tag{A.8}$$

This is a linear, hyperbolic equation, and their characteristics are the ensemble trajectories defined by

$$\begin{aligned} \dot{\mathbf{x}}_i &= \mathbf{v}_i \\ \dot{\mathbf{v}}_i &= \frac{1}{m}\mathbf{F}_i, \qquad\qquad i = 1,\ldots,M. \end{aligned} \tag{A.9}$$

along with the initial condition

$$f(\mathbf{x},\mathbf{v},t=0) = f_{in}(\mathbf{x},\mathbf{v})\,. \tag{A.10}$$

In this case, $f(\mathbf{x},\mathbf{v},t)$ is the joint position-velocity probability density of the M-particle ensemble at time t and the probability to find the M-particle ensemble in a subset A of the $6M$ position-velocity space at time t is

$$P_M(A,t) := \int\int_A f(\mathbf{x},\mathbf{v},t)\,d\mathbf{x}\,d\mathbf{v}\,. \tag{A.11}$$

It is very important to study in deep the initial value problem for Eq.(A.8) with initial condition (A.10), for $\mathbf{x} \in \mathbb{R}^{3M}_{\mathbf{x}}$, $\mathbf{v} \in \mathbb{R}^{3M}_{\mathbf{v}}$, also regards the implications of the Liouville theorem [87]. From (A.5), if a solution exists, $f(\mathbf{x},\mathbf{v},t) \geq 0$ for all $t \geq 0$, if $f_{in}(\mathbf{x},\mathbf{v}) \geq 0$. This means that the evolution process described by Liouville equation preserves the non-negativity of f. We assume for the force field $\mathbf{F}$ that

$$\nabla \cdot \mathbf{F} = 0 \tag{A.12}$$

for $\mathbf{x} \in \mathbb{R}^{3M_{\mathbf{x}}}$, $\mathbf{v} \in \mathbb{R}^{3M}_{\mathbf{v}}$, $t \geq 0$.

Integrating Eq. (A.8) over $\mathbb{R}^{3M}_{\mathbf{x}} \times \mathbb{R}^{3M}_{\mathbf{v}}$, assuming that the solution decays to zero sufficiently fast as $|\mathbf{x}| \to \infty$, $|\mathbf{v}| \to \infty$ and considering the condition (A.12), we have

$$\int_{\mathbb{R}^{3M}_{\mathbf{v}}} \mathbf{F} \cdot \nabla_{\mathbf{v}} f \, d\mathbf{v} = -\int_{\mathbb{R}^{3M}_{\mathbf{v}}} f \nabla \cdot \mathbf{F} \, d\mathbf{v} = 0, \tag{A.13}$$

and we obtain

$$\frac{d}{dt} \int_{\mathbb{R}^{3M}_{\mathbf{x}}} \int_{\mathbb{R}^{3M}_{\mathbf{v}}} f(\mathbf{x},\mathbf{v},t) \, d\mathbf{v} \, d\mathbf{x} = 0, \tag{A.14}$$

i.e.

$$\int_{\mathbb{R}^{3M}_{\mathbf{x}}} \int_{\mathbb{R}^{3M}_{\mathbf{v}}} f(\mathbf{x},\mathbf{v},t) \, d\mathbf{v} \, d\mathbf{x} = \int_{\mathbb{R}^{3M}_{\mathbf{x}}} \int_{\mathbb{R}^{3M}_{\mathbf{v}}} f_{in}(\mathbf{x},\mathbf{v}) \, d\mathbf{v} \, d\mathbf{x} = 1, \quad t \geq 0. \tag{A.15}$$

Thanks to the preservation of the non-negativity of f and the conservation of the whole-space integral (A.15), the solution of the initial value problem for the Liouville equation can have a full probabilistic interpretation. The classical Liouville equation holds when the particles move in a vacuum without interactions, neither with the environment nor between themselves. This is mathematically clear if we consider that the unique solution f of (A.8), (A.10) is

$$f(\mathbf{x},\mathbf{v},t) = f_{in}(w^{-1}(t;\mathbf{x},\mathbf{v})), \tag{A.16}$$

if the maps $w(t;\cdot,\cdot) : \mathbb{R}^{3M}_{\mathbf{x}} \times \mathbb{R}^{3M}_{\mathbf{v}} \to \mathbb{R}^{3M}_{\mathbf{x}} \times \mathbb{R}^{3M}_{\mathbf{v}}, t \geq 0$, are sufficiently smooth and one-to-one and if f_{in} is sufficiently differentiable. In this way, the required invertibility of w doesn't permit the existence of any type of collisions into the ensemble, i.e. the trajectors can't intersect. Using the canonical equations of motion [88], we can write the Liouville equation in the $6M$-dimensional ensemble phase-space $(\mathbf{x},\mathbf{p})$ of coordinate and momentum:

$$\partial_t f + \frac{\mathbf{p}}{m} \cdot \nabla_{\mathbf{x}} f - e\mathbf{E} \cdot \nabla_{\mathbf{p}} f = 0. \tag{A.17}$$

In the semiclassical Liouville equation we can consider the effects of the periodic potential on the charged particles due to the ions of the crystal lattice structure. The infinite periodic

crystal lattice is denoted by

$$L = \{i\mathbf{a}_1 + j\mathbf{a}_2 + l\mathbf{a}_3 \,|\, i, j, l \in \mathbb{Z}\}, \tag{A.18}$$

where $\mathbf{a}_1$, $\mathbf{a}_2$, $\mathbf{a}_3$ are the primitive lattice vectors; the reciprocal lattices is

$$\hat{L} = \{i\mathbf{b}_1 + j\mathbf{b}_2 + l\mathbf{b}_3 \,|\, i, j, l \in \mathbb{Z}\}, \tag{A.19}$$

where $\mathbf{b}_1$, $\mathbf{b}_2$, $\mathbf{b}_3$ are the reciprocal primitive lattice vectors and it holds

$$\mathbf{a}_i \cdot \mathbf{b}_j = 2\pi\delta_{ij}. \tag{A.20}$$

The primitive cell is a connected subset $A \in \mathbb{R}^3$ such that is volume is equal to $|\mathbf{a}_1 \cdot (\mathbf{a}_2 \wedge \mathbf{a}_3)$ and $\mathbb{R}^3 = \bigcup_{\mathbf{x}\in\mathbb{R}^3} T_{\mathbf{x}}A$, where $T_{\mathbf{x}}A$ is the translate of A by the lattice vector $\mathbf{x}$, i.e. the whole space is covered by the union of translates of A by lattice vectors. The primitive cell of the reciprocal space, that contains the points closer to the origin than to any other point of $\hat{L}$, is called the (first) Brillouin zone B. B is point symmetric to the origin, i.e. $\mathbf{k} \in B$ if and only if $-\mathbf{k} \in B$.
Given the Schroedinger equation

$$H_L\psi = \varepsilon\psi, \tag{A.21}$$

where H_L is the quantum Hamiltonian

$$H_L = -\frac{\hbar}{2m}\Delta - eV_L \tag{A.22}$$

and V_L the periodic potential due to the crystal lattice

$$V_L(\mathbf{x}+\mathbf{X}) = V_L(\mathbf{x}), \qquad \mathbf{x} \in \mathbb{R}^3_{\mathbf{x}}, \qquad \mathbf{X} \in L, \tag{A.23}$$

for the Bloch theorem the wave-functions ψ can be written as

$$\psi(\mathbf{x}) = e^{i\mathbf{k}\cdot\mathbf{x}}u_{\mathbf{k}}(\mathbf{x}), \tag{A.24}$$

where $u_{\mathbf{k}}(\mathbf{x}+\mathbf{X}) = u_{\mathbf{k}}(\mathbf{x})$ takes into account the periodicity of the lattice and $\mathbf{k}$ is an arbitrary wave-vector (of the reciprocal lattice) in $\mathbb{R}^3_{\mathbf{k}}$. Using (A.24), (A.21) can be written as

$$-\frac{\hbar^2}{2m}(\Delta u_{\mathbf{k}} + 2i\mathbf{k}\cdot\nabla u_{\mathbf{k}}) + \left(\frac{\hbar^2}{2m}|\mathbf{k}|^2 - eV_L(\mathbf{x})\right)u_{\mathbf{k}} = \varepsilon u_{\mathbf{k}}, \tag{A.25}$$

subject to the periodicity condition of $u_{\mathbf{k}}(\mathbf{x})$. This, for given $\mathbf{k} \in \mathbb{R}^3_{\mathbf{k}}$, is a second order self-adjoint elliptic eigenvalue problem on the primitive lattice cell, and we may have an infinite sequence of eigenpairs $\varepsilon = \varepsilon_l(\mathbf{k})$, $u_{\mathbf{k}}(\mathbf{x}) = u_{\mathbf{k},l}(\mathbf{x})$, $l \in \mathbb{N}$. Using

$$\psi(\mathbf{x}+\mathbf{X}) = e^{i\mathbf{k}\cdot\mathbf{X}}\psi(\mathbf{x}) \tag{A.26}$$

and considering that $e^{i\mathbf{k}\cdot\mathbf{X}} = 1 \; \forall \mathbf{k} \in \hat{L}$, $\mathbf{X} \in L$, the set of ψ and ε are identical for any two vectors differing by a reciprocal lattice vector. We can assign $l \in \mathbb{N}$ io order to have $\varepsilon_l(\mathbf{k})$ and $\psi_{\mathbf{k},l}(\mathbf{x}) = e^{i\mathbf{k}\cdot\mathbf{x}}u_{\mathbf{k},l}(\mathbf{x})$ periodic on the reciprocal lattice:

$$\varepsilon_l(\mathbf{k}+\mathbf{K}) = \varepsilon_l(\mathbf{k}), \tag{A.27}$$

$$\psi_{\mathbf{k}+\mathbf{K},l} = \psi_{\mathbf{k},l}, \tag{A.28}$$

where $\mathbf{K} \in \hat{L}$. In this way, we can consider only the Brillouin zone B and not the whole space, without losing any information.
$\varepsilon_l = \varepsilon_l(\mathbf{k})$ is a continuous function on B and represents the lth energy band of the crystal, while the corresponding mean velocity (the group velocity) is

$$\mathbf{v}_l(\mathbf{k}) = \frac{1}{\hbar}\nabla_{\mathbf{k}}\varepsilon_l(\mathbf{k}). \tag{A.29}$$

Consider an ensemble of M electrons in the same energy band ε_l; any band transition is forbidden because the band index is fixed; the wave-function of the ith electron is given by a linear combination of eigenstates $\psi_{\mathbf{k},l}(\mathbf{x})$ over $\mathbf{k} \in B$:

$$\psi_i(\mathbf{x},t) = \int_B c_i(\mathbf{k},t)\,\psi_{\mathbf{k},l}(\mathbf{x})\,d\mathbf{k}, \qquad i = 1,\ldots,M. \tag{A.30}$$

Considering the crystal momentum vector of the ith electron, $p_i = \hbar\mathbf{k}_i$, the semiclassical equations of motion in $(\mathbf{x},\mathbf{k})$ phase-space, i.e.

$$\begin{aligned} &\dot{\mathbf{x}}_i = \mathbf{v}(\mathbf{k}_i) \\ &\hbar\dot{\mathbf{k}}_i = \mathbf{F}_i, \qquad i = 1,\ldots,M \end{aligned} \tag{A.31}$$

where $\mathbf{F} = (\mathbf{F}_1,\ldots,\mathbf{F}_M)$, with $\mathbf{F}_i = \hbar\dot{\mathbf{k}}$, is the vector driving force, periodic in $\mathbf{k}_i$, the semiclassical ensemble Hamiltonian

$$H(\mathbf{x},\mathbf{p},t) = \sum_{i=1}^{M} \varepsilon\left(\frac{\mathbf{p}_i}{\hbar}\right) - eV(\mathbf{x},t), \tag{A.32}$$

one obtains the semiclassical electron-ensemble Liouville equation

$$\partial_t f + \sum_{i=1}^{M} \mathbf{v}(\mathbf{k}_i) \cdot \nabla_{\mathbf{x}_i} f + \frac{1}{\hbar} \mathbf{F} \cdot \nabla_{\mathbf{k}} f = 0\,. \tag{A.33}$$

The following periodic boundary conditions hold for $\mathbf{k}_i$:

$$f(\mathbf{x}, \mathbf{k}_1, \ldots, \mathbf{k}_i, \ldots, \mathbf{k}_M, t) = f(\mathbf{x}, \ldots, -\mathbf{k}_i, \ldots, \mathbf{k}_M, t), \qquad \mathbf{k}_i \in \partial B. \tag{A.34}$$

The main limits of Liouville equation arises when we have to specify the driving force field, including short and long range interactions, and when we have to deal with a too large number of M particles in practical applications. Thus, we would have a model able to describe at least the long range interactions between particles, for example the Coulomb ones, and with a reduced dimensionality. Assuming that the particles of a small subensemble move independently of each other, one can derive a system of equations for the position-velocity densities of a subensemble with d electrons, and d in principle can vary from 1 to M. Dealing with the variation of d, modeling the force field as a weak two-particles interaction and integrating the Liouville equation with respect to the positions and velocities of the remaining $M-d$ particles, we have the BBGKY hierarchy (Bogoliubov [91], Born and Green [92], Kirkwood [93] and Yvon [94]). Carrying out the limit $M \to \infty$, the Vlasov equation is obtained, which has a more macroscopic nature and whose solution is a single function of three position and three velocity coordinates and represents the electron number density in the physical space $\mathbb{R}^3_{\mathbf{x}} \times \mathbb{R}^3_{\mathbf{v}}$.

We have M electrons with equal mass, with position $\mathbf{x}_i \in \mathbb{R}^3_{\mathbf{x}}$ and velocity $\mathbf{v}_i \in \mathbb{R}^3_{\mathbf{v}}$. $\mathbf{E}_i \in \mathbb{R}^3$ is the field exerted on the ith electron (per unit charge) that we write as sum of the electric field and of the sum of the $M-1$ two-particles forces that the other electrons of the ensemble exert on the ith electron:

$$\mathbf{E}_i(\mathbf{x}, t) = \mathbf{E}_{ext}(\mathbf{x}_i, t) + \sum_{i=1, i \neq j}^{M} \mathbf{E}_{int}(\mathbf{x}_i, \mathbf{x}_j), \tag{A.35}$$

where $\mathbf{E}_{ext}$ is the external electric field and E_{int} is the two particle interaction field. The electrons are indistinguishable, i.e. $\mathbf{E}_{int}$ doesn't depend from the particles indexes, and the action-reaction law holds:

$$\mathbf{E}_{int}(\mathbf{x}_i, \mathbf{x}_j) = -\mathbf{E}_{int}(\mathbf{x}_j, \mathbf{x}_i)\,, \tag{A.36}$$

with $\mathbf{E}_{int}(\mathbf{x},\mathbf{x}) = 0$. The ensemble Liouville equation for $f = f(\mathbf{x}_1,\dots,\mathbf{x}_M,\mathbf{v}_1,\dots,\mathbf{v}_M,t)$ is

$$\partial_t f + \sum_{i=1}^{M} \mathbf{v}_i \cdot \nabla_{\mathbf{x}_i} f - \frac{e}{m}\sum_{i=1}^{M} \mathbf{E}_{ext}(\mathbf{x}_i,t)\cdot\nabla_{\mathbf{v}_i} f - \frac{e}{m}\sum_{i=1}^{M}\sum_{j=1}^{M} \mathbf{E}_{int}(\mathbf{x}_i,\mathbf{x}_j)\cdot\nabla_{\mathbf{v}_i} f = 0\,. \tag{A.37}$$

For the assumption (A.36), if the density f doesn't initially depend from the numbering of the particles, it holds for all times, i.e.

$$f(\mathbf{x}_1,\dots,\mathbf{x}_M,\mathbf{v}_1,\dots,\mathbf{v}_M,t) = f(\mathbf{x}_{\pi(1)},\dots,\mathbf{x}_{\pi(M)},\mathbf{v}_{\pi(1)},\dots,\mathbf{v}_{\pi(M)},t) \tag{A.38}$$

is valid for all permutations π of $\{1,\dots,M\}$ and $\forall t$, if it holds for $f_{in} = f(t=0)$. The joint position-velocity density $f^{(d)}$ of a subensemble of d electrons is

$$f^d(\mathbf{x}_1,\dots,\mathbf{x}_d,\mathbf{v}_1,\dots,\mathbf{v}_d,t) = \tag{A.39}$$

$$= \int_{\mathbb{R}^{3(M-d)}_{\mathbf{x}}}\int_{\mathbb{R}^{3(M-d)}_{\mathbf{v}}} f(\mathbf{x}_1,\dots,\mathbf{x}_M,\mathbf{v}_1,\dots,\mathbf{v}_M,t)\,d\mathbf{x}_{d+1}\dots d\mathbf{x}_M d\mathbf{v}_{d+1}\dots d\mathbf{v}_M\,, \tag{A.40}$$

with $1 \le d \le M-1$. By integrating (A.37) with respect to $3(M-d)$ position and velocity coordinates and by assuming that f decays to zero fast enough as $|\mathbf{x}_i| \to \infty$, $|\mathbf{v}_i| \to \infty$, one obtains

$$\partial_t f^{(d)} + \sum_{i=1}^{d} \mathbf{v}_i \cdot \nabla_{\mathbf{x}_i} f^{(d)} - \frac{e}{m}\sum_{i=1}^{d} \mathbf{E}_{ext}(\mathbf{x}_i,t)\cdot\nabla_{\mathbf{v}_i} f^{(d)} - \frac{e}{m}\sum_{i=1}^{d}\sum_{j=1}^{d} \mathbf{E}_{int}(\mathbf{x}_i,\mathbf{x}_j)\cdot\nabla_{\mathbf{v}_i} f -$$

$$\frac{e}{m}(M-d)\times\sum_{i=1}^{d}\nabla_{\mathbf{v}_i}\cdot\left(\int_{\mathbb{R}^{3(M-d)}_{\mathbf{v}_*}}\int_{\mathbb{R}^{3(M-d)}_{\mathbf{x}_*}} \mathbf{E}_{int}(\mathbf{x}_i,\mathbf{x}_*) f_*^{(d+1)} d\mathbf{x}_* d\mathbf{v}_*\right) = 0\,, \tag{A.41}$$

where $f_*^{(d+1)} = f_*^{(d+1)}(\mathbf{x}_1,\dots,\mathbf{x}_d,\mathbf{x}_*,\mathbf{v}_1,\dots,\mathbf{v}_d,\mathbf{v}_*,t)$. In the previous equation, the terms with index $i \ge d+1$ in the sum with external fields E_{ext} vanish by the divergence theorem, and vanish in the terms involving spatial derivatives and in the double sum with the interaction field E_{in}. Moreover, the last sum represents the contribution of each term with $1 \le i \le d$, that, by (A.38), is the same for each $j \ge d$, $j \ne d$. The Eq. (A.41) for $1 \le d \le M-1$ is the Bogoliubov-Born-Green-Kirkwood-Yvon (BBGKY) hierarchy for the classical Lioville equation [87]. Although the system of equation cannot be solved explicitly, we can perform an asymptotic analysis for $M \gg d$; this is reasonable because in the semiconductor there are ensemble with a large number of particles. For carrying out the limit $M \to \infty$, it is to be assumed that $|\mathbf{E}_{int}|$ is of the order of magnitude $1/M$ for M large; this means that the total

field strength is finite as $M \to \infty$. Given d fixed, as $M \to \infty$, the Eq.(A.41) becomes:

$$\partial_t f^{(d)} + \sum_{i=1}^{d} \mathbf{v}_i \cdot \nabla_{\mathbf{x}_i} f^{(d)} - \frac{e}{m} \sum_{i=1}^{d} \mathbf{E}_{ext}(\mathbf{x}_i, t) \cdot \nabla_{\mathbf{v}_i} f^{(d)}$$
$$- \frac{e}{m} \sum_{i=1}^{d} \nabla_{\mathbf{v}_i} \cdot \left(\int_{\mathbb{R}^3_{\mathbf{v}_*}} \int_{\mathbb{R}^3_{\mathbf{x}_*}} M f_*^{(d+1)} \mathbf{E}_{int}(\mathbf{x}_i, \mathbf{x}_*) d\mathbf{x}_* d\mathbf{v}_* \right) = 0 . \tag{A.42}$$

Since the electrons of a subensemble small with respect to the total number of electrons move independently, for the joint probability density we have that

$$f^{(d)}(\mathbf{x}_1, \ldots, \mathbf{x}_d, \mathbf{v}_1, \ldots, \mathbf{v}_d, t) = \prod_{i=1}^{d} P(\mathbf{x}_i, \mathbf{v}_i, t), \tag{A.43}$$

where $P = f^1$ is the one-particle density. From (A.42) with $d = 1$, by using (A.43) with $d = 2$, we obtain

$$\partial_t P + \mathbf{v} \cdot \nabla_{\mathbf{x}} P - \frac{e}{m} \mathbf{E}_{eff}(\mathbf{x}, t) \cdot \nabla_{\mathbf{v}} P = 0 , \tag{A.44}$$

with

$$\mathbf{E}_{eff}(\mathbf{x}, t) = \mathbf{E}_{ext}(\mathbf{x}, t) + \int_{\mathbb{R}^3_{\mathbf{x}_*}} \int_{\mathbb{R}^3_{\mathbf{v}_*}} M P(\mathbf{x}_*, \mathbf{v}_*, t) \mathbf{E}_{int}(\mathbf{x}, \mathbf{x}_*) d\mathbf{v}_* d\mathbf{x}_* . \tag{A.45}$$

If P is a solution of (A.44), (A.43) is an arbitrary solution of (A.44) for arbitrary $d \in \mathbb{N}$. In the same way, if the initial $f^{(d)}$ can be factored as in the (A.43), this is also possible for the solution of BBGKY hierarchy (A.42).

The number of electron per unit volume in a neighborhood of $(\mathbf{x}, \mathbf{v})$ at time t, i.e. the expected electron number density in phase space is defined as

$$F(\mathbf{x}, \mathbf{v}, t) = M P(\mathbf{x}, \mathbf{v}, t). \tag{A.46}$$

The expected electron number density in the position space and the macroscopic charge current density are, respectively,

$$n(\mathbf{x}, t) = \int_{\mathbb{R}^3_{\mathbf{v}}} F(\mathbf{x}, \mathbf{v}, t) d\mathbf{v} , \tag{A.47}$$

$$\mathbf{J} = -e \int_{\mathbb{R}^3_{\mathbf{v}_*}} \mathbf{v} F(\mathbf{x}, \mathbf{v}, t) d\mathbf{v} . \tag{A.48}$$

By multiplying (A.44) by M [87, 95], we finally obtain the classical Vlasov equation:

$$\partial_t F + \mathbf{v} \cdot \nabla_{\mathbf{x}} F - \frac{e}{m} \mathbf{E}_{eff} \cdot \nabla_{\mathbf{v}} F = 0 , \tag{A.49}$$

with

$$\mathbf{E}_{eff}(\mathbf{x},t) = \mathbf{E}_{ext}(\mathbf{x},t) + \int_{\mathbb{R}^3_{\mathbf{x}_*}} n(\mathbf{x}_*,t)\mathbf{E}_{int}(\mathbf{x},\mathbf{x}_*)d\mathbf{v}_* d\mathbf{x}_* \,. \tag{A.50}$$

This is as a single particle Liouville equation, where the many-body effects are taken into account only by the effective field $\mathbf{E}_{eff}$, that in turn depends on the number density n. The trajectories of electrons under the effect of the field $\mathbf{E}_{eff}$ are the characteristics

$$\dot{\mathbf{x}} = \mathbf{v}, \qquad \dot{\mathbf{v}} = -\frac{e}{m}\mathbf{E}_{eff}(\mathbf{x},t), \tag{A.51}$$

that in turn can be understood as the limiting $(\mathbf{x}_i,\mathbf{v}_i)$ trajectories of the Lioville equation (A.37) as $M \to \infty$. $F(\mathbf{x},\mathbf{v},t)$ is also considered as the existence probability of a particle in the state $(\mathbf{x},\mathbf{v})$ at time t, and then it has to obey to the Pauli principle

$$0 \leq F(\mathbf{x},\mathbf{v},t) \leq 1 \,. \tag{A.52}$$

If the Pauli principle is respected for the initial datum

$$0 \leq F(\mathbf{x},\mathbf{v},t=0) \leq 1 \,, \tag{A.53}$$

using (A.51), we can conclude that the Pauli principle is conserved in time by Vlasov equation (A.49).

The Vlasov equation then gives a more mascrocopic description into a kinetic framework when there are weak long range forces, so on a time scale much shorter than the mean time of, for example, two scattering events between particles due to short range forces. It is mandatory in this case to resort to the Boltzmann equation. Moreover, Vlasov equation is nonlinear with a nonlocal nonlinearity of quadratic type [86]. Starting from the semiclassical Liouville equation (A.33), with the same procedure, one has the semiclassical Vlasov equation

$$\partial_t F + \mathbf{v}(\mathbf{k}) \cdot \nabla_{\mathbf{x}} F - \frac{e}{\hbar}\mathbf{E}_{eff} \cdot \nabla_{\mathbf{k}} F = 0 \,, \tag{A.54}$$

with

$$\mathbf{E}_{eff}(\mathbf{x},t) = \mathbf{E}_{ext}(\mathbf{x},t) + \int_{\mathbb{R}^3_{\mathbf{x}_*}} n(\mathbf{x}_*,t)\mathbf{E}_{int}(\mathbf{x},\mathbf{x}_*)d\mathbf{v}_* d\mathbf{x}_* \,. \tag{A.55}$$

The electron number density and current density are respectively

$$n(\mathbf{x},t) = \int_B F(\mathbf{x},\mathbf{k},t)d\mathbf{k}, \tag{A.56}$$

$$\mathbf{J}(\mathbf{x},t) = -e\int_B \mathbf{v}(\mathbf{k})F(\mathbf{x},\mathbf{k},t)d\mathbf{k}. \tag{A.57}$$

The phase-space number density F satisfies the periodic boundary conditions in $\mathbf{k}$:

$$F(\mathbf{x},\mathbf{k},t) = F(\mathbf{x},-\mathbf{k},t), \qquad \mathbf{x} \in \mathbb{R}^3_{\mathbf{x}}, \mathbf{k} \in \partial B, t > 0. \tag{A.58}$$

The Boltzmann equation takes into account the short range forces and, in particular, collisions between particles and with the crystal lattice; the particles instantaneously change their state, so their velocity vectors and, consequently, their wave-vectors and their momentum change in a very fast way, while the position vectors change slowly. Without collisions, the number density $F = F(\mathbf{x},\mathbf{v},t)$ is conserved along the characteristics (A.51) under the effect of the convection due to the effective field $\mathbf{E}_{eff}$, i.e.

$$\left(\frac{dF}{dt}\right)_{conv} = 0. \tag{A.59}$$

By postulating that there is a balance between the rate of change of F due to the convection and that due to the collisions, we can write

$$\left(\frac{dF}{dt}\right)_{conv} = \left(\frac{dF}{dt}\right)_{coll}, \tag{A.60}$$

or, explicitly, the following Boltzmann equation:

$$\partial_t F + \mathbf{v}\cdot\nabla_{\mathbf{x}} F - \frac{e}{m}\mathbf{E}_{eff}\cdot\nabla_{\mathbf{v}} F = \left(\frac{dF}{dt}\right)_{coll}, \tag{A.61}$$

where the effective field $\mathbf{E}_{eff}$ is given by (A.50). Given a particle at time t, with position vector $\mathbf{x}$ and velocity vector $\mathbf{v}'$, the rate $P(\mathbf{x},\mathbf{v}' \to \mathbf{v},t)$ to change its velocity $\mathbf{v}'$ in $\mathbf{v}$ after a scattering event is proportional to the occupation probability $F(\mathbf{x},\mathbf{v}',t)$ of the initial state $(\mathbf{x},\mathbf{v}')$ and, according to the Pauli principle, also to $1 - F(\mathbf{x},\mathbf{v},t)$, that is the probability that the final state is available at time t:

$$P(\mathbf{x},\mathbf{v}' \to \mathbf{v},t) = s(\mathbf{x},\mathbf{v}',\mathbf{v})F(\mathbf{x},\mathbf{v}',t)\left(1 - F(\mathbf{x},\mathbf{v},t)\right). \tag{A.62}$$

s is the *scattering rate* and $s(\mathbf{x},\mathbf{v}',\mathbf{v})d\mathbf{v}'$ the *transition rate*.

The total rate of change of the number density F at $(\mathbf{x},\mathbf{v},t)$ due to the collisions is the difference between the sum of the rates of the particles scattered from all possible states $(\mathbf{x},\mathbf{v}')$ into the state $(\mathbf{x},\mathbf{v})$ at time t and the sum of the rates of particles scattered from the

state $(\mathbf{x},\mathbf{v})$ into any possible state $(\mathbf{x},\mathbf{v}')$ at time t, i.e.

$$\left(\frac{dF}{dt}\right)_{coll}(\mathbf{x},\mathbf{v},t) = \int_{\mathbb{R}^3_{\mathbf{v}'}} \left[P(\mathbf{x},\mathbf{v}' \to \mathbf{v},t) - P(\mathbf{x},\mathbf{v} \to \mathbf{v}',t)\right] d\mathbf{v}' \tag{A.63}$$

By inserting (A.62) into (A.63), one obtains

$$\begin{aligned} C[F](\mathbf{x},\mathbf{v},t) = \int_{\mathbb{R}^3_{\mathbf{v}'}} \big[&s(\mathbf{x},\mathbf{v}',\mathbf{v})F(\mathbf{x},\mathbf{v}',t)\,(1-F(\mathbf{x},\mathbf{v},t)) - \\ &s(\mathbf{x},\mathbf{v},\mathbf{v}')F(\mathbf{x},\mathbf{v},t)\left(1-F(\mathbf{x},\mathbf{v}',t)\right)\big]\, d\mathbf{v}' \end{aligned} \tag{A.64}$$

where

$$C[F] := \left(\frac{dF}{dt}\right)_{conv}. \tag{A.65}$$

C is the collision operator and $C[F]$ the collision integral. Thus, the Boltzmann equation reads

$$\partial_t F + \mathbf{v}\cdot\nabla_{\mathbf{x}}F - \frac{e}{m}\mathbf{E}_{eff}\cdot\nabla_{\mathbf{v}}F = C[F] \tag{A.66}$$

The effective self-consistent field already introduces a non linearity, the collision integral $C[F]$ introduces another non linearity, quadratic and non-local in the velocity. If we initially consider the semiclassical Vlasov equation (A.54) and the semiclassical expression for the effective field (A.55) the semiclassical Boltzmann equation reads

$$\partial_t F + \mathbf{v}(\mathbf{k})\cdot\nabla_{\mathbf{x}}F - \frac{e}{\hbar}\mathbf{E}_{eff}\cdot\nabla_{\mathbf{k}}F = C[F] \tag{A.67}$$

where

$$\begin{aligned} C[F](\mathbf{x},\mathbf{k},t) = \int_B \big[&s(\mathbf{x},\mathbf{k}',\mathbf{k})F(\mathbf{x},\mathbf{k}',t)\,(1-F(\mathbf{x},\mathbf{k},t)) - \\ &s(\mathbf{x},\mathbf{k},\mathbf{k}')F(\mathbf{x},\mathbf{k},t)\left(1-F(\mathbf{x},\mathbf{k}',t)\right)\big]\, d\mathbf{k}'. \end{aligned} \tag{A.68}$$

The Boltzmann equation has to respect the boundary condition

$$F(\mathbf{x},\mathbf{k},t) = F(\mathbf{x},-\mathbf{k},t), \qquad \mathbf{x}\in\mathbb{R}^3_{\mathbf{x}}, \mathbf{k}\in\partial B, t>0\,. \tag{A.69}$$

Moreover, we impose the initial condition

$$F(\mathbf{x},\mathbf{k},t=0) = F_{in}(\mathbf{x},\mathbf{k}) \tag{A.70}$$

and we assume that it obeys to the Pauli exclusion principle:

$$0 \leq F_{in}(\mathbf{x},\mathbf{k}) \leq 1\,. \tag{A.71}$$

We report a sketch of the proof for existence and uniqueness for the Boltzmann-Poisson problem in the whole space as in [96, 86]; for further details we refer to [19, 20]. This also shows the intrinsic importance of the Pauli principle for the Boltzmann equation. It is used a decoupling iterative approach. We set $F^{(0)} = 0$ and construct a sequence of approximations $\left\{F^{(l)}\right\}_{l\in\mathbb{N}_0}$ as follows. Given $F^{(l)}$, the number density is

$$n^{(l)} = \int_B F^{(l)} d\mathbf{k} \tag{A.72}$$

and the effective field $\mathbf{E}^{(l)}_{eff}$ is calculated by inserting $n^{(l)}$ into (A.50) using the Poisson kernel

$$\mathbf{E}_{int}(\mathbf{x},\mathbf{y}) = -\frac{e}{4\pi\varepsilon_s}\frac{\mathbf{x}-\mathbf{y}}{|\mathbf{x}-\mathbf{y}|^3}\,, \qquad \mathbf{x},\mathbf{y}\in\mathbb{R}^3, \quad \mathbf{x}\neq\mathbf{y} \tag{A.73}$$

where ε_s is the permittivity. One obtains

$$\partial_t F^{(l+1)} + \mathbf{v}(\mathbf{k})\cdot\nabla_{\mathbf{x}} F^{(l+1)} - \frac{e}{\hbar}\mathbf{E}^{(l)}_{eff}\cdot\nabla_{\mathbf{k}} F^{(l+1)} = C_{lin}[F^{(l+1)}, F^{(l)}] \tag{A.74}$$

with the initial condition (A.70) and the periodic boundary condition on ∂B. The collision integral is written as

$$\begin{aligned} C_{lin}[F^{(l+1)}, F^{(l)}] = \int_B \Big[& s(\mathbf{x},\mathbf{k}',\mathbf{k}) F^{(l)}(\mathbf{x},\mathbf{k}',t)\left(1 - F^{(l+1)}(\mathbf{x},\mathbf{k},t)\right) - \\ & s(\mathbf{x},\mathbf{k},\mathbf{k}') F^{(l+1)}(\mathbf{x},\mathbf{k},t)\left(1 - F^{(l)}(\mathbf{x},\mathbf{k}',t)\right)\Big] d\mathbf{k}'\,. \end{aligned} \tag{A.75}$$

Defining

$$A^{(l)} = \int_B s(\mathbf{x},\mathbf{k}',\mathbf{k}) F^{(l)}(\mathbf{x},\mathbf{k}',t) d\mathbf{k}'\,, \tag{A.76}$$

$$B^{(l)} = \int_B s(\mathbf{x},\mathbf{k},\mathbf{k}') F^{(l)}\left(1 - F^{(l)}(\mathbf{x},\mathbf{k}',t)\right) d\mathbf{k}'\,, \tag{A.77}$$

one has

$$C_{lin}(F^{(l+1)}, F^{(l)}) = A^{(l)}(1 - F^{(l+1)}) - B^{(l)} F^{(l+1)}\,. \tag{A.78}$$

The linear transport equation (A.74) can be solved by the method of characteristics or by the semigroup theory. Along the characteristics

$$\dot{\mathbf{x}} = \mathbf{v}(\mathbf{k}), \qquad \hbar\dot{\mathbf{k}} = -e\mathbf{E}_{eff}(l), \tag{A.79}$$

the (A.74) can be written as

$$\frac{dF^{(l+1)}}{dt} + \left(A^{(l)} + B^{(l)}\right) F^{(l+1)} = A^{(l)}. \tag{A.80}$$

Since $s > 0$, from (A.76) $A^{(l)} \geq 0$, if $F^{(l)} \geq 0$. By integrating (A.80), we have $F^{(l+1)} \geq 0$. Setting $G := 1 - F^{(l+1)}$, one obtains

$$\frac{dG^{(l+1)}}{dt} + \left(A^{(l)} + B^{(l)}\right) G^{(l+1)} = B^{(l)}. \tag{A.81}$$

If $F^{(l)} \leq 0$, we have $B^{(l)} \geq 0$ and, by integrating (A.81), $G^{(l+1)} \geq 0$. We can conclude that, if the initial datum F_{in} satisfies the Pauli principle, this holds for all iterates $F^{(l)}$ for all times $t > 0$. By passing to the limit $l \to \infty$, we have that the Boltzmann equation conserves the upper and the lower bounds, i.e 1 and 0, and the solution F satisfies the Pauli principle

$$0 \leq F(\mathbf{x},\mathbf{k},t) \leq 1, \qquad t \geq 0\,. \tag{A.82}$$

When the transition rate is regular and positive enough, then the sequence $\left\{F^{(l)}\right\}_{l\in\mathbb{N}_0}$ converges to the unique solution of the Boltzmann-Poisson problem.

By integrating (A.68) we obtain

$$\begin{aligned}\int_B C[F]d\mathbf{k} = \int_B\int_B \big[&s(\mathbf{x},\mathbf{k}',\mathbf{k})F(\mathbf{x},\mathbf{k}',t)\,(1-F(\mathbf{x},\mathbf{k},t)) - \\ &s(\mathbf{x},\mathbf{k},\mathbf{k}')F(\mathbf{x},\mathbf{k},t)\left(1-F(\mathbf{x},\mathbf{k}',t)\right)\big]\,d\mathbf{k}'d\mathbf{k} = 0\,,\end{aligned} \tag{A.83}$$

and it is clear how the scattering processes produce neither a destruction nor a generation of particles, and both the continuity equation and the conservation of the total number of electrons are respected. A fundamental property of the collision operator prescribes that the state of the particles ensemble has to relax towards a local thermodynamical equlibrium. For the *detailed balance principle* the local scattering probabilities vanish for all states $(\mathbf{x},\mathbf{k})$, $(\mathbf{x},\mathbf{k}')$ in thermal equilibrium [89, 97, 90]:

$$s(\mathbf{x},\mathbf{k}',\mathbf{k})F_{eq}(\mathbf{x},\mathbf{k}',t)\left(1-F_{eq}(\mathbf{x},\mathbf{k},t)\right) = s(\mathbf{x},\mathbf{k},\mathbf{k}')F_{eq}(\mathbf{x},\mathbf{k},t)\left(1-F_{eq}(\mathbf{x},\mathbf{k}',t)\right), \tag{A.84}$$

where F_{eq} is the equilibrium number density that is equal to the Fermi-Dirac distribution

$$F_{eq}(\mathbf{k}) = \frac{1}{1+\exp\left(\frac{\varepsilon(\mathbf{k})-\varepsilon_F}{k_B T}\right)}, \tag{A.85}$$

where $\varepsilon(\mathbf{k})$ is the energy of the considered energy band, ε_F is the Fermi level, k_B is the Boltzmann constant and T is the lattice temperature. From (A.84) one has

$$s(\mathbf{x},\mathbf{k},\mathbf{k}') = \exp\left(\frac{\varepsilon(\mathbf{k}')-\varepsilon(\mathbf{k})}{k_B T}\right) s(\mathbf{x},\mathbf{k}',\mathbf{k}), \tag{A.86}$$

that [96] is a sufficient and necessary condition on s in order to have the Fermi-Dirac distribution as the null manifold of the collision operator C, i.e if we have that

$$C[F] = 0, \qquad 0 \leq F \leq 1, \tag{A.87}$$

then F is given by (A.85) for $-\infty \leq \varepsilon_F \leq +\infty$, if (A.86) holds.

We define the strength of the interaction at the state $(\mathbf{x},\mathbf{k})$ related to the scattering rate s as the collision frequency λ

$$\lambda(\mathbf{x},\mathbf{k}) := \int_B s(\mathbf{x},\mathbf{k},\mathbf{k}')d\mathbf{k}'; \tag{A.88}$$

The relaxation time is the reciprocal of the collision frequency and gives the average time between two consecutive scattering events at $(\mathbf{x},\mathbf{k})$ and is the time scale of the relaxation of a density F towards the equilibrium Fermi-Dirac distribution.

We would analyze more in deep this property because it is one of the most important peculiarities of the Boltzmann equation, just considering [86] a simplified case, when the density is low enough to use the Maxwellian distribution $M(\mathbf{k})$ in place of the Fermi-Dirac one,

$$M(\mathbf{k}) = \tilde{N}\exp\left(\frac{\varepsilon(\mathbf{k})}{k_B T}\right), \tag{A.89}$$

with

$$\tilde{N} = \left(\int_B \exp\left(\frac{\varepsilon(\mathbf{k})}{k_B T}\right) d\mathbf{k}\right)^{-1}, \tag{A.90}$$

and the initial datum F_{in} is very close to the Maxwellian distribution; in this case we can write a very simplified expression for a linear and local in $\mathbf{k}$ collision operator:

$$\tilde{C}[F](\mathbf{x},\mathbf{k},t) = -\frac{1}{\tau(\mathbf{x},\mathbf{k})}\left(F(\mathbf{x},\mathbf{k},t) - M(\mathbf{k})n(\mathbf{x},t)\right). \tag{A.91}$$

Along the characteristics $(\mathbf{x}(t),\mathbf{k}(t))$ the Boltzmann equation reads

$$\frac{d}{dt}F = -\frac{1}{\tau}\left(F - Mn\right), \tag{A.92}$$

leading to

$$F\left(\mathbf{x}(t),\mathbf{k}(t),t\right) = e^{-t/\tau}\left(F_{in}(\mathbf{x}_0,\mathbf{k}_0) + \frac{1}{\tau}\int_0^t n\left(\mathbf{x}(s),s\right)M(\mathbf{k}(s))e^{s/\tau}ds\right). \tag{A.93}$$

Assuming τ constant and n known, one has that

$$F\left(\mathbf{x}(t),\mathbf{k}(t),t\right)) - n\left(\mathbf{x}(t),t\right)M(\mathbf{k}(t)) \sim e^{-t/\tau}, \qquad \text{as} \quad t \to \infty. \tag{A.94}$$

The Vlasov equation doesn't have this property because it doesn't take into account the collisions and it is time-reversible, with a static exterior field, but when the collisions are introduced, so with the Boltzmann equation, they drive the ensemble towards a thermodynamical equilibrium in the large time limit. This is one of the most important consequences of the H-Theorem [87, 96].

References

[1] C. Jacoboni, Theory of Electron Transport in Semiconductors. Springer-Verlag Berlin Heidelberg (2010).

[2] C. Cercignani, The Boltzmann Equation and its Applications, volume 67 of Applied Mathematical Sciences. Springer, New York. (1988).

[3] K. S. Novoselov, A. K. Geim, S. V. Morozov, D. Jiang, Y. Zhang, S. V. Dubonos, I. V. Grigorieva, and A. A. Firsov, Electric Field effect in atomically thin carbon films. Science, 306:666-669, (2004).

[4] A. H. Castro Neto, F. Guinea, N. M. R. Peres, K. S. Novoselov, A. K. Geim, The electronic properties of graphene, (2009). *Rev. Mod. Phys.* 81: 109–162.

[5] S. Das Sarma, Shaffique Adam, E. H. Hwang, E. Rossi, Electronic transport in two-dimensional graphene. Rev. Mod. Phys., Vol. **83**, No. 2, (April-June 2011).

[6] K. S Novoselov, A. K. Geim, S. V. Morozov, D. Jiang, M. I. Katsnelson, I. V. Grigorieva, S. V. Dubonos, A. A. Firsov. Two-dimensional gas of massless Dirac fermions in graphene. Nature, **438**, 197-200 (2005).

[7] P. R. Wallace. The band theory of graphite. Phys. Rev., 71(9):622-634, (May 1947).

[8] K. M. Borysenko, J. T. Mullen, E. A. Barry, S. Paul, Y. G. Semenov, J. M. Zavada, M. Buongiorno Nardelli, K. W. Kim. First-principles analysis of electron-phonon interactions in graphene. Phys. Rev. B **11**, 121412(R) (2010)

[9] N. Metropolis, S. Ulam. J. Am. Stat. Assoc. **247**, 335 (1949).

[10] T. Kurosawa, in Proceedings of the International Conference on the Physics of Semiconductors, Kyoto, J. Phys. Soc. Jpn. Suppl. **21**, 424 (1966).

[11] P.J. Price, in Proceedings of the 9th International Conference on the Physics of Semiconductors, ed. by S.M. Ryvkin (Nauka, Leningrad), p. 753 (1968).

[12] A.D. Boardman, W. Fawcett, H.D. Rees, Solid State Commun. **6**, 305 (1968).

[13] W. Fawcett, A.D. Boardman, S. Swain, J. Phys. Chem. Solids **31**, 1963 (1970).

[14] C. Jungemann, B. Meinerzhagen, Hierarchical Device Simulation – The Monte Carlo Perspective. Springer, Wien. (2003).

[15] D. Vasileska, D. Mamaluy, H.R: Khan, K. Raleva, S:M: Goodnick, Semiconductor Device Modeling. J. Comp. Theor. Nanosci., **5**, 1-32 (2008).

[16] R.M. Yorston, J. Comp. Phys., **64**, 177 (1986).

[17] X. Li, E. A. Barry, J. M. Zavada, M. Buongiorno Nardelli, K. W. Kim, Surface polar phonon dominated electron transport in graphene. Appl. Phys. Lett., **97**, 232105 (2010).

[18] A. Jüngel, Transport Equations for Semiconductors Lecture Notes in Physics, vol. 773, Springer, Berlin (2009).

[19] A. Majorana, S. Marano, Space homegeneous solutions to the Cauchy problem for semiconductor Boltzmann equations. SIAM J. Math. Anal. **28**, 1294-1308 (1997).

[20] A. Majorana, S. Marano, On the Cauchy problem for spatially homogeneous semiconductor Boltzmann equations: existence and uniqueness. Annali di Matematica, **184**, 275-296 (2005).

[21] M.H.Kalos and P.A.Whitlock, Monte Carlo Methods, Wiley, New York (1986).

[22] E.T. Jaynes, Information Theory and Statistical Mechanics. *Phys. Rev. B* **106**:620-630 (1957).

[23] H.D. Rees, Phys. Lett. A **26**, 416 (1968).

[24] H.D. Rees, J. Phys. Chem. Solids **30**, 643 (1969).

[25] M. Coco, A. Majorana, G. Mascali, V. Romano, Comparing kinetic and hydrodynamical models for electron transport in monolayer graphene, VI International Conference on Computational Methods for Coupled Problems in Science and Engineering COUPLED PROBLEMS (2015).

[26] V. Romano, A. Majorana, M. Coco, DSMC method consistent with the Pauli exclusion principle and comparison with deterministic solutions for charge transport in graphene. *Journal of Computational Physics* 302:267–284 (2015).

[27] S. Bosi, C. Jacoboni, Monte Carlo high-field transport in degenerate GaAs. *J. Phys. C: Solid State Phys.* **9**: 315–319 (1976).

[28] P. Lugli, D. K. Ferry, Degeneracy in the Ensemble Monte Carlo Method for High-Field Transport in Semiconductors. *IEEE Trans. on Elect. Devices* **ED-32** (11): 2431–2437 (1985).

[29] C. Jacoboni and P. Lugli, *The Monte Carlo method for Semiconductor Device Simulation*, Springer-Verlag (1989).

[30] C. Jacoboni, L. Reggiani, Rev. Mod. Phys. **55**, 645 (1983).

[31] P. Borowik, J. L. Thobel, Improve Monte Carlo method for the study of electron transport in degenerate semiconductors, J. Appl. Phys. 84, 3706 (1998).

[32] P. Borowik, L. Adamowciz, Improved algorithm for Monte Carlo studies of electron transport in degenerate semiconductors, Physica B 365, 235–239 (2005).

[33] M. V. Fischetti, S. E. Laux, Monte Carlo analysis of electron transport in small semiconductor devices including band-structure and space-charge effects, Phys. Rev. B 38, 9721 (1988).

[34] M. Zebarjadi, C. Bulutay, K. Esfarjani, A. Shakouri, Monte Carlo simulation of electron transport in degenerate and inhomogeneous semiconductors, Appl. Phys. Letters 90, 092111 (2007) .

[35] A. Tomadin, D. Brida, G. Cerullo, A. C. Ferrari, M. Polini, Nonequilibrium dynamics of photoexcited electrons in graphene: Collinear scattering, Auger processes, and the impact of screening, Physical Review B 88, 035430 (2013).

[36] R. S. Shishir and D.K. Ferry, Velocity saturation in intrinsic graphene. *J. Phys. Condens. Matter* **21**:344201 (2009).

[37] T. Fang, A. Konar, H. Xing, and D. Jena, High-field transport in two-dimensional graphene. *Phys. Rev. B* **84**:125450 (2011).

[38] P. Lichtenberger, O. Morandi, F. Schürrer, High-field transport and optical phonon scattering in graphene. *Physical review B* 84: 045406 (2011).

[39] P. Tadyszak, F. Danneville, A. Cappy, L. Reggiani, L. Varani, L. Rota, Monte Carlo calculations of hot-carrier noise under degenerate conditions. *Appl. Phys. Lett.* **69** (10): 1450–1452 (1996).

[40] Y. Cheng, I. M. Gamba, J. Proft, Preserving Discontinuous Galerkin Schemes for Linear Vlasov-Boltzmann Transport Equations, Mathematics of Computation 81, 153–190 (2012).

[41] J. M. Burt, I. D. Boyd, A low diffusion particle method for simulating compressible inviscid flows, J. Comp. Phys 227, 4653–4670 (2008).

[42] Y. Cheng, I.M. Gamba, A. Majorana, C.-W. Shu, A discontinuous Galerkin solver for Boltzmann-Poisson systems in nano devices. *Computer Methods in Applied Mechanics and Engineering* **198 (37-40)**: 3130–3150 (2009).

[43] Y. Cheng, I.M. Gamba, A. Majorana, C.-W. Shu, A brief survey of the discontinuous Galerkin method for the Boltzmann-Poisson equations. *Boletin de la Sociedad Espanola de Matematica Aplicada* **54**: 47–64 (2011).

[44] V. D. Camiola, V. Romano, Hydrodynamical model for charge transport in graphene, Journal of Statistical Physics **157**: 11141137 (2014).

[45] N. Zamponi, L. Barletti, Quantum electronic transport in graphene: a kinetic and fluid-dynamical approach, Math. Methods Appl. Sci. 34, 807–818 (2011).

[46] G. Mascali, V. Romano, A comprehensive hydrodynamical model for charge transport in graphene, 978-1-4799-5433-9/14/$31.00 © 2014 IEEE, IWCE-2014 Paris (2014).

[47] G. Alì, G. Mascali, V. Romano, C.R. Torcasio, A Hydrodynamical Model for Covalent Semiconductors, with Applications to GaN and SiC. Acta Appl. Math. 122 (1):335 (2012).

[48] L. Barletti, Hydrodynamic equations for electrons in graphene obtained from the maximum entropy principle. *J. Math. Phys.* 55:083303(21), (2014).

[49] O. Morandi, F. Schürrer, Wigner model for quantum transport in graphene. *J. Phys. A: Math. Theor.* 44:265301(32), (2011).

[50] M. J. Cáceres, J. A. Carrillo, A. Majorana, Deterministic simulation of the Boltzmann-Poisson system in GaAs-based semiconductors, SIAM J. Sci. Comput. 27 (6), 1981–2009 (2006).

[51] M. Galler, A. Majorana, Deterministic and Stochastic Simulations of Electron Transport in Semiconductors, Bulletin of the Institute of Mathematics - Academia Sinica New Series 2, 349–365 (2007).

[52] B. Cockburn, C.-W. Shu, The local discontinuous Galerkin method for convection-diffusion systems, SIAM J. Numer. Anal. 35, 2440–2463 (1998).

[53] V.D. Camiola, G. Mascali, V. Romano, Simulation of a Double-Gate MOSFET by a Nonparabolic Hydrodynamical Subband Model for Semiconductors Based on the Maximum Entropy Principle. *Mathematical and Computer Modelling* **58**:321-343 (2013).

[54] C.-W. Shu, S. Osher, Efficient implementation of essentially non-oscillatory shock capturing schemes, J. Comp. Phys. 77, 439–471 (1988).

[55] R. J. LeVeque, Numerical Methods for Conservation Laws. Birkhäuser, Basel, (1992).

[56] A. Harten, S. Osher, Uniformly high-order accurate non-oscillatory schemes. I. SIAM J. Numer. Anal. **24**, 279-309 (1987).

[57] M. Coco, A. Majorana, V. Romano, Cross validation of discontinuous Galerkin method and Monte Carlo simulations of charge transport in graphene on substrate. *Ricerche Math.* DOI 10.1007/s11587-016-0298-4 (2016).

[58] M. Coco, A. Majorana, G. Nastasi, V. Romano, High-field mobility in graphene on substrate with a proper inclusion of the Pauli exclusion principle. *Accepted in Atti dell'Accademia Peloritana dei Pericolanti* , (2016).

[59] G. Kané, M. Lazzeri, F. Mauri, High-field transport in graphene: the impact of Zener tunneling, J. Phys.: Condensed Matter 27, 164205 (11pp) (2015).

[60] E. H. Hwang, S. Adam, S. Das Sarma, Carrier Transport in Two-Dimensional Graphene Layers, Phys. Rev. Lett. 98:186806 (2007).

[61] E. H. Hwang, S. Das Sarma, Dielectric function, screening, and plasmon in two-dimensional graphene, J. Phys. Rev. B 75: 205418 (2007).

[62] M. Lundstrom, Fundamentals of carrier transport, Cambridge University Press, (2000).

[63] K. Tomizawa, Numerical Simulation of Submicron Semiconductor Devices, Artech House, Inc., (1993).

[64] H. Hirai, H. Tsuchiya, Y. Kamakura, N. Mori, M Ogawa, Electron mobility calculation for graphene on substrates, J. Appl. Phys. 116:083703 (2014).

[65] M. Coco, G. Mascali, V. Romano, Monte Carlo analysis of thermal effects in monolayer graphene. *J.Computational and Theoretical Transport*, Vol. 45 (7): 540-543 (2016).

[66] M. Coco, V. Romano, A complete electron-phonon transport model in suspended monolayer graphene, submitted (2017).

[67] O. Morandi, Charge transport and hot-phonon activation in graphene. *J.Computational and Theoretical Transport* 43: 162-182 (2014).

[68] E.N. Koukaras, G. Kalosakas, C. Galiotis, P. Konstantinos, Phonon properties of graphene derived from molecular dynamics. Scientific Reports 5:12923. simulations (2015).

[69] D.L. Nika, A.A. Balandin, Two-dimensional phonon transport in graphene. *J. Phys.: Condens. Matter* 24: 233203 (2012).

[70] E. Pop, V. Varshney, A.K. Roy, Thermal properties of graphene: Fundamentals and applications. *MRS Bull* 37: 1273 (2012).

[71] N. Mounet, N. Marzari, First-principles determination of the structural, vibrational, and thermodynamical properties of diamond, graphite, and derivatives. Physical Review B 71, 205214 (2005).

[72] G. Mascali, A hydrodynamic model for silicon semiconductors including crystal heating. *European Journal of Appl. Math.* 26: 447– 496 (2015).

[73] N. Bonini, M. Lazzeri, N. Marzari, F. Mauri, Phonon anharmonicities in graphite and graphene. *Phys. Rev. Letters* 99: 176802 (2007).

[74] M. Freitag, M. Steiner, Y. Martin, V. Perebeinos, Z. Chen, J.C. Tsang, P. Avouris, Energy dissipation in graphene field-effect transistor. *Nano Letters* 9: 1883-1888 (2009).

[75] T. Feng, X. Ruan, Z. Ye, B. Cao, Spectral phonon mean free path and thermal conductivity accumulation in defected graphene: The effects of defect type and concentration. Phys. Rev. B 91:224301-01–12 (2015).

[76] E. Pop, S. Sinha, K.E. Goodson, Heat generation and transport in nanometer-scale transistors. Proc. IEEE 94:1587–160 (2006).

[77] O. Muscato, V. Di Stefano, Local equilibrium and off-equilibrium thermoelectric effects in silicon semiconductors. J. of Appl. Phys. 110:093706-1–10 (2010).

[78] O. Muscato, V. Di Stefano, W. Wagner, A variance-reduced electrothermal Monte Carlo method for semiconductor device simulation. Comput. Math. Appl. 65:520–527 (2013).

[79] V.E. Dorgan, M.H. Bae, E. Pop, Mobility and saturation velocity in graphene on SiO2. *Appl. Phys. Lett.* 97: 082112 (2010).

[80] I. Gierz, C. Riedl, U. Starke, C.R. Ast, Atomic hole doping of graphene. *Nano letters* 8: 4603-4607 (2008).

[81] P. L. Bhatnagar, E. P. Gross, and M. Krook. A model for collision processes in gases. I. small amplitude processes in charged and neutral one-component systems. Phys. Rev., **94**(3):511-524 (1954).

[82] A.M. Anile and V. Romano, Non parabolic band transport in semiconductors: closure of the moment equations, Cont. Mechan. Thermodyn. **11** (5) 307-325 (1999).

[83] V. Romano, Non parabolic band transport in semiconductors: closure of the production terms in the moment equations, Cont. Mechan. Thermodyn. **12** (1) 31-51 (2000).

[84] G. Mascali and V. Romano, Hydrodynamical model of charge transport in GaAs based on the maximum entropy principle, Continuum Mechanics and Thermodynamics **14** 405-423 (2002).

[85] G. Mascali, V. Romano, Exploitation of the Maximum Entropy Principle in Mathematical Modeling of Charge Transport in Semiconductors, Entropy, 19(1), 36; doi:10.3390/e19010036 (2017).

[86] P.A. Markowich, C.A. Ringhofer, C. Schmeiser, Semiconductor Equations. Springer-Verlag Wien New York (1990).

[87] C. Cercignani, The Boltzmann Equation and Its Applications. Applied Mathematical Sciences, vol. **67**. Springer-Verlag, Berlin (1988).

[88] L.D. Landau, E.M. Lifsits, Meccanica. Editori Riuniti (2004).

[89] N.C. Ashcroft, N.D. Mermin, Solid State Physics. Holt-Sounders, New York (1976).

[90] C. Kittel, Introduction to Solid State Physics. J. Wiley and Sons, New York (1968).

[91] N.N. Bogoliubov. Problems of a Dynamical Theory in Statistical Physics. In: Studies in Statistical Mechanics, Vol I (J. de Boer, G.E. Uhlenbeck, eds.). North-Holland, Amsterdam, p.5 (1962).

[92] M. Born, H.S. Green. A General Kinetic Theory of Fluids. Cambridge University Press. Cambridge (1949).

[93] J.G. Kirkwood. J. Chem. Phys. **14**, 180 (1946).

[94] J. Yvon. La Thorie Statistique des Fluides. Actualiés Scientifiques et Industrielles, No. 203. Hermann, Paris (1935).

[95] N.A. Krall, A.W. Trivelpiece. Principles of Plasma Physics. McGraw-Hill, New York (1973).

[96] F. Poupaud. On a System of Nonlinear Boltzmann Equations of Semiconductor Physics. SIAM. J. Appl. Math. **50**, 1593-1606 (1990).

[97] J. S. Blakemore. Semiconductor Statistics. Pergamon Press, Oxford (1962).

[98] D. Hilbert. Math. Ann. **72**, 562 (1912).

[99] F. Poupaud. Etude Mathematique et Simulations Numeriques de Quelques Equation de Boltzmann. Thesis, Univ. Paris, 6 (1988).